Electrochemical Society

UNIV. OF MICHIGAN
AUG 11 1953
EAST ENGINEERING
LIBRARY

ELECTROCHEMICAL INDUSTRY

Milwaukee-Chicago-Gary Area

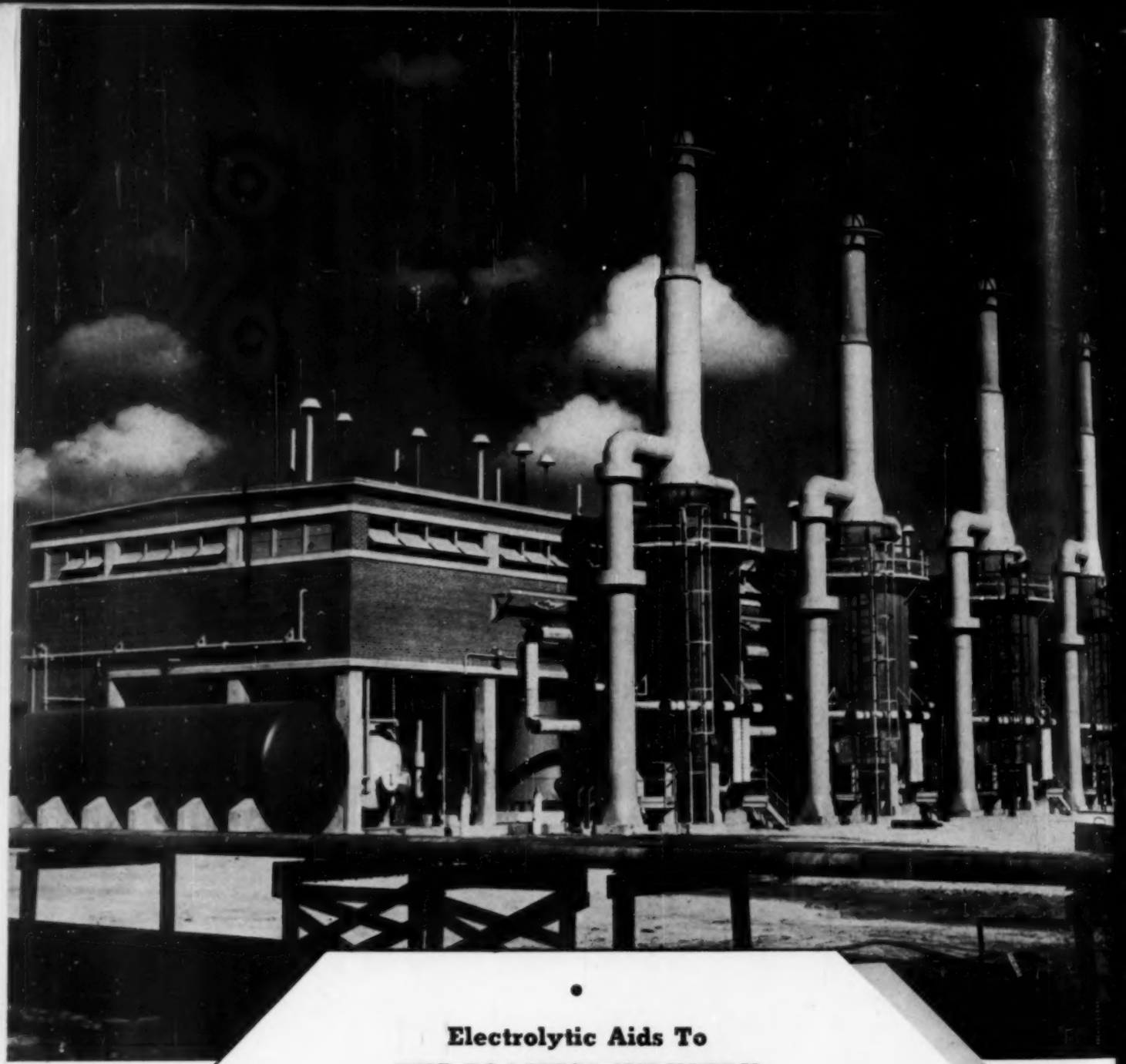

Electrolytic Aids To
THE PLASTICS INDUSTRY

Chlorine and caustic soda, products of the electrolytic industry, are important in the behind-the-scenes steps essential to the production of many plastic materials.

Uniformly high quality **GLC Graphite Anodes** are doing their share to help the electrolytic industry meet the ever increasing civilian and defense demands for chlorine and caustic soda.

ELECTRODE DIVISION

Great Lakes Carbon Corporation

Niagara Falls, N. Y. GLC Morganton, N. C.

Graphite Anodes, Electrodes and Specialties

Sales office: Niagara Falls, N. Y. **Other offices:** New York, N. Y., Chicago, Ill., Pittsburgh, P

Sales Agents: J. B. Hayes, Birmingham, Ala., George O'Hara, Long Beach, Cal., Great Northern Carbon & Chemical Co. Ltd., Montreal, Can

EDITORIAL STAFF

R. M. Burns, *Chairman*
Norman Hackerman, *Technical Editor*
Ruth G. Sterns, *Managing Editor*
Cecil V. King, *Associate Editor*
U. B. Thomas, *News Editor*
Mary F. Murray, *Assistant Editor*

DIVISIONAL EDITORS

J. V. Petrocelli, *Corrosion*
Abner Brenner, *Electrodeposition*
W. C. Vosburgh, *Battery*
H. C. Froelich, *Electronics*
W. C. Gardiner, *Industrial Electrolytic*
S. J. Sindeband, *Electrothermic*
John J. Chapman, *Electric Insulation*
L. B. Rogers, *Theoretical*
Sherlock Swann, Jr., *Electro-Organic*

REGIONAL EDITORS

Joseph Schulein, *Pacific Northwest*
J. C. Schumacher, *Los Angeles*
O. W. Storey, *Chicago*
G. W. Heise, *Cleveland*
Paul S. Brallier, *Niagara Falls*
Oliver Osborn, *Houston*
Earl A. Gulbransen, *Pittsburgh*
A. C. Holm, *Canada*
J. W. Cuthbertson, *Great Britain*
T. L. Rama Char, *India*

ADVERTISING OFFICE

Jack Bain
Advertising Manager
545 Fifth Avenue
New York 17, N. Y.
Phone—*Murray Hill 2-3345*

Journal of the
Electrochemical Society

AUGUST, 1953 VOL. 100 · NO. 8

CONTENTS

Editorial

"Gypping" the Gullible 209C

Regional Feature

The Milwaukee-Chicago-Gary Industrial Area. *O. W. Storey* .. 211C

Technical Papers

Corrosion of Steel by Air-Free, Dilute, Weak Acids. *Norman Hackerman and E. E. Glenn, Jr.* 339
The Kinetics of the Initial Corrosion of Copper in Aqueous Solutions. *George Richard Hill* 345
The Manufacture, Properties, and Uses of Polyvinyl Formal. *Andrew F. Fitzhugh, Edward Lavin, and George O. Morrison* 351
The Chemistry of Traps in Zinc Sulfide Phosphors. *W. Hoogenstraaten* 356
Some Properties of Zinc Sulfide Activated with Copper and Cobalt. *W. Hoogenstraaten and H. A. Klasens* 366
Anodic Formation of Coatings on Magnesium, Zinc, and Cadmium. *Kurt Huber* 376

Feature Section

Mechanism of Electropolishing of Copper in Phosphoric Acid Solutions, II. The Mechanism of Smoothing. *J. Edwards* 223C
Society Progress and Comment on a National Problem (Presidential Address). *J. C. Warner* 231C

Current Affairs

Palladium Medal Award to Furman 233C
Further Details on Fall Meeting at Wrightsville Beach 234C

News Notes	235C	Book Reviews	237C
Section News	236C	New Products	239C
Personals	236C	Recent Patents	240C
New Members	237C	Employment Situations	242C

Published monthly by The Electrochemical Society, Inc., Mount Royal and Guilford Aves., Baltimore 2, Md., combining the JOURNAL and TRANSACTIONS OF THE ELECTROCHEMICAL SOCIETY. Editorial offices: 216 West 102nd Street, New York 25, N. Y. Statements and opinions given in articles and papers in the JOURNAL OF THE ELECTROCHEMICAL SOCIETY are those of the contributors, and The Electrochemical Society assumes no responsibility for them. Subscription $11.25 to members, $15.00 to nonmembers. Single copies $1.25 to members, $1.50 to nonmembers. Copyright 1953 by The Electrochemical Society, Inc. Entered as second-class matter November 15, 1947, at the Post Office at Baltimore, Md., under the act of August 24, 1912.

Model 622—Ultra-Sensitive Instruments

Portable d-c and a-c thermo instruments for precision measurement of potentials and minute currents in electronics or laboratory research.

Model 901
Portable Test Instruments

Available in d-c, Model 901—and a-c, Model 904, single and multiple ranges of wide coverage. Excellent scale readability and shielding. Accuracy within ½ of 1%.

A-C Clamp Volt-Ammeter

(Model 633, Type VA-1) For convenient and rapid measurement of a-c voltage and current without breaking the circuit. Jaws take insulated or non-insulated conductors up to 2" diameter. Safe, rugged, versatile. Also available as a-c clamp ammeter, without voltage ranges.

Specialized and Multi-purpose

INSTRUMENTS

for

- **RESEARCH**
- **PRODUCTION**
- **MAINTENANCE**

For complex, or just routine measurement jobs, these and other specialized WESTON Instruments save time and assure dependable measurements. For information on the complete line, see your local Weston representative, or write . . . WESTON Electrical Instrument Corp., 614 Frelinghuysen Ave., Newark 5, N. J.

WESTON
Instruments

Sensitive Relays

A line of sensitive relays including the Model 705 which provides positive operation at levels as low as ½ microampere. Non-chattering magnetic contacts handle up to 10 watts at 120 volts.

Panel and Switchboard Instruments

A complete line of instruments in all types, sizes and ranges required for switchboard and panel needs . . . including d-c, a-c power frequencies and radio frequency, rectifier types and D.B. meters.

Model 697 Volt-Ohm-Milliammeter

One of a line of pocket-size meters, Model 697 combines a selection of a-c and d-c current, and resistance ranges. Ideal for maintenance testing and many inspection requirements.

Model 1411 Inductronic D-C Amplifier

Stable amplifier provides high degree of resolution even at fractional loads. Reaches steady full scale deflection in a fraction of a second. Interchangeable plug-in range standards for either microamperes or millivolts.

Industrial Circuit Tester—Model 785

A multi-range, multi-purpose, ultra-sensitive analyzer, for laboratory and industrial checking of electrical and electronic circuits. Has 28 practical scale ranges; measures d-c and a-c voltage, d-c and a-c current, and resistance. Accessories available to extend ranges. Compact and portable; furnished in either oak or steel case.

Model 686
Electronic Tube Analyzer

Tests tubes under exact operating potentials. Accurately determines true mutual conductance of all tubes, in accordance with manufacturers' rated operating conditions, or under special operating conditions.

High Frequency Electronic Analyzer
Model 769

A three-in-one instrument providing a self-contained Volt-Ohm-Milliammeter, a high impedance electronic D-C Volt-Ohmmeter, and a probe type Vacuum Tube Voltmeter for use to 300 megacycles. Exceptionally stable and accurate. Has specially designed extremely small RF and D-C probes.

Corrosion of Steel by Air-Free, Dilute, Weak Acids[1]

NORMAN HACKERMAN AND E. E. GLENN, JR.[2]

Department of Chemistry, The University of Texas, Austin, Texas

ABSTRACT

The corrosion of mild steel by a spray of dilute acetic acid solutions in an air-free CO_2 atmosphere was studied. With less than 500 ppm acetic acid, the corrosion rate of steel varied inversely with acid concentration at constant partial pressure of CO_2. Using 500 to 1000 ppm acetic acid, the corrosion rate was low, following initial rapid attack, and independent of the partial pressure of CO_2. The corrosion rate was independent of CO_2 pressure at 1 atm or below for all acid concentrations used, except the lowest, 50 ppm. At 1.5 atm CO_2, a substantial rate increase was observed at all acid concentrations. The corrosion product formed in the presence of CO_2 was largely iron(II) carbonate. This carbonate film offered some protection to the metal surface until it became thick enough to part because of internal stresses.

It is postulated that higher acid concentrations led to the lowest continuing corrosion rate because fine particles precipitated during the rapid initial attack, and the resulting film on the metal was relatively less permeable to the corrosive fluids. At lower acid concentrations, the precipitate was coarser and the resulting film was more porous, leaving considerable metal surface exposed to the corrosive medium. Experiments to support this view are described.

INTRODUCTION

This study grew out of investigations of corrosion in natural gas condensate wells. In spite of a total lack of oxygen in these wells, steel surfaces, as well as numerous alloys, were frequently quite badly attacked by the corrosive components of the fluid stream: water, carbon dioxide, and the lower fatty acids (1, 2). It was decided to study the kinetics of the reaction between steel and the materials named above without the complicating influence of a non-aqueous phase and under controlled conditions wherein only the concentration of the acidic constituents varied.

EXPERIMENTAL

The reaction was made to take place between a thin liquid film and the metal coupons to which it adhered. The liquid film was replenished by a spray drawn from a reservoir into which liquid dripped from the coupons. The apparatus is shown schematically in Fig. 1.

The reaction chamber was a five-cm diameter glass pipe cross, and the reservoir a four-liter glass container. The gas and liquid were circulated in the system by a pump in which the corrosive fluid did not come in contact with any metal parts (3). Auxiliary equipment such as a Bakelite coupon holder, sight-feed bubbler, manometer, spray nozzle, and the like are all indicated in the diagram. All connections were made with plastic tubing to insure a tight but flexible system with little susceptibility to breakage.

The gaseous atmosphere, nitrogen, carbon dioxide, or a mixture of both, flowed from a cylinder over heated copper to remove oxygen, through the system, and to the atmosphere. The pressure, in any case, was never less than 2.0 cm Hg above that of the atmosphere, and the gas went to the atmosphere through a mercury bubbler. Some of the flowing gas was utilized to help bring liquid from the reservoir to the spray nozzle by making use of the gas-lift principle. The compressed gas from the larger tube of the spray nozzle met the liquid falling from the smaller tip and produced a fine spray which fell parallel to the major coupon faces. The spray spread so that all seven coupons in the holder were wet uniformly and continuously. The gas was saturated by passing it through water (this also served as a sight-feed bubbler). C. P. acetic acid, tank nitrogen, and high purity tank CO_2 were used. The coupons were cut from a sheet of SAE 1020 steel to the dimensions 1.9 x 3.17 x 0.16 cm. On one corner, a small extension was left to fit into the holes of the Bakelite holder.

Procedure

The coupons were abraded on a polishing wheel with No. 2 emery paper, dropped into acetone, rinsed twice in fresh acetone to remove adhering solids, and left under acetone until weighed. Coupons were kept as free of moisture as possible until placed in the reaction chamber.

After weighing to 0.1 mg, they were placed in the

[1] Manuscript received October 8, 1952. This paper was prepared for delivery before the Montreal Meeting, October 26 to 30, 1952.

[2] Present address: Magnolia Petroleum Company, Field Research Laboratories, Dallas, Texas.

reaction chamber. The system was evacuated with a water aspirator and then flushed three times with the gas to be used to remove all air. Then the gas flow was regulated to a rate (usually 10 cc per minute) adequate to maintain the desired pressure inside the system. The pump was then started and adjustments made to obtain a satisfactory spray over the coupons.

Coupons were removed from the coupon holder through a 2.5-cm ID Pyrex glass pipe fitting, closed by a tight-fitting rubber stopper. To keep air out of the system, the pump was stopped, the gas flow rate was increased to 500 cc per minute, and the rubber stopper was replaced by one carrying a mechanical finger. Each coupon was removed by the remotely operated mechanical finger and the original stopper was then replaced. The high gas flow rate prevented

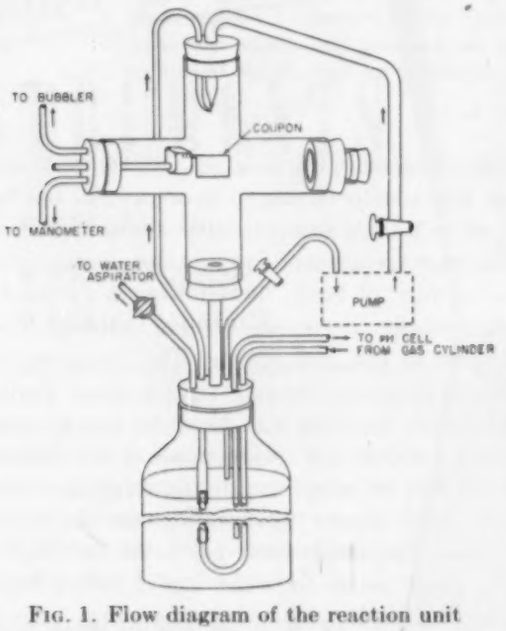

FIG. 1. Flow diagram of the reaction unit

air in-leakage.[3] The gas flow was maintained at the high rate for about five minutes after the system was again closed.

The extracted coupon was placed in acetone for a short time, removed, and dried thoroughly by evaporation. It was then scrubbed with a bristle brush and pumice soap to remove the scale, and finally dried and weighed. In some experiments the coupon was weighed with the scale in place to give the "as-removed" weight.

During the first day of each run, the *p*H of the reservoir liquid, generally between 4 and 5, increased by 0.1 to 0.3 unit, but remained constant thereafter. With the large volume of solution used, depletion was negligible.

[3] A trace of air in the system produced red rust on the coupons, and therefore acted as an efficient indicator of air in-leakage.

Duplicate runs were made in all cases, and least square plots showed that corresponding data agreed to better than 10 per cent.

RESULTS

Experiments were carried out in N_2 at 1 atm, in 0.25 atm CO_2 plus 0.75 atm N_2, in 1 atm CO_2, and in 1.5 atm CO_2. For each of these, the acetic acid concentration was varied from 0 to 1000 ppm (0 to 0.017*M*). Other possible variables, such as solid surface to fluid volume ratio, pump speed, flow rate, and metal, were held constant. All runs were made at 30° ± 2°C, and lasted either 7 or 14 days.

The data obtained in these experiments are plotted in Fig. 2 through 5. In the absence of CO_2, the metal loss generally increased with acid concentration except that maximum total loss was obtained with 200 ppm acid (Fig. 2). At all three partial pressures of CO_2, the total metal loss as well as the rates after a short initial time were lowest in the most concen-

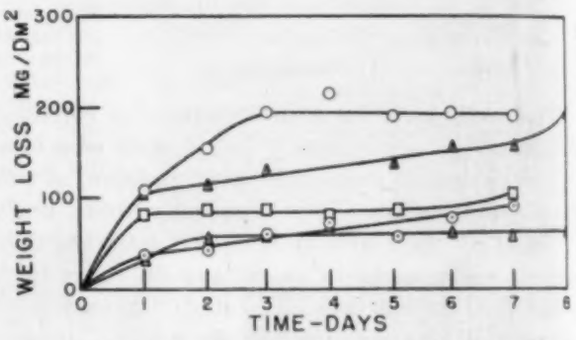

FIG. 2. Partial pressure of N_2—1.0 atm. Acetic acid concentrations: ⊙ = 0; △ = 50; ○ = 200; □ = 500; ▲ = 1000 ppm.

trated solutions. Also the rate went through a maximum, with acid concentration for each pressure as shown by the slopes of the curves of Fig. 3, 4, and 5. With 0.25 atm CO_2, it occurred between 100 and 200 ppm acetic acid; with 1.0 atm CO_2, between 50 and 100 ppm; and with 1.5 atm CO_2, at about 50 ppm.

The rate curves of the experiments with CO_2 at 0.25 and at 1 atm were quite similar, but weight losses with 1.5 atm CO_2 were generally about twice as great. With all three CO_2 pressures, the 500, 750, and 1000 ppm acetic acid experiments gave very similar results. In each case, there is a marked change in slope at 1 day, and, in 1.5 atm, a second change is evident (Fig. 5).

The solid reaction product was identified (4) without removing it from the coupon by use of an x-ray spectrometer.[4] Iron(II) carbonate was found in all cases where CO_2 was employed. Samples of scale were scraped off and electron diffraction studies made. The crystallites were apparently very small

[4] North American Philips unit.

since measurable patterns could not be obtained. The product of the CO_2-free system gave a pattern which could not be identified, but was probably a basic iron acetate.

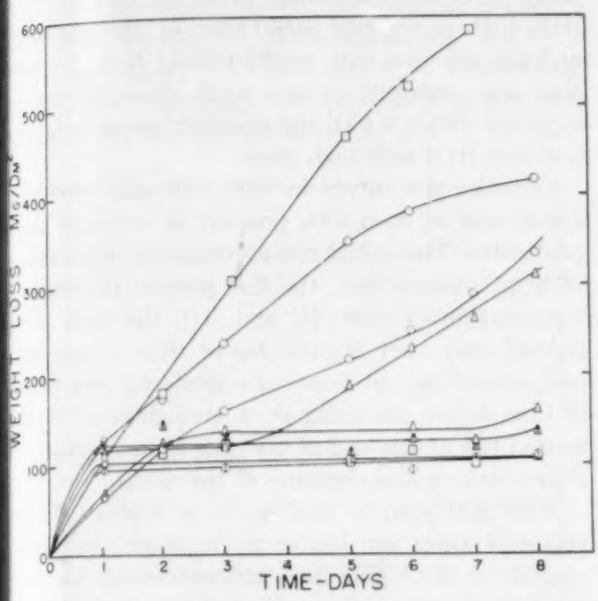

FIG. 3. Partial pressure of CO_2—0.25 atm; partial pressure of N_2—0.75 atm. Acetic acid concentrations: ⊙ = 0; △ = 50; ⊡ = 100; ○ = 200; △ = 300; □ = 500; ⊕ = 750; ◬ = 1000 ppm.

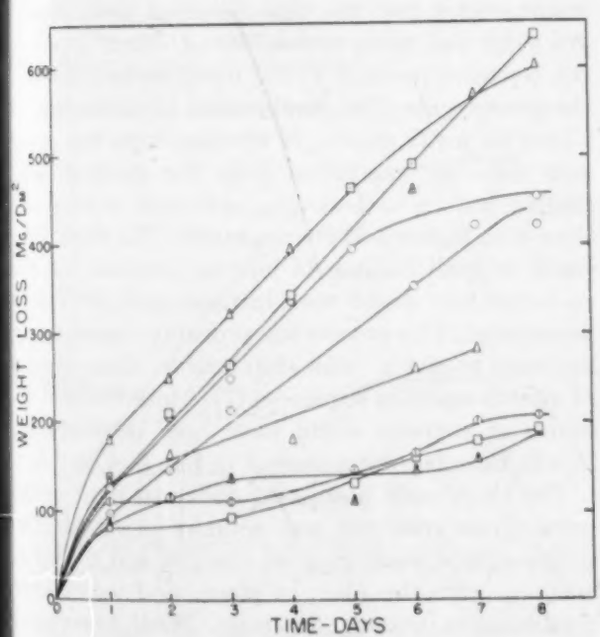

FIG. 4. Partial pressure of CO_2—1.0 atm. Acetic acid concentrations same as for Fig. 3.

The scale formed at highest CO_2 pressures was more adherent than that in the other cases. There was no evidence of pitting except at the highest CO_2 pressure where appreciable pitting occurred. Shock (5) also has observed pitting in similar systems only at CO_2 pressures above 1 atm.

Some experiments were carried out at 1.0 atm CO_2 with either 50, 500, or 1000 ppm acetic acid plus 1000 ppm NaCl (Fig. 6). The rate was unaffected for the most concentrated acid system, but increased in the other two systems.

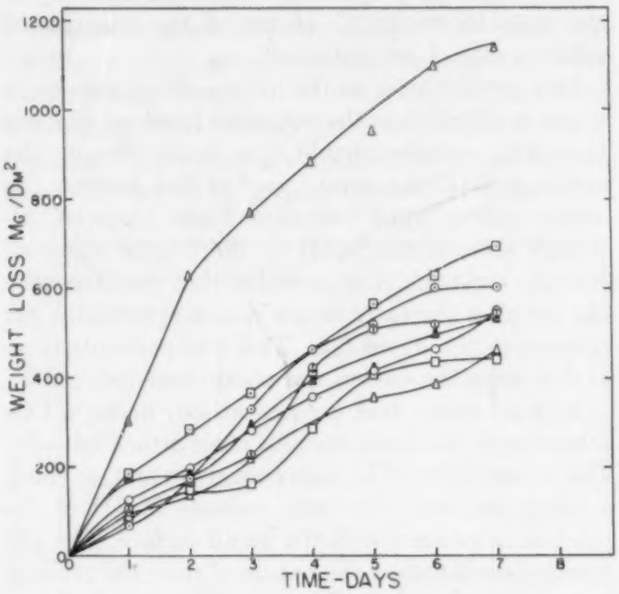

FIG. 5. Partial pressure of CO_2—1.5 atm. Acetic acid concentrations same as for Fig. 3.

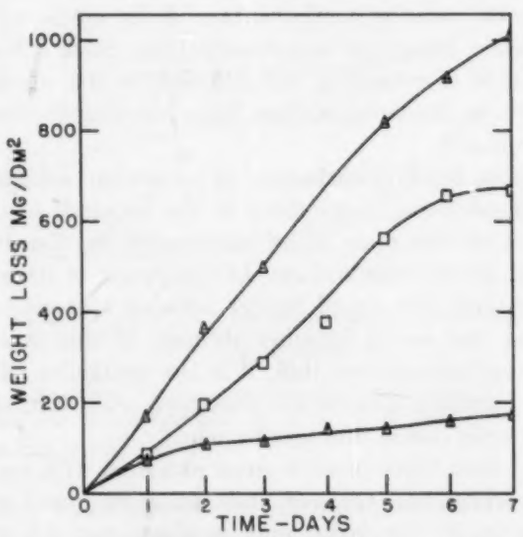

FIG. 6. Partial pressure of CO_2—1.0 atm. NaCl concentration—1000 ppm. Acetic acid concentrations: △ = 50; □ = 500; ◬ = 1000 ppm.

DISCUSSION

Aside from temperature, composition of the system, and nature of the metal surface, the kinetics of this reaction is a function of the history of the reaction and of the nature of the solid reaction product formed. It appears that the manner in which the solid product is formed on the metal eventually controls the course of the reaction. Under the conditions

of these experiments, a steady state is approached which depends on the following competitions in the reaction system: (*a*) rate of scale thickening vs. rate of scale dissolution; (*b*) change in acid concentration in the liquid film on the metal surface vs. change in scale thickness; (*c*) scale thickness vs. tendency of the scale to crack; (*d*) nature of the precipitated solid vs. rate of precipitation.

In a system such as this only a small volume of liquid is effective as the corrosive phase at any one time, i.e., a replenishable thin liquid film on the metal surface. As spray reaches the coupon, an approximately equal volume of liquid drops off. Although some of the liquid on the coupon was continually replaced, it is probable that reaction with the metal in the early stages causes appreciable *p*H changes in the liquid film. This was particularly so at first since the system was poorly buffered.

At high acetic acid concentrations, under a CO_2 atmosphere, the metal sustains rapid attack initially. The initial rate may be high enough, in fact, to cause a rapid and relatively large increase in *p*H of the solution in contact with the metal surface. The *p*H increase should affect the nature of the solid product formed, i.e., the iron(II) carbonate produced should come out of solution as very small particles because of rapid precipitation (6). Fine particles are capable of close packing on the surface of the metal, giving a dense, relatively impermeable film. Such a film is capable of retarding the diffusion of the corrosive fluids to the metal surface, thus lowering the corrosion rate.[5]

Since iron(II) carbonate is somewhat soluble in acid solutions, particularly in the presence of CO_2, some of the scale must continually be dissolving from the exterior surface. As dissolution of the scale continues, the actual barrier between corrosive medium and metal becomes thinner. If this type of barrier becomes too thin, it is less protective. Thus the corrosion process involves both scale formation and scale dissolution simultaneously.

At least three possible situations exist with regard to competition between dissolution rate and scale growth: [I] the latter may predominate; [II] they may be equal; [III] the former may predominate. With [I], gradual thickening of the scale would occur until internal stresses caused cracking, whereupon new metal surface would be exposed to the corrosive medium and the reaction rate should increase markedly. With [II], the reaction rate should be essentially constant after some scale has formed. With [III], little or no scale would form to offer protection and the reaction rate would remain high. No such case was apparent in this work. Case [I] may be expected with low CO_2 and acetic acid concentrations and case [III] with high ones.

Consider the curves for 500, 750, and 1000 ppm acetic acid at each CO_2 pressure in terms of these postulates. The initial rise corresponds to formation of a fine, dense film; the flat portion illustrates a combination of cases [I] and [II], the scale being formed only very slightly faster than it dissolved, and, accordingly, it required a relatively long period of time before becoming thick enough to crack; the second rise at the end of the runs is then caused by scale cracking and exposure of the metal.

With 200 ppm or less acetic acid plus CO_2, the corrosion rates are higher throughout[6] than those caused by the higher acid concentrations. In these solutions the precipitate is probably formed more slowly because of a lower initial reaction rate. Such a precipitate should be coarser and more likely to form a more permeable film. Since the acid concentrations were low, the film dissolved more slowly, yet there was more probability of direct access of the corrosive medium to the metal surface through the porous scale. This combination of circumstances allows for faster growth of the film from the metal side than for dissolution from the solution side, thereby leading to thick films in a much shorter time than with higher acid concentration. The thick films crack or spall because of internal stresses and the corrosion rate should then increase until the cracks are covered. This process was probably repeated over and over to give a "stair-step" curve, characteristic of growth-cracking sequences (7). More frequent removal of coupons would have been necessary for this to have become apparent in Fig. 3, 4, and 5.

The thick scale postulated above to form in the more dilute solutions was actually observed. The coupons were weighed, after removal and drying in acetone, with the scale in place, and again after scrubbing to remove the scale. With lower acid concentrations, the average total scale weight was about 3 mg. With higher concentrations, it averaged about 1 mg. For the former, the amount of scale was relatively constant for each experiment but with the latter it fluctuated from 0.2 mg to 1.7 mg in any given run. It is interesting that in the second case more scale was found on coupons removed at

[5] The rate might be controlled by ionic movement through the crystal lattice. Then the large number of boundaries the ions must cross in a scale composed of a fine precipitate should impede this movement. However, this neglects the possibility of an equal or greater rate of diffusion via grain boundaries. It suggests that fine grain scale would be more retarding if it exhibited no ionic conduction, or, conversely, that with ionically conducting scale coarser grains are more favorable to slower corrosion rates. Subsequent work in this laboratory with solid $FeCO_3$ indicates that it does not conduct ionically at all.

[6] In one or two cases the difference in initial slopes cannot be distinguished.

times when the corrosion rate showed an increase, and less scale was formed on coupons removed during the periods of the flatter portion of the rate curves. These observations lend credence to the idea that when the scale thickens sufficiently, it cracks and permits an increase in corrosion rate.

The rate in 50 ppm acid and 0.25 atm CO_2 is much lower than might be predicted, unless one considers the low partial pressure of CO_2 present.

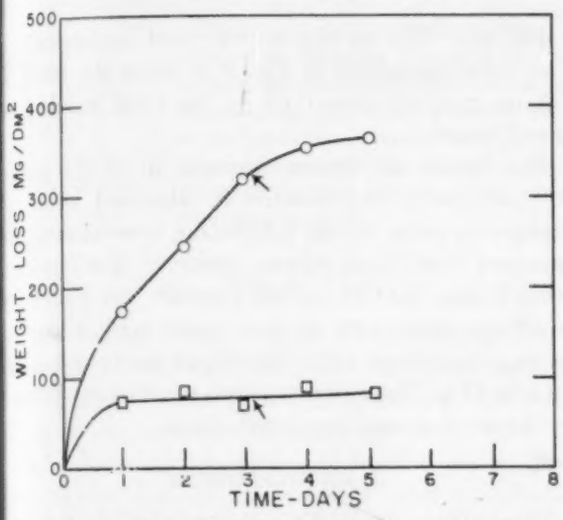

FIG. 7. Partial pressure of CO_2—10.0 atm. Acetic acid concentrations: ○ 50 changed to 1000 ppm; □ 1000 changed to 50 ppm at end of 3 days (arrows show data taken just *before* change in acid concentration).

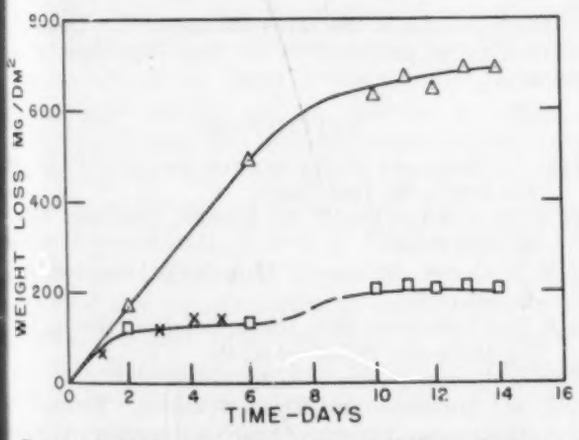

FIG. 8. Partial pressure of CO_2—1.0 atm. Acetic acid concentrations: △ = 50; □ = 1000; × = data from Fig. 4.

Even though the particle size of the precipitate should be fairly large, the small amount of CO_2 and acetic acid present probably permitted the film to grow more slowly and perhaps pack somewhat more closely, resulting in a more protective film than in the other cases.

In the absence of CO_2, the metal loss after 2 to 3 days was greater at higher acid concentration, except that the greatest loss occurred in 200 ppm acid (Fig. 2). The maximum suggests that again more rapid precipitation occurs, as described above, in the more acidic systems. The film apparently cracked near the end of the 1000 ppm run, giving rise to an increase in the corrosion rate.

Tests of the Postulated Mechanism

Several experiments were designed to check the validity of the proposed corrosion mechanism. If the coupons were permitted to drain dry in the closed system, increased internal stresses should accentuate cracking of the carbonate scale. On re-exposure, rate of attack should be greater because of greater exposure of bare metal to the corrosive medium. During the course of experiments using 50 and 1000 ppm acetic acid with 1 atm of CO_2, the pump was shut off after 1 day and the coupons permitted to drain in the air-free atmosphere until the coupons appeared to be completely dry (about 5 hours). After resumption of the experiment, the rate of attack increased greatly. The very high rates of attack observed show that further exposure did not heat the cracks; or, that in the process of healing, the scale on each set of coupons thickened to such an extent that it continued to crack.

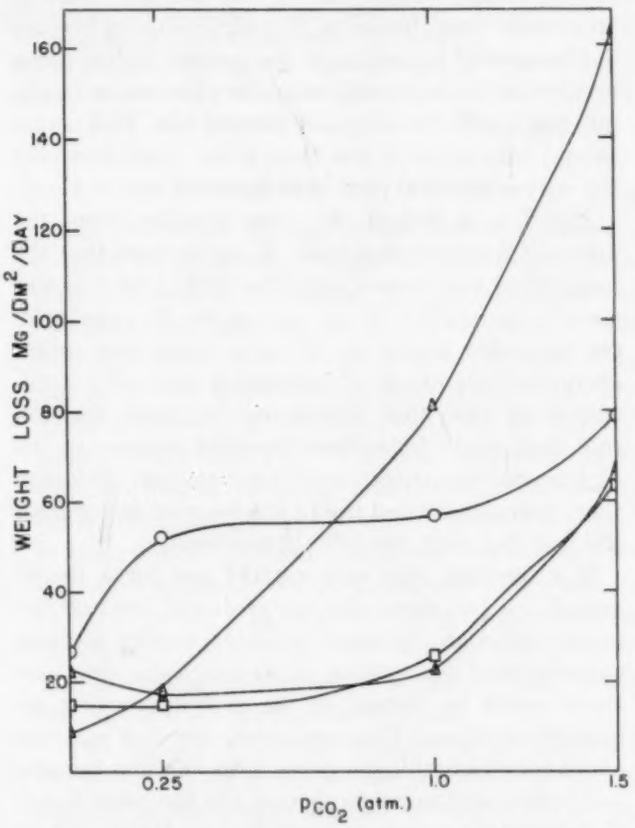

FIG. 9. Effect of p_{CO_2} on corrosion rate after 7 days. Acetic acid concentrations: △ = 50; ○ = 200; □ = 500; ⚠ = 1000 ppm.

In another experiment, the acid concentration at fixed CO_2 pressure was changed during the run. If a

fine, dense, impervious film does form on the metal with 1000 ppm acetic acid and 1 atm CO_2, there should be little change in slope of the rate curve if the acid concentration were decreased quickly to 50 ppm. This is so because the lower acid concentration dissolves the scale less readily, and the film should be equally impervious to either solution. On the other hand, for the reverse experiment the rate curve should level off rather rapidly—although perhaps after a sharp initial rise. This is because the precipitate formed originally is coarse and relatively permeable. Therefore, contact with the more concentrated acid should cause a rate increase initially. In a short time, however, the curve should become flat because of formation of the postulated fine dense precipitate which would be quite effective in blocking openings in the originally formed film. This action should take place in less than a day since normally the curves for 1000 ppm acid flattened out in a day.

Fig. 7 is a plot of the data obtained from the "mixed" concentration runs. It can be seen that the predictions were borne out. The 1000 ppm run was essentially unaffected by change to 50 ppm acid. On the other hand, the 50 ppm curve was rather abruptly flattened by the change of the acid concentration to 1000 ppm. The sharp rise in the reaction rate that might have been expected because of the higher acid concentration was not noticed, although there was a continued rise in the reaction rate during the first day with the 1000 ppm solution.

If a 50 ppm run were carried out for a longer period, e.g., 14 days, the curve should level off because, although the scale consisted mainly of large particles and was porous in nature, some fine particles would be formed as the growth-cracking sequence continued. These relatively few fine particles could eventually fill the pores until the film became less porous and more protective. On the other hand, if a 1000 ppm run were extended over a longer period, the protective film would thicken sufficiently to crack, permitting access of the corrosive medium to the metal surface, and thus causing an increase in the rate of attack until the cracks healed. The curves obtained for experiments such as these are shown in Fig. 8 and bear out the predictions.

Effect of NaCl *Addition*

The presence of NaCl in solutions containing between 50 and 500 ppm acetic acid increased the corrosion rate considerably, but in 1000 ppm acid the rate was essentially unchanged (Fig. 6). An increase in corrosion rate is to be expected because of improved solution conductivity which permits the cooperation of more distant anode and cathode areas (8). If, as is postulated, the 1000 ppm solution provides a less permeable scale, the increase in conductivity of the solution would be of little consequence.

Effect of CO_2

The rate data at the several acid concentrations have been regrouped in Fig. 9 to show the effect of CO_2 on integral rates (i.e., ½ the total weight loss after 7 days).

The curves are drawn through all of the points but no special significance is attached to small changes in slope. Some interesting observations are apparent from these curves, however. For instance, below 1 atm, the CO_2 partial pressure had essentially no effect except with 50 ppm acetic acid. A marked increase did occur with the others between 1.0 and 1.5 atm CO_2. These observations are also explainable by the mechanisms suggested above.

Acknowledgment

The authors gratefully acknowledge the support, both financial and otherwise, given to this work by the Natural Gasoline Association of America Corrosion Project Research Committee.

Any discussion of this paper will appear in a Discussion Section, to be published in the June 1954 issue of the Journal.

References

1. D. A. Shock and N. Hackerman, *Ind. Eng. Chem.*, **39**, 863 (1947); **39**, 1283 (1947).
2. N. Hackerman and H. R. Schmidt, *Ind. Eng. Chem.*, **41**, 1721 (1949).
3. E. E. Glenn, Jr. and N. Hackerman, *Rev. Sci. Instr.*, **21**, 148 (1950).
4. X-Ray Diffraction Data Cards, American Society Testing Materials, Philadelphia, Pa.
5. D. A. Shock, private communication.
6. I. M. Kolthoff and E. B. Sandell, "Textbook of Quantitative Inorganic Analysis," revised ed., p. 99, The Macmillan Company, New York (1943).
7. U. R. Evans, "Metallic Corrosion, Passivity, and Protection," p. 148, Edward Arnold and Company, London (1946).
8. H. H. Uhlig, "The Corrosion Handbook," (H. H. Uhlig, Editor), p. 130, John Wiley and Sons, Inc., New York (1948).

The Kinetics of the Initial Corrosion of Copper in Aqueous Solutions[1]

GEORGE RICHARD HILL

Fuel Technology Department, University of Utah, Salt Lake City, Utah

ABSTRACT

In order to determine the mechanism and rate of corrosion of copper in aqueous solution before diffusion through a film of products becomes rate-determining, a system involving an electroreduction cell coupled to a recording electronic voltmeter has been constructed that makes possible the determination of the thickness of very thin films of corrosion products on the copper surface. These data are used to determine the rate laws regulating the corrosion of the metal and to evaluate the specific rate constant for the initial corrosion process. A mechanism and rate law are proposed for the initial corrosion process.

INTRODUCTION

Theoretical treatments have been proposed to account for corrosion rates under conditions such that diffusion of electrons, ions, or atoms through surface films is the rate-determining step (1–5). Few data are available on the corrosion for the period during which this film of oxide forms, and no complete theory has been developed to account for the rapid initial rate.

Experimental and theoretical work has also been done on corrosion in which diffusion of ions to or from the metal surface through a concentration gradient in the aqueous solution determines the rate of the reaction (6–9). Data obtained under these conditions give, for the rate of corrosion of copper in sulfuric acid solutions saturated with oxygen, values of 40 mg/dm²/day (10) and 0.020 cm/year (11). (This is approximately 50 mg/dm²/day.) Corrosion rates obtained in 0.1*N* and 1*N* NaCl saturated with oxygen are 1.25 and 11.3 mg/dm²/day (12).

Initial rate measurements at one temperature by Brown, Roetheli, and Forrest (13), who measured the rate of disappearance of oxygen as it corroded copper in water solution, gave a value of 0.0054 ml of oxygen consumed/dm²/min/average ml of oxygen per liter of solution. This corresponds to about 2500 mg of copper/dm²/day,[2] as Cu(I). The experiments carried out in this laboratory using a completely different technique indicate that this value represents the rate of corrosion before diffusion through a film of products becomes rate-determining.

[1] Manuscript received February 27, 1951. This paper was prepared for delivery before the Buffalo Meeting, October 11 to 14, 1950.

[2] The rate of corrosion of 2500 mg of copper/dm²/day is obtained by assuming an average concentration of oxygen in the solution of 28 ml O_2/liter.

EXPERIMENTAL PROCEDURE

The procedure followed in the current research is to allow an oxide-free, cleaned sample of electrolytic copper to corrode in a stirred, thermostatted solution of known *p*H, ionic strength, and constant oxygen concentration for a measured time interval. The sample is then transferred rapidly to an oxygen-free solution where it is made one electrode of two electrical circuits (see Fig. 1). In the reduction circuit the thin film of corrosion products is reduced at a constant current. Two platinum wires serve as anodes in this circuit—to obtain fairly uniform current distribution on both sides of the sample. They are enclosed in glass tubing, open at the bottom to prevent diffusion of oxygen or chlorine into the solution. The current is maintained at a constant 0.92 ± 0.01 ma during the reduction in each run.

The measuring circuit consists of an electronic voltmeter which measures the potential of the cell formed by the copper and its corrosion film as one electrode against a silver-silver chloride electrode. During the reduction process, the potential read on the electronic voltmeter remains fairly constant while a particular compound on the surface is being reduced. The potential changes rapidly following complete reduction of that compound until a value is reached at which another compound on the surface is reduced or until the potential at which water will be reduced is attained. A plot of observed voltages vs. time gives one or more "plateaus" from which the thickness of each corrosion film can be determined (14). During the latter part of the work the potential vs. reduction-time curves were plotted directly, using a Speedomax Type G, 0 to 10 mv recorder coupled to the voltmeter in the measuring circuit.

In using the apparatus for film thickness deter-

minations, one must have in the cell a solution of electrolyte (1*N* KCl) boiled and aspirated absolutely free from oxygen. Oxygen is excluded from the system during the complete electroreduction period by the continuous introduction of nitrogen which has been passed over heated copper turnings.

Experimental Results

The initial samples were cleaned by conventional "abrasion" techniques. It was found that various compounds remained on the surface after such cleaning. Fig. 2 illustrates typical electroreduction curves

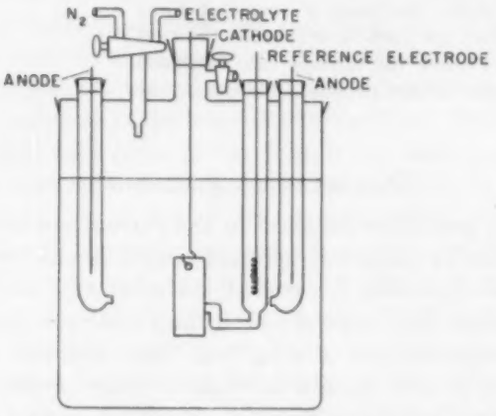

Fig. 1. Schematic diagram of cathodic reduction apparatus.

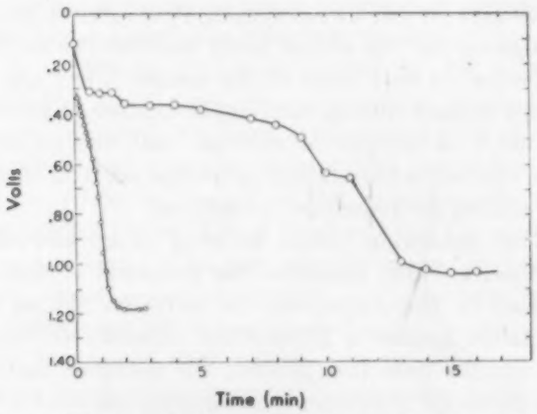

Fig. 2. Electroreduction of "abrasion" and "chemically" cleaned samples. ○, pure Cu cleaned by abrasion; ○, pure Cu cleaned with 10 per cent ammonium persulfate.

obtained on the same metal sample following cleaning by abrasion and following cleaning with 10 per cent ammonium persulfate solution. The electroreduction curve for the persulfate-cleaned sample is nearly identical with the curve for an electroreduced sample, there being no indication of any plateaus during the 80-sec period before hydrogen evolution. At least three "compounds" were present on the sample cleaned by abrasion as indicated by the plateaus and by the 12 min required before the hydrogen evolution potential was attained. It is to be noted that the emf at which hydrogen evolution occurs is a function of the nature of the surface present after the electroreduction has been completed. All samples used in the corrosion rate measurements were cleaned with ammonium persulfate.

The sample whose electroreduction curve is X in Fig. 3, was placed for 10 min in 1*N* KCl corrosion solution at *p*H 8.5 and at an oxygen pressure of 626 mm. Curve Z is the reduction blank for the same sample. The plateau of curve X represents reduction of a film of about 300 Å apparent thickness. The film thickness is calculated from the relationship,

$$T = \frac{\frac{it}{\mathbf{F}} \times \frac{M}{nD}}{a} \times 10^5,$$

where: T is film thickness in Å; i is reduction current in ma; t is the time in sec; **F** is the Faraday; M is

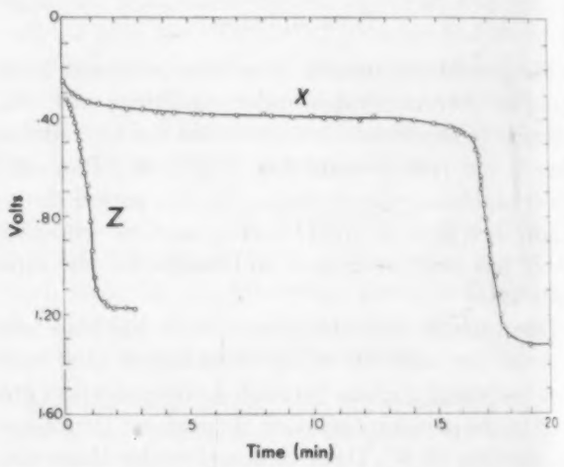

Fig. 3. Electroreduction of oxide-free and corroded samples. Z = Cu, cleaned with persulfate; × = same after 10 min corrosion; *p*H = 8.5; temp = 26°C; P_{O_2} = 626 mm; soln. *N* KCl.

the gram molecular weight of the compound composing the film; n is the number of Faradays required to reduce one gram molecular weight of the film; D is the film density; a is the apparent area of the metal in cm². The selection of the corrosion product undergoing reduction on the plateau makes a small difference in the value of M/nD and in the calculated film thickness. Values of M/nD for three probable corrosion products are 14.5 for cupric hydroxide, 12 for cuprous oxide, and 14.2 for atacamite, a basic copper chloride. Cuprous oxide was assumed to be the product on the surface of the metal in each case. The uncertainty due to this selection is less than the experimental error in runs of short duration.

It was found necessary to correct for the amount of corrosion occurring during the transfer of the samples to and from the corrosion solutions. Blank runs, before and after each experimental run, consisted of electroreduction plateau determinations for samples treated identically except for the period of suspen-

sion in the corrosion cell. The average blank thus determined was subtracted from the time of the corresponding plateau for the experimental run.

The amount of corrosion occurring in transferring the cleaned samples to the corrosion cell and back to the electroreduction cell was of the same order of magnitude as that produced in a 5-sec immersion in the corrosion cell solution. Corrosion run data for periods shorter than 5 sec were, therefore, not significant. From three to six runs were made at each

TABLE I. *Effect of corrosion time on film thickness*

Corrosion time	No. of samples	Avg plateau time	Film thickness, Å*
sec		*sec*	
5	4	53	3
10	3	146	7.6
20	3	238	12.5
30	3	360	18.8
40	4	405	21.2
50	6	480	25
60	5	500	26

* The real surface area of the samples is 5 times the apparent surface area. The surface area was determined, using a modification of the polarization technique suggested by Bowden and Rideal (15, 16). The calculated film thickness assumes uniform, complete coverage which probably is not the case.

TABLE II. *Effect of long corrosion time on film thickness*

Corrosion time	No. of samples	Avg plateau time	Film thickness, Å
min		*sec*	
2	3	580	39
5	3	1280	86
10	3	1820	121
20	2	2070	138
40	2	2450	164

TABLE III. *Effect of pH on film thickness*

*p*H	Corrosion time	No. of samples	Avg film thickness, Å
	min		
7.0	2	3	40
8.3	2	3	8

corrosion time and average values were used in the rate constant determinations.

Table I lists the plateau time and corrosion film thickness obtained for corrosion times of from 5 to 60 sec on samples of copper whose surface areas, as determined from the dimensions of the samples, were 44 cm². The pressure of oxygen in equilibrium with the system was 625 mm and the temperature was 25°C in each run. The *p*H was 7 in each run. The plateau times are considered reproducible within ±20 per cent.

The data for corrosion periods of from 2 to 40 min are shown in Table II. The samples for these runs were 33.3 cm² in apparent area, the true surface area being five times the apparent area. The other variables were the same as for Table I.

The corrosion rate was found to increase with hydrogen ion concentration between *p*H 8.3 and *p*H 7. In solutions more acid than *p*H 7, the corrosion product dissolved from the surface as it formed; in more basic solutions an impervious, self-quenching film formed. Since the addition of buffers changed the conditions on the metal surface (traces of impurities in the buffer would alter the reduction potential curves tremendously), it was necessary to use

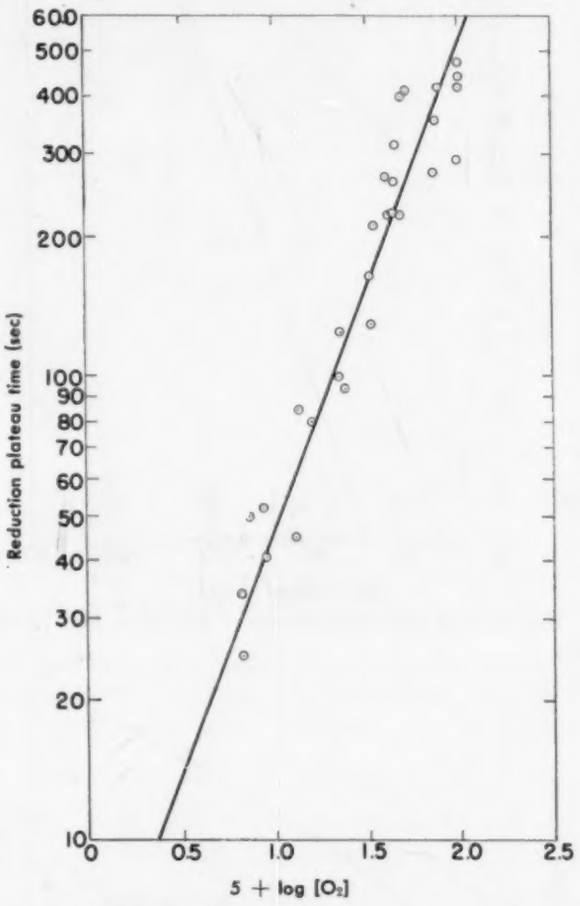

FIG. 4. Log corrosion vs. log oxygen concentration. Temp = 25°C; soln = 0.1*N* KCl; corrosion time = 60 sec.

unbuffered solutions in the narrow *p*H interval indicated to determine semi-quantitatively the hydrogen ion dependence. From the data of Table III the reaction is seen to be between one-half and first order with respect to hydrogen ion. The latter was assumed to be the true dependency.

The dependence of the initial corrosion process upon oxygen concentration was determined by making a series of runs at constant corrosion time with the partial pressure of oxygen maintained at values from 42 mm to 626 mm in individual runs. Fig. 4 is a plot of the log of the reduction plateau time vs. the log of the oxygen concentration for these runs.

The slope of the best line through the data is one, indicating first order dependence upon oxygen concentration for the slow step in the initial corrosion process.

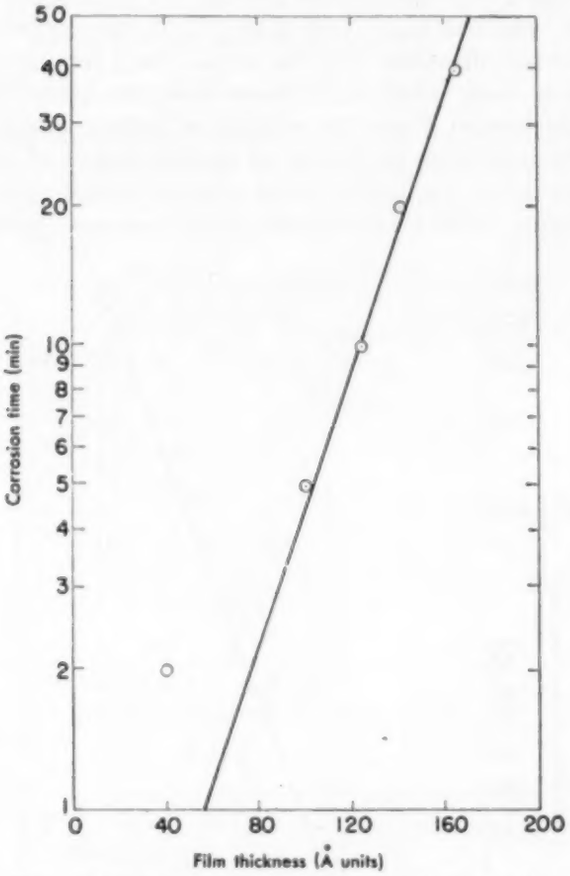

FIG. 5. Log time dependence of corrosion film formation.

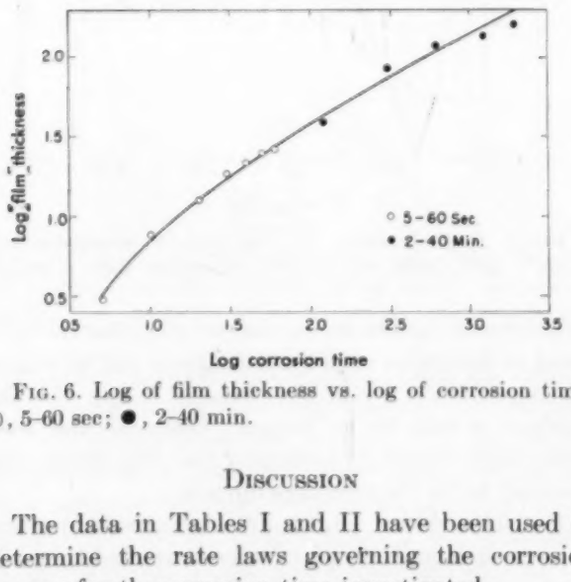

FIG. 6. Log of film thickness vs. log of corrosion time. ○, 5–60 sec; ●, 2–40 min.

DISCUSSION

The data in Tables I and II have been used to determine the rate laws governing the corrosion process for the corrosion time investigated.

Fig. 5 shows the reaction rate to be dependent upon the logarithm of the corrosion time for the period from 10 to 40 min (and presumably for longer corrosion times). Such time dependence suggests that the slow step in the reaction is dependent upon a process or surface, the nature of which is itself changing with time (17–19).

The data indicate that for corrosion time intervals between one and five minutes after the initial film formation, the parabolic rate law seems to be followed. Wagner (1) has developed the theory explaining this rate dependence. Wagner's model, which accounts very well for the parabolic rate dependence, assumes that diffusion through a film of corrosion products is the slow step in the reaction. Fig. 6, a plot of log film thickness vs. log of corrosion time, shows the transition from one rate-controlling step to the next to be smooth, which would be expected.

During the initial phases of the corrosion, i.e., for periods of corrosion less than 60 sec, such a film of products would be only partially formed. The following mechanism, which is consistent with the observed data, is proposed to account for the corrosion of copper during this initial period.

Assume the rate of corrosion to be proportional to the number of sites on which the initial process can occur. The number of available sites will decrease from an initial number, S_0, to $(S_0 - Cu_2O)$ at time, t. Cu_2O represents the amount of corrosion (number of occupied sites) at time, t. The rate expression for this condition (including the observed oxygen and hydrogen ion dependence) is,

$$\frac{d(Cu_2O)}{dt} = k_1(O_2)(H^+)(S)$$

$$= k_1(O_2)(H^+)(S_0 - Cu_2O).$$

Integrating, one obtains,

$$-\ln \frac{(S_0 - Cu_2O)}{S_0} = k_1(O_2)(H^+)(t - t_0)$$

provided the concentrations of oxygen and hydrogen ion remain constant during the corrosion process.

A logarithmic plot of $(S_0 - Cu_2O)$ vs. time is shown in Fig. 7. The value of S_0 which causes the points for 50- and 60-sec corrosion to fall on the straight line determined by the 5- to 40-sec corrosion runs is (in the units of the plot) 650 plateau sec. This corresponds to a surface layer of 35 Å. Physically this would mean that each copper atom or pair of atoms in the first ten layers, more or less, would be the site on which the initial phase of the corrosion could occur. After these atoms were converted to oxide, diffusion of copper ions through the oxide would become rate-determining and a parabolic rate law would be observed.

Based upon all of the experimental data and the

above considerations, the following reaction sequence is suggested for the corrosion process:

$$2Cu + O_2 + H^+ \xrightarrow{k_1} 2Cu^+ + HO_2^- \quad (I)$$

$$2Cu^+ + HO_2^- + 2Cu \rightarrow 2Cu_2O + H^+. \quad (II)$$

In step (I), the slow step in the reaction, an oxygen molecule occupies a site consisting of a pair of copper atoms, removing two electrons and becoming peroxide ion. A proton associates with this peroxide ion at the same time forming the biperoxide ion HO_2^-. A second, rapid step in the reaction involves the reduction of the biperoxide ion to two oxide ions, the electrons coming from an adjacent pair of copper atoms as indicated in equation (II). Each of the $O^=$ ions would associate with a pair of the Cu^+ ions (still in the surface) releasing the proton to the solution. The rate constant, k_1, determined from the data in Fig. 7 is 3×10^5 liter mole^{-1} atm^{-1} sec^{-1}.

It is possible that diffusion of the oxygen molecule to the site upon which it becomes HO_2^- is the slow step in the reaction. If this is the case, the treatment of the data would be like that proposed by King (6, 20). The observed initial rate could be obtained using a diffusion coefficient for oxygen of 1 cm^2/day and a diffusion layer thickness of 0.01 cm. Preliminary temperature coefficient measurements indicate a very small heat of activation for the process (about 1 kcal). This small activation energy would be expected if the process is under oxygen diffusion control. Since the solution was stirred by the oxygen as it bubbled in through a sintered Pyrex disk, it would be unusual if the diffusion layer increased in thickness with time, which is a necessary condition for diffusion control. It may have been achieved, however, during runs of very short duration. Additional experiments, in which the corroding copper sample is rotated at various speeds in the corrosion solution, and precise temperature coefficient measurements will help to confirm this observation and will enable a decision to be made between the two alternative slow steps.

Results in Presence of Acetate Ion

Some important conclusions were reached as a result of observations made on samples allowed to corrode in a solution containing 0.9N KCl and 0.1N $KC_2H_3O_2$, saturated with O_2. In this solution the acetate ion (or acetic acid present due to hydrolysis) adsorbed on the clean copper surface and prevented the formation of any film. The data obtained for a sample which remained 90 min in the solution are shown as curve V in Fig. 8. At a potential of −0.87 volt, a plateau occurred corresponding to the electroreduction of the adsorbed layer. The number of equivalents of electricity consumed during the reduction was 4.3×10^{-7}. This would mean that

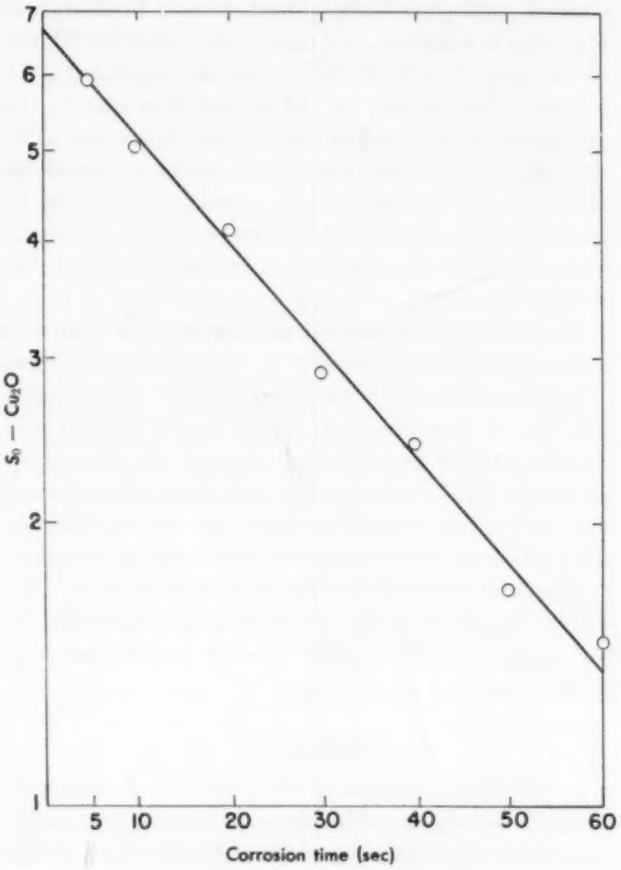

Fig. 7. Log corrosion sites vs. corrosion time. Temp = 25°C; P_{O_2} = 625 mm; S_0 = 650 plateau sec.

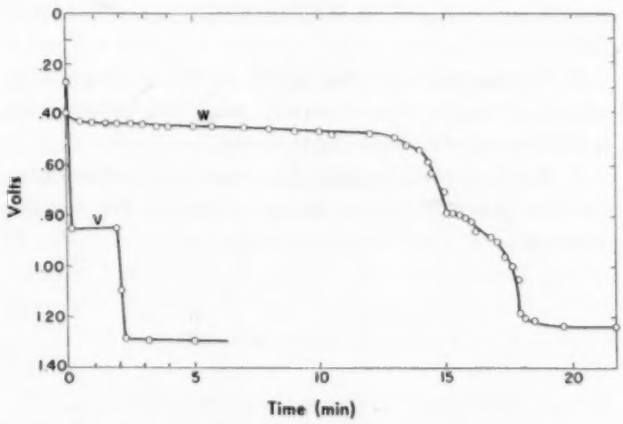

Fig. 8. Electroreduction of samples corroded in acetate solutions. V = Cu corroded in 0.1N KAc + 0.9N KCl for 90 min; W = Cu corroded in 0.1N KAc + 0.9N KCl for 1 min, then in N KCl for 90 min. Temp = 26°C; P_{O_2} = 625 mm.

2.6×10^{17} molecules or ions were adsorbed on an area of 2×10^{18} Å^2. This suggests that a double layer of acetic acid molecules adsorbed on the copper

surface was reduced to hydrogen and acetate ion, if the interpretation is correct.

The sample represented by curve W in Fig. 8 was cleaned with persulfate, rinsed, placed for 1 min in the acetate solution, and then transferred for 90 min to an acetate-free N KCl solution aspirated with oxygen. The plateau at -0.45 volt was due to the formation of a corrosion film during the period after the adsorbed acetate had been partly removed by diffusion into the acetate-free corrosion solution. It was not as thick as the film formed during corrosion tests of 10 min on samples not initially wet with the acetate solution.

From these observations the necessity of complete cleaning of the solid surface becomes apparent. Also of great importance is the absence from the corrosion solution of any chemical which might adsorb and thereby reduce the effective area of the sample or otherwise inhibit the reaction. Acetate treatment of a clean copper surface changes the net reaction or the surface in such a way that the film of corrosion products is diminished by a factor of 9 or 10. The stabilizing effect of the adsorbed polar molecules on the surface of the copper should prove useful in electroreduction processes.

Conclusions

1. The initial process of the corrosion of copper in aqueous potassium chloride solutions is first order with respect to the oxygen concentration and to the hydrogen ion concentration, and depends upon the number of available sites (free copper atoms) on and near the copper surface. The specific rate constant for the process is 3×10^5 liter mole^{-1} atm^{-1} sec^{-1} at 25°C.

2. Subsequent to the initial reaction the mechanism changes, the observed rate dependence becomes parabolic, then logarithmic.

3. Acetate ion changes the process by adsorption, no film of copper oxide being formed in the acetate solution.

Acknowledgment

This research has been supported by the Office of Naval Research. Appreciation is also due Dr. Richard C. Gilmore and Mr. George W. Petty for their assistance with some of the experimental rate measurements.

Any discussion of this paper will appear in a Discussion Section, to be published in the June 1954 issue of the Journal.

References

1. C. Wagner, *Z. phyzik. Chem.*, **21B**, 25 (1933); **32B**, 447 (1936); **40B**, 445 (1938).
2. H. A. Miley, *Trans. Electrochem. Soc.*, **81**, 391 (1942).
3. U. R. Evans, *Trans. Electrochem. Soc.*, **83**, 335 (1943).
4. N. Mott, *Trans. Faraday Soc.*, **35**, 1175 (1939); **36**, 472 (1940).
5. A. Dravnieks and H. J. McDonald, *J. Electrochem. Soc.*, **93**, 177 (1948).
6. C. V. King, *Trans. N. Y. Acad. Sci.*, [2], **10**, (7), 202 (1948).
7. C. V. King, *J. Am. Chem. Soc.*, **57**, 828 (1935).
8. R. G. Van Name and D. V. Hill, *Am. J. Sci.*, **36**, 543 (1913); **42**, 307 (1916).
9. C. V. King and W. H. Cathcart, *J. Am. Chem. Soc.*, **59**, 63 (1937).
10. G. H. Damon and R. C. Cross, *Ind. Eng. Chem.*, **28**, 231 (1936).
11. R. P. Russell and A. White, *Ind. Eng. Chem.*, **19**, 116 (1927).
12. F. J. Asselin and F. A. Rohrman, *Ind. Eng. Chem.*, **32**, 1015 (1940).
13. R. H. Brown, B. E. Roetheli, and H. O. Forrest, *Ind. Eng. Chem.*, **23**, 350 (1931).
14. W. E. Campbell and U. B. Thomas, *Trans. Electrochem. Soc.*, **76**, 303 (1939).
15. J. R. Weeks and G. R. Hill, Technical Report No. 6, AEC AT(11-1)-82, Project No. 1, University of Utah (1951).
16. F. P. Bowden and E. K. Rideal, *Proc. Roy. Soc. London*, **A120**, 49, 80 (1928).
17. H. A. Miley, *Trans. Electrochem. Soc.*, **81**, 391 (1942); O. H. Hamilton and H. A. Miley, *ibid.*, 413.
18. U. R. Evans, *Trans. Electrochem. Soc.*, **83**, 335 (1943).
19. N. Mott, *Trans. Faraday Soc.*, **35**, 1175 (1939); **36**, 472 (1940).
20. C. V. King, private communication.

The Manufacture, Properties, and Uses of Polyvinyl Formal[1]

ANDREW F. FITZHUGH AND EDWARD LAVIN

Shawinigan Resins Corporation, Springfield, Massachusetts

AND

GEORGE O. MORRISON

Shawinigan Products Corporation, New York, New York

ABSTRACT

Polyvinyl formal ("Formvar" ®) is manufactured by simultaneous hydrolysis and acetalization of polyvinyl acetate. Composition and resulting properties can be varied. These resins uniquely combine rigidity and toughness. Moldability is improved by lowered molecular weight and plasticizers. Solvents are few. Retention of more acetate groups leads to more general solubility and lowered strength and dimensional stability.

A major application is in wire enamel, where cross-linking occurs. Solutions are also used for solenoid bonding and metal priming. Other applications include injection molding, calendering, reinforcement of more brittle resins, thermal adhesives for metals, and plasticized compositions.

INTRODUCTION

Polyvinyl formal is a leading synthetic resin in the enameled wire field, and possesses several unique properties for other applications.

The starting material for its manufacture is vinyl acetate (1–3), which is polymerized, using peroxide type initiation, controlled to give polyvinyl acetates in a wide range of average viscosities. Commercially, solution (4), suspension (5, 6), and emulsion (7) polymerization processes are used.

A predominantly head-to-tail linkage occurs, thus:

$$n\ CH_2{=}CHOCOCH_3 \rightarrow \left(\begin{array}{l}-CH_2-CH- \\ \qquad\quad | \\ \qquad\quad OCOCH_3\end{array}\right)_n.$$

It has been established that monomer transfer reactions give rise to head-to-head configuration and branching (8–10).

Since polyvinyl acetate is an ester, acetate groups can be removed, giving new bodies which contain free hydroxyl groups. These, in turn, can be reacted with substances containing a reactive carbonyl group to form acetals. It is thus possible to make a large variety of resins, each containing hydroxyl, acyl, and acetal groups in various proportions (11).

The simultaneous hydrolysis and acetalization of polyvinyl acetate may be represented by the equation

$$\begin{array}{l}CHOAc \\ | \\ CH_2 \\ | \\ CHOAc \\ | \\ CH_2 \\ |\end{array} + H_2CO + H_2O \xrightarrow{H^+}$$

$$\begin{array}{l}CH \\ | \\ CH_2 \\ | \\ CH \\ | \\ CH_2 \\ |\end{array}\begin{array}{l}\quad -O \\ \diagup\ \diagdown \\ \quad\ O \\ \diagdown\ \diagup \\ \quad -O \\ \quad\ |\end{array} + 2HOAc$$

The reaction is catalyzed by strong mineral acids. It will be understood that, because of steric and equilibrium limitations, this reaction never goes to completion, so that both hydroxyl and acetyl groups remain attached to the vinyl chain.

Processes for the manufacture of polyvinyl acetal resins fall roughly into two main classes—sequential and simultaneous. In a sequential or two-stage process the polyvinyl acetate is first hydrolyzed and this product is then reacted to form the acetal resin. In a simultaneous or one-stage process, hydrolysis and acetal formation are carried on at the same time. There can be semisequential processes intermediate between these two, in which the aldehyde is added after the hydrolysis has progressed to a certain point, but without separation of the hydrolysis product.

Commercial polyvinyl formal[2] is manufactured by a simultaneous process in acetic acid solution, shown schematically in Fig. 1.

Polyvinyl acetate of the proper viscosity is dissolved in a mixture of acetic acid, water, and formalin, and pumped into a heated kettle. Sulfuric acid catalyst is added and the mixture maintained at an elevated temperature until the desired reaction has been completed. The sulfuric acid catalyst is

[1] Manuscript received November 24, 1952. This paper was prepared for delivery before the Montreal Meeting, October 26 to 30, 1952.

[2] Known as "Formvar" ®

then neutralized and water added to the reaction mixture under rapid agitation, which results in precipitation of the resin as spongy granules of fairly uniform size (12). After washing and (for some products) steeping in a stabilizing solution (13), the resin is centrifuged and dried.

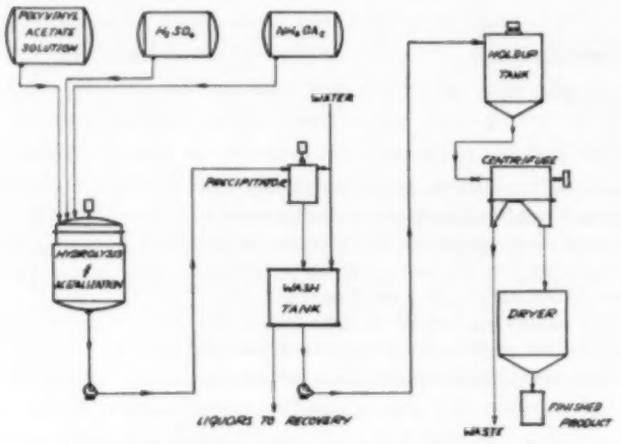

FIG. 1. Polyvinyl formal flowsheet (schematic)

By varying the charge composition and reaction conditions, an almost endless series of polyvinyl acetal resins may be obtained, with wide variations in properties. For example, with increasing acetalization a wide range of properties is possible from water soluble materials to water impervious resins. The bulk density and grain structure can be controlled by the conditions for precipitation, a more dilute solution giving a finer, more spongy grain. As in most organic reactions, longer times at lower temperatures give lighter colors, a fact utilized along with stabilization in the production of resins for molding.

Table I lists the principal types of polyvinyl formal on the market. The numerators of the grade designations are the approximate viscosities of the parent polyvinyl acetates in centipoises of benzene solutions containing 86 grams per liter (and hence represent the molecular weights); the denominators indicate the "percentage hydrolysis" or extent to which acetate groups have been replaced by hydroxyl and formal groups.

"E" indicates a material most suitable for wire enamel; "S", a thermally stabilized material.

In Fig. 2, the lower left corner represents polyvinyl acetate, the lower right corner represents 100 per cent polyvinyl alcohol, and the top represents a hypothetical pure polyvinyl formal. Weight percentages are used.

The parallelograms represent the specification limits for various degrees of hydrolysis: E and S, 95 per cent; M, 85 per cent; and W, 70 per cent. The oval F represents the approximate composition of fiber-forming materials which have been made by reaction of paraformaldehyde with polyvinyl alcohol under extreme condensation conditions (14), and I the approximate composition of an extremely soft, tough and absorbent sponge recently patented (15).

TABLE I. *General properties of polyvinyl formal*

Property	ASTM test method	Formvar, type				
		15/95E	15/95S	7/95S	12/85	7/70
Average degree of polymerization	—	500	500	350	430	350
Polyvinyl alcohol, %	(a)	5–6	7–9	7–9	5–7	5–7
Polyvinyl acetate, %	(b)	9.5–13	9.5–13	9.5–13	20–27	40–50
Viscosity, cp	(c)	40–60	40–60	15–22	18–22	8–10
Stability (minimum), 1 hr @ °C	—	120	150	150	120	120
Specific gravity	—	1.2	1.2	1.2	1.2	1.2
Refractive index, n_D^{25}	D542-42	1.5	1.5	1.5	1.5	1.5
Flow temperature, °C	D569-48	160–170	160–170	140–145	145–150	—
Heat distortion point, °C	D648-49T	88–93	88–93	88–93	75–80	50–60
Inflection temperature, °C	D1043-49T	103–108	100–105	100–105	90–95	75–80
Apparent modulus of elasticity, 10^5 psi	D1043-49T	3.5–6.0	3.5–6.0	3.5–6.0	4–6	4–6
	D638-41T	—	2.5–3.0	—	—	—
Tensile strength, 10^4 psi	D638-41T	1.0–1.1	1.0–1.1	1.0–1.1	1.0–1.1	1.0–1.1
Elongation, %	D638-41T	7–20	10–50	10–50	4–5	3–4
Deformation, 4000 psi load, %, 50°C	D621-48T	0.2–0.4	0.2–0.4	0.2–0.4	4–6	V. high
Deformation, 4000 psi load, %, 70°C	D621-48T	1–3	1–3	1–3	V. high	V. high
Impact strength, Izod, notched, ½ × ½ compr.	D256-43T	1.2–2.0	1.2–2.0	1.0–1.4	0.5–0.7	0.4–0.6
Impact strength, Izod, notched, ½ × ⅛ inj.	D256-43T	—	—	1.3–2.0	—	0.4–0.6
Impact strength, Izod, unnotched	D256-43T	>60	>60	>60	—	—
Water absorption, %	D570-40T	0.75	1.1	1.1	1.5	1–5

(a) By acetylation; (b) by saponification; (c) 5 g resin in 100 ml ethylene dichloride solution at 20°C.

PHYSICAL PROPERTIES

The properties of polyvinyl formal are largely determined by the high polarity of the alcohol and

acetal groups. It differs from other highly polar resins, such as polyamides and polyvinyl alcohol, in tending less toward crystallinity because of the completely random arrangement of methylal, acetate, and hydroxyl groups.

Table I lists a number of properties of the principal types of polyvinyl formal. It will be observed that, in general, strength, rigidity, and characteristic temperatures become lower as the proportion of polyvinyl acetate increases. Changes of molecular

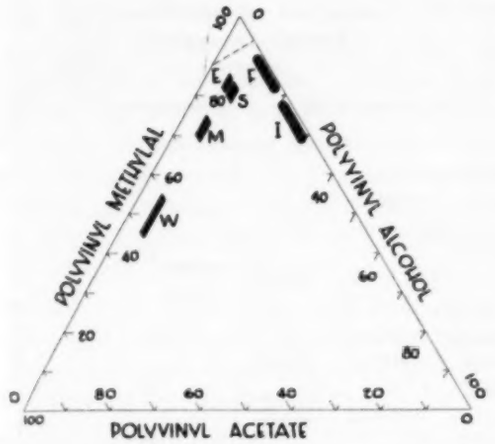

FIG. 2. Range of composition of commercial polyvinyl formal.

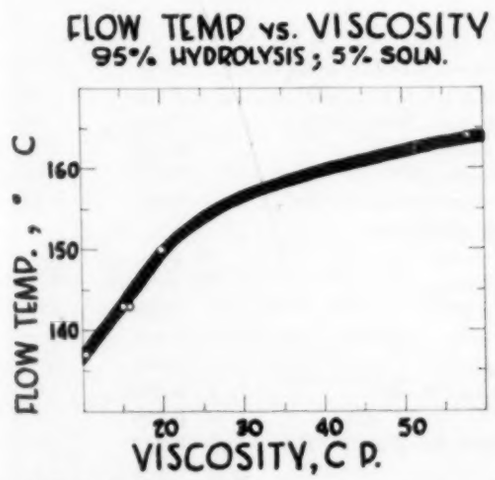

FIG. 3. Relationship of flow temperature to solution viscosity.

weight within the range of these materials will be seen to have little effect on properties below the inflection temperature. Flow temperature, on the other hand, is dependent upon molecular weight as shown in Fig. 3. It is practically independent of acetate content.

Increasing polyvinyl acetate content lowers the inflection temperature, with resultant greater flow as shown by the values for heat distortion temperature and deformation under load (see Fig. 4). The heat distortion temperature is independent of molecular weight between a degree of polymerization of about 350 to over 1000, as shown in Table II.

A reduction in elongation and impact strength also results from increasing the proportion of polyvinyl acetate.

Water absorption increases with polyvinyl alcohol content. Unexpectedly, the elongation becomes greater with a higher proportion of alcohol groups, possibly because of an increase in the water absorption when conditioned at 50 per cent relative humidity.

Plasticizers, even in small quantities, increase cold flow, as shown in Fig. 5.

In comparison to other resins, polyvinyl formal uniquely combines rigidity, toughness, and dimen-

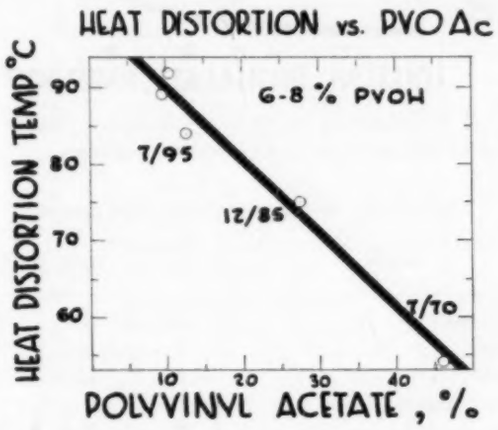

FIG. 4. Relationship of heat distortion temperature to acetate content.

TABLE II. *Heat distortion vs. molecular weight*

Formvar type	DP	Polyvinyl acetate, %	Heat distortion Temp, °C
7/95	350	10.2	92
15/95	500	10.9	91
100/95	>1000	10.2	93

sional stability, although excelled by another resin in each property separately (16). Its electrical properties have already been reported (17, 18).

Table III lists pure solvents of the 7/95 and 15/95 types, together with a partial list of solvents for higher acetate types. The solubilizing effect of the acetate groups is marked. All solvents for type 15/95 for which data have been obtained have audio dielectric constants between 7 and 13 (except dioxane) and Hildebrand's solubility parameter (19) of 9.8 to 10.7, showing the dependence of solubility on polarity and "internal pressure." Solutions in many of these solvents will tolerate high dilution with nonsolvents. All types containing less than ten per cent of polyvinyl alcohol are soluble in mixtures of aliphatic alcohols with aromatic hydrocarbons such as 30 parts

ethanol to 70 parts toluene. Methanol through the various butanols can be mixed with benzene, toluene, or xylene, depending upon the volatility and toxicity requirements. Polyvinyl formal containing more than

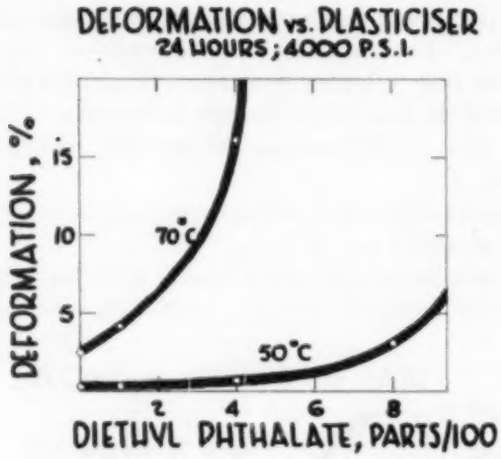

FIG. 5. Relationship of 24-hr deformation under 4000 psi load to temperature and plasticizer content.

TABLE III. *Solubility of polyvinyl formal*

Solvent	7 & 15/95 E & S	12/85	7/70
Acetic acid	S	S	S
Acetone	I	I	S
Alcohols	I	I	I
Alcohol-toluene (30:70)	S	S	S
Aniline	S	S	S
n-Butyl acetate	I	I	S
Cellosolve acetate	PS	S	S
Chloroacetic acids	S	S	S
Chloroform	S	S	S
Cresylic acid	S	S	S
Cyclohexanone	I	S	S
Cyclohexyl acetate	I	I	S
Diacetone alcohol	I	S	S
Dichloroethyl ether	S	S	S
Dioxane	S	S	S
Ethyl acetate	I	I	S
Ethylene dichloride	S	S	S
Furfural	S	S	S
Hydrocarbons	I	I	I
Isophorone	PS	S	S
Methyl cellosolve	I	S	S
Methyl cellosolve acetate	I	S	S
1-Nitropropane	S	S	S
Pyridine	S	S	S
Tetrachloroethane	S	S	S

S = soluble; I = insoluble; P = partly soluble.

ten per cent polyvinyl alcohol is soluble only in liquids which are completely miscible with water.

The thermal degradation of polyvinyl formal results predominantly from surface atmospheric oxidation. Spongy granules of type S resin become discolored and largely insoluble after one hour at 160°C, whereas the same material, molded into disks 10 mm thick was heated for one hour at 200°C with the formation of 0.7 per cent insolubles, only slight discoloration, and about 1 per cent increase in viscosity. Oxidative changes are greatly reduced by the use of phenolic stabilizers such as para-tertiary-amylphenol (20).

APPLICATIONS

The first and most extensive application of polyvinyl formal is in the manufacture of a tough, heat-

TABLE IV. *Comparison of oleoresinous and polyvinyl formal wire enamels*

Test and description	Heavy enamel	Heavy polyvinyl formal
Elongation, %	35	75
Abrasion resistance:		
Revolving drum, 25°C, turns	30	200
130°C, turns	5	75
Inca paddle, turns	150	2400
Scrape, 0.009-in. blade, 25°C, oz	20	50
Scrape, 0.016-in. blade, 105°C, oz	20	55
GE needle, 10 oz load, strokes	47	1640
GE needle, 20 oz load, strokes	7	210
Compression:		
Lb to cause failure at 25°C	1800	5500
20 lb load, 24 hr, 125°C	Fails	Passes
20 lb load, 24 hr, 150°C	Fails	Passes
Heat aging, 105°C, hr	50–100	3000–3500
Heat aging, 125°C, hr	12–24	400–700
Heat shock, 2 hr at 105°C	Fails	Passes
Solvent resistance:		
Kerosene	Sl. softened	No effect
Naphtha	Sl. softened	No effect
Toluene	Fails	No effect
Acetone	Fails	No effect
Ethanol	Fails	No effect
Power factor, 30°C	0.0085	0.0076
75°C	0.036	0.0046
Dielectric constant, 30°C	3.0	3.6
75°C	3.6	3.4
Loss factor, 30°C	0.025	0.028
75°C	0.12	0.025

resistant wire enamel. An alkyl phenolic resin is combined with it in a solvent mixture of cresylic acid or furfural and naphtha (20–24). After application to the wire, this coating is cured to a cross-linked material harder than its components and virtually incapable of flow.

As may be seen in Table IV, there is no significant difference between the dielectric strengths of this wire and conventional enameled wire. However, the greater toughness and adhesion of enamels contain-

ing polyvinyl formal better assure maintaining dielectric strength by retaining integrity of the coating during winding, treatment, and service. Such enamel is seen to have abrasion resistance 2.5 to 30 times that of oleoresinous wire enamel of the same thickness, depending upon the testing method. It will stand 30 to 60 times the heat aging, and resists solvents, many of which cause failure of conventional enamels.

A related application is the bonding of solenoid coils by means of solutions of Formvar 7/70 applied in ketone or ester solution.

A revolution in aeroplane construction has been accomplished by the "Redux" adhesive process, in which surfaces are first coated with phenolic resins, then dusted with polyvinyl formal, and finally cured under heat and pressure to give greater structural strength than welding or rivetting (25).

In several applications such as metal coatings the unique properties of polyvinyl formal justify its relatively high cost. It has been used for food can lining (26). A high-performance steel priming composition has been developed consisting of Formvar 7/70 and passivating agents. Resistance to salt water is especially good. This primer may make even small shops largely self-contained in preparing metallic surfaces for painting.

Calendering and extrusion of polyvinyl formal sheet stock has recently shown considerable promise.

Increasing interest is being shown in the use of polyvinyl formal for injection molding applications. Molding temperatures of 150°–200°C, pressures of 10,000 to 20,000 lb/in.^{2}, and relatively large gates are generally desirable. While plasticizers improve flow, their use should be kept to a minimum in order to preserve high dimensional stability.

Polyvinyl formal has been used in two types of compositions for phonograph records: as a major constituent to produce high quality, unbreakable records; and, in much smaller proportions, to toughen inexpensive materials to give products similar to shellac records (27, 28).

The resin may be plasticized to form tough, elastomeric compositions. A war-time use of one such material was in self-sealing gasoline tanks. It can be used for safety glass, although polyvinyl butyral appears superior for this application.

ACKNOWLEDGMENTS

The authors wish to thank General Electric Company for Fig. 6 and wire enamel data; Phelps Dodge Copper Products Corporation for wire enamel data; and Shawinigan Resins Corporation for permission to publish the remaining data in this paper.

Any discussion of this paper will appear in a Discussion Section, to be published in the June 1954 issue of the JOURNAL.

REFERENCES

1. P. D. COPPOCK AND D. J. HADLEY, U. S. Pat. 2,398,820, April 23, 1946.
2. G. O. MORRISON AND T. P. G. SHAW, *Trans. Electrochem. Soc.*, **63**, 425 (1933).
3. F. W. SKIRROW AND G. O. MORRISON, U. S. Pat. 1,710,197, April 23, 1929.
4. K. G. BLAIKIE AND R. N. CROZIER, *Ind. Eng. Chem.*, **28**, 1155 (1936).
5. C. L. BOYCE, U. S. Pat. 2,486,855, Nov. 1, 1949.
6. C. L. BOYCE, U. S. PAT. 2,555,286, May 29, 1951.
7. W. K. WILSON, U. S. Pat. 2,508,341, May 16, 1950.
8. P. J. FLORY AND F. S. LEUTNER, *J. Polymer Sci.*, **3**, 880 (1948).
9. O. L. WHEELER, S. L. ERNST, AND R. N. CROZIER, *J. Polymer Sci.*, **8**, 409 (1952).
10. O. L. WHEELER, E. LAVIN, AND R. N. CROZIER, *J. Polymer Sci.*, **9**, 157 (1952).
11. G. O. MORRISON, F. W. SKIRROW, AND K. G. BLAIKIE, U. S. Reissue 20,430 (6–29–37) of Pat. 2,036,092 (orig. date 3–31–36) appl. March 25, 1929.
12. J. DAHLE, U. S. Pat. 2,282,037, May 5, 1942.
13. J. DAHLE, U. S. Pat. 2,258,410, Oct. 7, 1941.
14. C. W. GAYLER, U. S. Pat. 2,487,864, Nov. 15, 1949.
15. C. L. WILSON, U. S. Pat. 2,609,347, Sept. 2, 1952.
16. Technical Data on Plastics, Manufacturing Chemists' Assn., Washington (1952).
17. Table of Dielectric Materials, Vol. II, National Defense Research Committee, Washington.
18. T. D. CALLINAN, Thermal Evaluation of Formvar Resin, NRL Report C-3397, Naval Research Laboratory, Washington, D. C. (Dec. 27, 1948).
19. J. C. HILDEBRAND, "The Solubility of Nonelectrolytes," p. 129, Reinhold Publishing Corp., N. Y. (1950).
20. K. G. BLAIKIE AND R. N. CROZIER, U. S. Pat. 2,166,856, July 18, 1939.
21. R. W. HALL, U. S. Pat. 2,114,877, April 19, 1938.
22. R. H. THIELKING, U. S. Pat. 2,154,057, April 11, 1939.
23. E. H. JACKSON AND R. W. HALL, U. S. Pat. 2,307,588, Jan. 5, 1943.
24. W. PATNODE, E. J. FLYNN, AND J. A. WEH, *Ind. Eng. Chem.*, **31**, 1063 (1939).
25. N. A. DE BRUYNE, U. S. Pat. 2,499,134, Feb. 28, 1950.
26. C. E. MCMANUS, U. S. Pat. 2,308,530, Jan. 19, 1943.
27. G. F. METZ, U. S. Pat. 2,563,792, Aug. 7, 1951.
28. G. F. METZ, U. S. Pat. 2,599,570, June 10, 1952.

The Chemistry of Traps in Zinc Sulfide Phosphors[1]

W. Hoogenstraaten

Philips Research Laboratories, N. V. Philips' Gloeilampenfabrieken, Eindhoven, Netherlands

ABSTRACT

Trap characteristics of zinc sulfide phosphors are studied as a function of chemical composition. The simplest phosphor systems are found to have simple, single-peaked glow curves. They contain only activators and coactivators in pure sulfide base materials. Coactivators are defined as impurities necessary to stabilize the activators in the zinc sulfide lattice. They are found to exert a major influence upon trap characteristics. The trap depths are found to be 0.37 electron volt (ev) for Cl^-, Br^-, and Al^{3+}, 0.51 ev for Sc^{3+}, 0.62 ev for Ga^{3+}, and 0.74 ev for In^{3+} as coactivators in ZnS-Cu. Additional glow peaks and traps are produced by oxygen and by the killers cobalt and nickel. The formation of mixed crystals with cadmium sulfide or zinc selenide generally results in a shift of the glow curves toward lower temperatures.

Introduction

The chemical nature of the luminescence centers in zinc sulfide phosphors is, in general, reasonably well known. On the other hand, the nature of the electron traps, which are thought to be responsible for the afterglow phenomena, is much less well understood. Although the traps are physically just as well defined as the activator levels, very little is found in the literature about their dependence upon the preparative conditions of the phosphors (1–5). In this paper an attempt is made to clarify this situation and to show that the trap population in zinc sulfide phosphors may be controlled by chemical means.

As a tool for identifying the different kinds of traps, use was made of thermal glow curves. The phosphors were cooled by liquid air, exposed to the exciting radiation of 3650 Å, and heated in the dark at a more or less constant rate of 3° per sec. The current of a photomultiplier on which the fluorescent light fell and the thermo emf by which the phosphor temperature was measured were simultaneously recorded on a rotating drum with photographic paper.

The theory of the glow curve has been extensively studied by various authors (3, 6–9). If only one species of traps is present, the glow curve is determined by the trap depth ϵ and the escape frequency s according to: $\gamma = s \exp - \epsilon/kT$. In addition, the glow curve is affected by the rate of heating and by the kinetics governing the recombination of electrons with traps and centers. It is not easy to make a conclusion whether a single glow peak is due to one trap species with discrete values of ϵ and s, or whether it is caused by a distribution of traps in depth or s-value. Although the latter possibility seems to be the most likely in general, it will be assumed here that a well separated glow maximum indicates a number of traps which are produced, at least in principle, by the same disturbance.

There are a few precautions to be taken in interpreting the glow curve. One of these (10) relates to the effect of temperature quenching of the phosphors which depends not only on the activator but also on the state of the base lattice. When, in the glow experiment, the temperature has reached the point where the fluorescence efficiency decreases, the glow curve must end there regardless of the presence of deep traps that are still filled with electrons. For this reason the glow curve may fail to show the presence of deep traps in a zinc sulfide phosphor activated with silver, which might be found in the same matrix activated by an impurity with a more favorable temperature dependence such as copper.

Another factor to be noted is that traps may not be revealed by the glow curve, either because they are not filled at the temperature of excitation, or because the electrons released from them are mostly retrapped by deeper traps which were not filled during the excitation. An example of the former type is KCl-Tl (11), the deep traps of which are hardly filled at 90° K, but are revealed by the glow curve after excitation at room temperature. An example of the latter type will be given below.

Finally, a remark must be made on the translation of the temperature of maximum glow into the corresponding trap depth. For this purpose, use is often made of a linear relationship such as 100° K corresponding to 0.2 ev trap depth (11). In most cases with zinc sulfide phosphors this relationship seems to hold approximately with heating rates of 2 to 3° per sec; yet there are cases where it leads to false

[1] Manuscript received May 13, 1952. This paper was prepared for delivery before the Philadelphia Meeting, May 4 to 8, 1952.

results. For the cobalt traps in ZnS-Cu-Co (12), for example, 100° K corresponds to only 0.12 ev, owing to the low value of s.

Preparation of Phosphors

It is obvious that a study of the relationship between trap population and phosphor constitution requires a knowledge of the physical and chemical composition of the systems. The amounts of the elements present in the finished products must be known, as well as the lattice structure, including its defects such as vacancies and interstitial disturbances. Especially the latter factors are difficult to control reproducibly, and it seems hardly possible to avoid lattice disturbances of a physical nature which may well give rise to traps. The method used by the author was to start with the simplest systems of bright fluorescence, and to investigate the changes in the glow curve produced by adding increasing amounts of certain impurities to these phosphors.

Accordingly, the zinc sulfide phosphors were prepared by firing ZnS mixed with the activators and other impurities in a stream of H_2S + HCl or, if halogen ions had to be avoided, in H_2S alone. Another method of introducing halogens into the sulfides, which was especially suitable if the influence of added oxygen had to be studied, was by firing the phosphors with $CaCl_2$, $BaCl_2$, or $ZnCl_2$ in nitrogen. In that case, the base material was previously freed from oxygen by firing it in H_2S. In order to obtain well crystallized products of a defined lattice structure (wurtzite), the firing was carried out at a temperature of 1100°C or higher.[2]

Results

Halogen Ions

The least complex zinc sulfide phosphors, which may be expected to have the simplest glow curves, contain [besides the elements of the base lattice] only the monovalent positive activator ions and the monovalent negative halogen ions needed to stabilize the activator; the latter are called the "coactivators" (13, 14). Comparing the glow curves (Fig. 1) of $ZnS - X^+ - Cl^-$, in which $X^+ = Ag^+$, Cu^+, Au^+, or Zn^+,[3] a striking resemblance among the simple glow peaks is observed. The glow maxima spread around −90°C within ±10°C. This spread is about the same as that usually found with a number of different products of the same composition. Hence it may be concluded that in these phosphors with different activators and a common coactivator, the traps are of the same kind and are probably produced by this coactivator.

With $ZnS\text{-}Cu^+\text{-}Br^-$ and $ZnS\text{-}Zn^+\text{-}Br^-$ a single glow peak is found at the same positions as with $ZnS\text{-}Cu^+\text{-}Cl^-$. For ZnS-Cu-Cl phosphors fired at 950°C, and having mainly sphalerite structure, the glow maximum is found at −120°C. This is a first indication

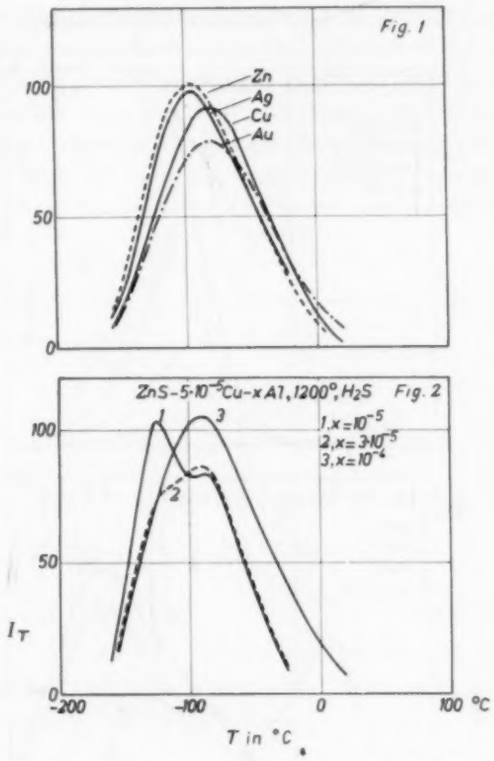

Fig. 1. Glow curves of ZnS-X, 1100°C, H_2S/HCl with X = Ag, Cu, Au, and Zn.

Fig. 2. Glow curves of ZnS−$5\cdot10^{-5}$ Cu-x Al, 1200°C, H_2S with $x = 10^{-5}$, $3\cdot10^{-5}$, and 10^{-4}.

of the influence of the base matrix upon the trap depth, for which a number of examples will be given below.

Trivalent Metal Ions

One of the main pieces of evidence for Kroeger's theory of the function of flux and halogen ions in zinc sulfide phosphors is the fact that the charge compensation can also be effected by trivalent positive ions like Al^{3+} and Ga^{3+}. It is possible to prepare brightly luminescent and completely halogen-free phosphors by adding small amounts of trivalent metal salts in addition to the activator (15, 16). Evidently the incorporation of the X^+ activator ions is accomplished here by the substitution of X^+ and Y^{3+} for two Zn^{2+} ions, whereas in the first case this

[2] The author wishes to express his gratitude to Mr. J. Dikhoff who carried out most of the phosphor preparations described here.

[3] Zn^+ denotes the agent thought to produce the activator level of self-activated ZnS. Although it is generally held that this agent is monovalent zinc, the author prefers to consider it merely as a symbol without attaching to it a definite significance.

was done by replacing Zn^{2+} and S^{2-} with X^+ and Cl^-.

The glow curves of ZnS-Cu (H_2S), coactivated with increasing amounts of Al (Fig. 2), show peaks at -125°C and -90°C, the -125°C peak being gradually replaced by the other one with increasing Al content. The author is uncertain about the interpretation of the -125°C peak which occurs at Al concentrations below that of Cu. Possibly it is caused by traps which are produced by sulfur vacancies due to the excess of copper. The development of the glow peak at -90°C with increasing concentrations of Al shows that these ions produce characteristic traps.

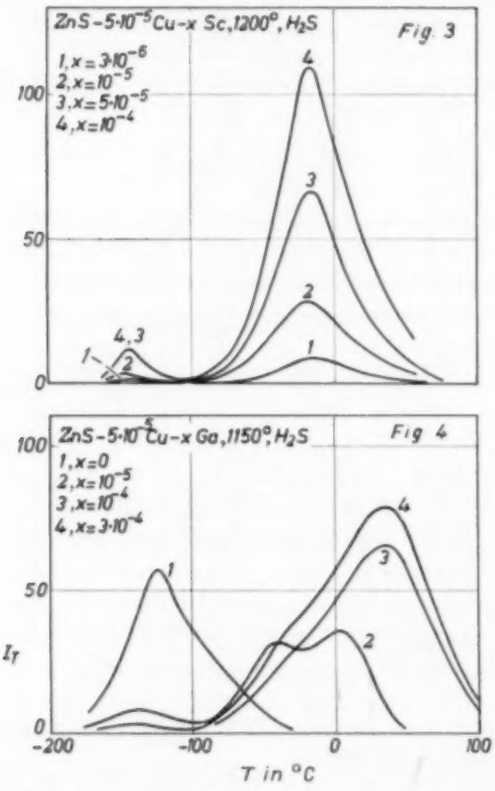

FIG. 3. Glow curves of ZnS$-5\cdot10^{-5}$ Cu- x Sc, 1200°C, H_2S with $x = 3\cdot10^{-6}$, 10^{-5}, $5\cdot10^{-5}$, and 10^{-4}.

FIG. 4. Glow curves of ZnS$-5\cdot10^{-5}$ Cu- x Ga, 1150°C, H_2S with $x = 0$, 10^{-5}, 10^{-4}, and $3\cdot10^{-4}$.

With scandium (Fig. 3), low peaks at -145°C and higher ones at -18°C are found. Especially the latter peak gains in height with increasing amounts of Sc.

The introduction of gallium in ZnS-Cu gives rise to the glow curves shown in Fig. 4. At low Ga concentrations, there is only one low temperature peak at -125°C which disappears with increasing Ga content. At the same time a new peak arises at 35°C, especially at Ga concentrations exceeding the Cu concentration. There is an intermediate case (curve 2 with $5\cdot10^{-5}$ Cu and 10^{-5} Ga)[4] where traps corresponding to -40°C and 0°C are apparently found. This, however, is a case, as already mentioned in the Introduction, where conclusions must be drawn judiciously. As is known from Kroeger's work, an excess of copper relative to the amount of the coactivator produces a blue emission band in addition to the normal green band due to copper; moreover, it seems to give rise to killer centers, for the temperature dependence of the green fluorescence is shifted to lower temperatures, while the blue emission is quenched at still lower temperatures. If a phosphor with an excess of copper contains deep traps such as are produced by Ga, there will occur, first, a change of emission color from blue to green during the warm-up, which causes a dip in the recorded glow curve because the photocell is more sensitive to blue than to green light. In addition, the low quenching temperature will cause an extinction of the glow

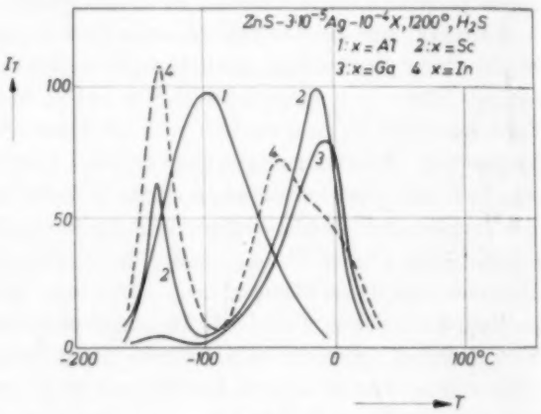

FIG. 5. Glow curves of ZnS$-3\cdot10^{-5}$ Ag $-$ 10^{-4} X, 1200°C, H_2S with X = Al, Sc, Ga, and In.

before the traps are empty, producing a glow maximum at a lower temperature. Indeed, it was observed that during the thermal glow the color of the emitted light changed from blue to green at about -40°C.

Precisely the same situation is found with ZnS-Cu-In. With zero In content only shallow traps appear; with In concentrations below that of Cu there is a complex glow curve with attendant color shift and quenching, and as soon as the ratio In/Cu exceeds 1, the glow curve consists again of a single peak with a maximum at 95°C. Thus for the four trivalent elements, the following characteristic glow peaks are found: Al at -90°C; Sc at -18°C; Ga at 35°C; and In at 95°C. If the s-values of these traps are not too different, the trap depth thus increases with the polarizability of the coactivator ion.

The glow curves of ZnS-Ag phosphors coactivated with the four trivalent elements in amounts exceeding the molar silver concentration, show, in prin-

[4] All activator concentrations given in this paper are expressed as gram-atoms of activator per mole of ZnS.

ciple, the same behavior (Fig. 5). However, the deep traps of Ga and In cannot show their true maximum, owing to the temperature quenching of the ZnS-Ag emission near room temperature. The three heavier metals produce low temperature peaks at −135°C; Al gives a single peak at −100°C; and Sc gives the glow maximum of its deeper trap at the same temperature as with ZnS-Cu (−12°C). With Ga, the glow is quenched at −5°C, and with In the glow is probably of a different nature than in the foregoing cases, for it is of yellow color instead of blue (14). Finally, the author found specific glow curves also with Ce^{3+} as coactivator in ZnS-Cu and ZnS-Ag. Shrader and coworkers (17) also report the occurrence of new traps in ZnS-Cu-Tb.

Oxygen

The three-peaked glow curves commonly reported in the literature (1–8, 18–21) for ZnS-Cu must be attributed to the incorporation of oxygen. Among the various glow curves published by Wells and Wilkins (1) there is one example of this oxygen effect. A ZnS-Cu phosphor fired at 1000°C with NaCl flux showed a single glow peak at −100°C; fired at 1000°C with ZnO, its glow curve showed three peaks. Leverenz (22) also found an enhancement of the "room temperature persistence" of ZnS-Cu with the addition of 2 per cent ZnO before firing. The formation of oxygen traps by the gradual introduction of ZnO in ZnS- 10^{-4} Cu - $CaCl_2$ (N_2) (Fig. 6) was studied. With 0.5 per cent ZnO there is a slight shift of the original −80°C peak to lower temperatures, and a new peak at 50°C is developed. With increasing amounts of ZnO, the new peak increases in height and at the same time shifts slightly to lower temperatures. At the low temperature side there is a gradual replacement of the original glow peak, which decreases in height [and shifts to lower temperatures] by a new peak at about −35°C; finally, the typical three-peaked glow curve is obtained with 2 per cent ZnO. This development suggests that the glow peak at the low temperature side is due to the original traps produced by Cl; its decrease in height and temperature may be due to an increasing degree of retrapping of its electrons by the newly-formed deeper traps produced by oxygen. This explanation, however, becomes doubtful in view of the glow curves shown in Fig. 7. If oxygen is present in the lattice it is possible to incorporate activator ions without the aid of coactivators (23). The glow curves of some of the products obtained in this way show again three peaks at approximately the same temperatures as in the presence of chlorine; in fact, the low temperature peak has now become the highest one. Further experiments are required to reach a definite conclusion about this problem.

The glow curves of ZnS-Au-ZnO-$CaCl_2$ phosphors show three maxima at the same temperatures as with Cu as activator. The introduction of ZnO in ZnS-Ag and in self-activated ZnS also complicates the originally simple glow curve. Glow curves with these activators show two maxima at the same temperatures as the first two peaks with Cu. The absence of the glow from the deepest traps is again easily explained with the temperature quenching effect of the activators.

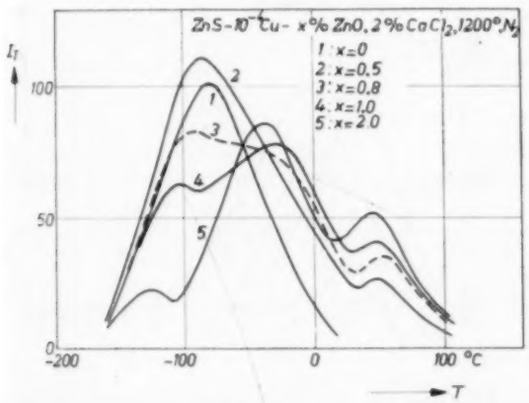

FIG. 6. Glow curves of ZnS−10^{-4} Cu - x % ZnO, 2% $CaCl_2$, 1200°C, N_2 with x = 0, 0.5, 0.8, 1.0, and 2.0.

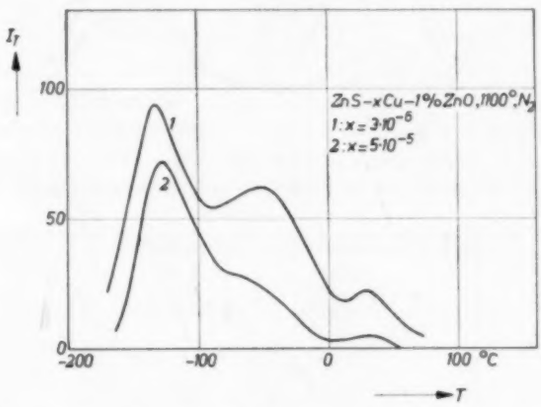

FIG. 7. Glow curves of ZnS- x Cu− 1% ZnO, 1100°C, N_2 with x = $3 \cdot 10^{-6}$ and $5 \cdot 10^{-5}$.

Cobalt and Nickel

The introduction of Co in ZnS-Cu-Cl produces a new peak at 110°C in the glow curve of this phosphor. This peak, which has already been mentioned by Krylova (5), increases in height with increasing amounts of Co as shown in Fig. 8. However, if the concentration of Co reaches that of Cu, the peak decreases again in height, as will be shown in more detail in a forthcoming publication (12). The low temperature glow peak is reduced with the incorporation of Co. This is most probably caused by an

increasing degree of retrapping of the electrons, after release from these traps, in the deeper Co traps. The suppression of the low temperature glow by Co is also mentioned by Garlick (24). This is possible because even after excitation to saturation the Co traps are never completely filled. The high temperature of the glow caused by Co makes it obvious that this glow cannot be found with Ag or Zn^+ as activators.

Nickel is known as a killer for the fluorescence and phosphorescence of both ZnS-Ag and ZnS-Cu. This

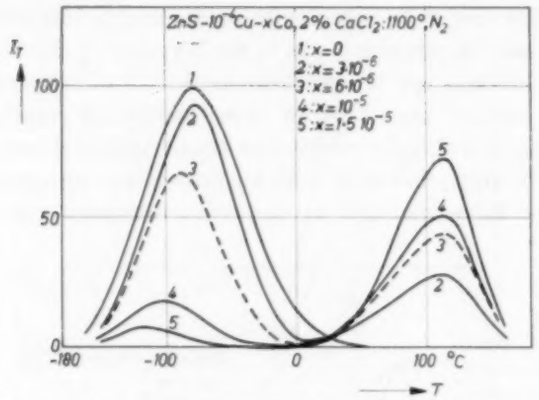

FIG. 8. Glow curves of ZnS—10^{-4} Cu - x Co, 2% $CaCl_2$, 1100°C, N_2 with $x = 0$, $3 \cdot 10^{-6}$, $6 \cdot 10^{-6}$, 10^{-5}, and $1.5 \cdot 10^{-5}$.

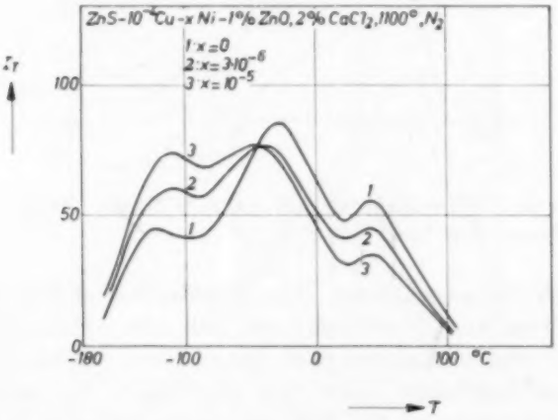

FIG. 9. Glow curves of ZnS—10^{-4} Cu - x Ni — 1% ZnO, 2% $CaCl_2$, 1100°C, N_2 with $x = 0$, $3 \cdot 10^{-6}$, and 10^{-5}.

makes it improbable that the traps formed by Ni will be found from the glow curves. Indeed, the only effect of Ni on the glow curve of ZnS-Cu is a decrease in height of the high temperature peaks, as shown in Fig. 9 for the case of traps produced by oxygen. Cobalt incorporated in ZnS-Cu-ZnO removes the original glow peaks (probably in the same manner as with the Cl glow of ZnS-Cu-Co) and replaces them by its own peak.

Cadmium Sulfide and Zinc Selenide

It has long been known that the introduction of CdS in ZnS, which form a complete series of mixed crystals, causes the absorption edge and the spectral emissions of the various activators to show a gradual shift toward longer wave lengths. If the position of the absorption edge or of the emission maxima is plotted on a frequency scale against the molar composition of the (Zn, Cd)S phosphors, a nearly linear relationship is found in most cases. From it, a mean shift of 150 ± 15 cm^{-1}/mole per cent CdS, or $1.85 \cdot 10^{-2}$ ev/mole per cent CdS, may be derived. With mixed crystals of ZnS and ZnSe, the situation is less simple, for here the shift is in most cases accompanied by the appearance of a new emission peak, suggesting that the introduction of Se produces new activator levels (14). The energy shift found here is smaller than with CdS and varies between 0.5 and $0.75 \cdot 10^{-2}$ ev/mole per cent ZnSe.

The influence of the formation of mixed crystals on the glow curves of ZnS phosphors has not been

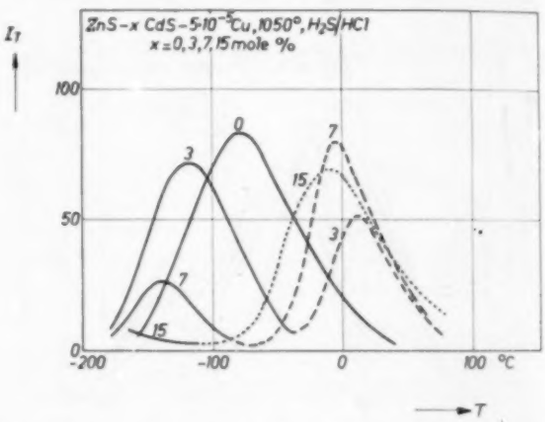

FIG. 10. Glow curves of ZnS- x CdS — $5 \cdot 10^{-5}$ Cu, 1050°C, H_2S/HCl with $x = 0$, 3, 7, and 15 mole%.

clear so far. From the glow curves of (Zn, Cd)S-Cu published by Garlick and coworkers (2, 3) one obtains the general impression of a shift to lower temperatures, but the shape of the curves varies in such an irregular manner that the behavior of the separate glow peaks cannot be followed. This is clear in view of the fact that these zinc cadmium sulfides, all containing oxygen, were far from simple phosphors with respect to their trap population. Moreover, it will be seen that in the very case of traps due to oxygen, the effect of the introduction of Cd differs from the other cases.

With the oxygen-free phosphors having simple glow curves produced by Cl, trivalent metals, and cobalt, a shift to lower temperatures with increasing concentration of cadmium is clearly seen. In Fig. 10, 11, and 12 this is shown for (Zn, Cd)S-Cu-Cl, (Zn, Cd)S-Cu-Al, and (Zn, Cd)S-Cu-Cl-Co. In the first case, a gradual shift of the original glow peak to lower temperatures is observed, until, with 15 per cent CdS, this peak apparently appears below

−180°C and cannot be shown by our glow curve. Furthermore, a new glow peak appears at 10°C, increasing in height relative to the other peak and also shifting to lower temperatures. The same situation obtains with (Zn, Cd)S-Cu-Al. In this case, the new glow peak is a very broad band, and with 7 per cent CdS there is even an indication of two maxima. This suggests that the new traps created with the introduction of cadmium have a very broad distribution of trap depths in this case. An additional cause for the broadness of the glow peaks in mixed

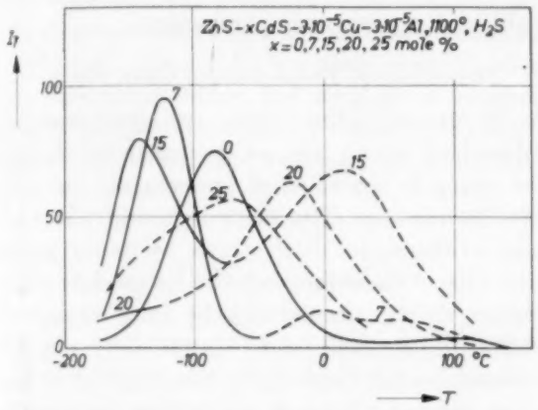

FIG. 11. Glow curves of ZnS- x CdS − $3 \cdot 10^{-5}$ Cu − $3 \cdot 10^{-5}$ Al, 1100°C, H_2S with x = 0, 7, 15, 20, and 25 mole%.

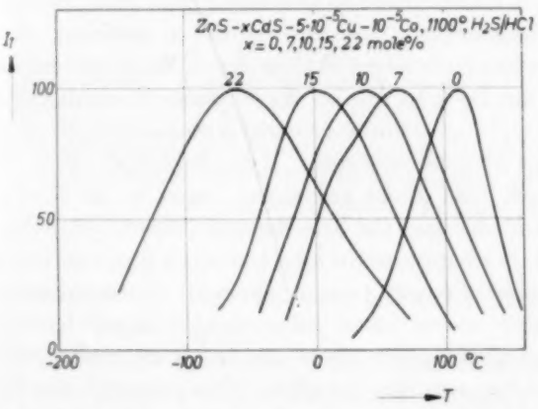

FIG. 12. Glow curves of ZnS- x CdS − $5 \cdot 10^{-5}$ Cu − 10^{-5} Co, 1100°C, H_2S/HCl with x = 0, 7, 10, 15, and 22 mole%.

crystals may be a certain inhomogeneity of the phosphor, i.e., a fluctuation of the distribution of Cd ions in the lattice.

The glow curves of (Zn, Cd)S-Cu-Co are shown in Fig. 12 where the low temperature peaks have been omitted for simplicity. The maxima of the cobalt glow show a continuous shift and, besides, a remarkable broadening. This is caused by two effects. First, there are new traps due to Cd which produce an additional glow peak at −5° to −30°C with 7 to 22 per cent CdS. Thus, the shifting Co peak will first be broadened at the low temperature side, and with higher Cd concentrations at the high temperature side. The second effect is the temperature quenching of the Cu emission which causes the glow to disappear at high temperatures. The temperature dependence, however, is not affected, or only slightly so, by the formation of mixed (Zn, Cd)S crystals, so that at higher Cd contents the glow peak will be fully developed.

Finally, the behavior of the oxygen glow in (Zn, Cd)S-Cu shown in Fig. 13 is considered. No shift is found here. Instead, the separate peaks seem to broaden and lose their sharpness, until they form

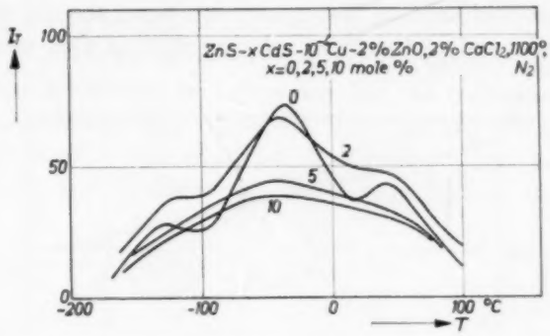

FIG. 13. Glow curves of ZnS- x CdS− 10^{-4} Cu − 2% ZnO, 2% $CaCl_2$, 1100°C, N_2 with x = 0, 2, 5, and 10 mole%.

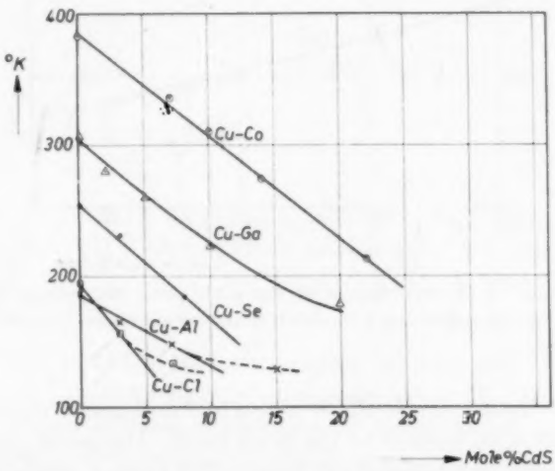

FIG. 14. Temperatures of the glow peak maxima of (Zn, Cd) S-phosphors as a function of the composition in mole% CdS.

one irregular broad band. Perhaps this merging is due to inhomogeneity of the phosphor, as well as to the appearance of the new cadmium glow.

In Fig. 14 the temperatures of the glow maxima of the various traps in (Zn,Cd)S-Cu are plotted against the mole fraction of CdS. In most cases there is a linear relationship. The deviations from linearity found for the shallow traps with Cl and Al may be explained with the proximity of these glow peaks to the starting temperature of the glow curves. The temperature shift expressed in °C per mole per cent CdS, (measured for the initial linear part where

there is a deviation from linearity at higher CdS contents), is found to be as follows: Cu-Co, 7.8 and 8.9 (for two series of preparations); Cu-Ga, 8.2; Cu-Sc, 8.7; Cu-Al, about 6; Cu-Cl, about 12; and Ag-Cl, about 10. On the average we find 8.8 ± 1.2°C per mole per cent CdS. Assuming that 100° K on the temperature scale of the glow curve correspond to 0.2 ev trap death, this would amount to a mean shift of $1.76 \cdot 10^{-2}$ ev per mole per cent CdS which is, within the limits of error, the same value as that found for the mean shift of absorption and emission.

The simplest way to explain this result is to assume a gradual shift of the conduction band toward the filled band in the band scheme of (Zn,Cd)S, while

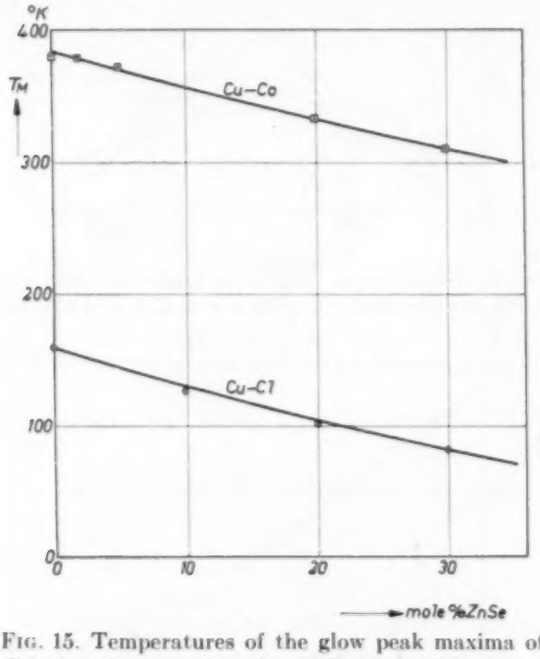

FIG. 15. Temperatures of the glow peak maxima of Zn (S, Se)-phosphors as a function of the composition in mole% ZnSe.

the discrete levels of the activators and traps remain fixed with respect to the filled band. The same conclusion was reached by Fonda (25) from a study of the decay of phosphorescence of (Zn,Cd)S-Cu phosphors. Another fact supporting this point of view is that the temperature at which the fluorescence is quenched is only slightly affected by the incorporation of CdS. This temperature is determined by the distance between the activator levels and the filled band.[5] Finally, some emissions have been found in ZnS phosphors which are probably caused by transitions from trap levels to the filled band; there is some evidence that these emissions do not shift upon formation of mixed crystals with CdS (14).

Only a few experiments have been carried out to determine the effect upon the glow curves of the formation of mixed crystals of ZnS and ZnSe. The main result of these is that the glow peaks produced by Cl, Al, and Co show a shift to lower temperatures as shown in Fig. 15. This shift is about 2.7°C or $0.55 \cdot 10^{-2}$ ev per mole per cent ZnSe, which is again of the same order of magnitude as that for the fluorescence emissions. A remarkable difference compared with the case of (Zn,Cd)S is the absence of a new peak in the Zn(S,Se)-Cu-Cl and Zn(S,Se)-Cu-Al series. The glow peaks produced by oxygen are not blurred as with CdS, but remain well separated with a slight shift to lower temperatures.

Indication of Traps without Glow Peaks

As mentioned before, there are sometimes traps in phosphors which are not revealed by the glow curve owing to the effect of temperature quenching of the fluorescence. However, it is still possible to obtain evidence for such traps by more indirect means. One of these methods can be used only if the phosphor shows stimulability by long wave-length radiation. Thus Bull and Mason (28) measured the stimulable light sum from deep traps after keeping the excited phosphor at various temperatures for a certain length of time. The derivative of this light sum as a function of the temperature of decay has in many cases the shape of a glow peak and gives an indication of the trap depths in question, which were not shown by the glow curve. When this method cannot be used due to the absence of stimulability, the buildup of fluorescence of a phosphor with empty traps may be measured. If the buildup is slow, this means that there are many traps to be filled on excitation, and the area between the buildup curve and its asymptote for long times is a measure for the number of empty traps at the start of the excitation. A glow curve taken subsequently should have the same area, unless there are losses by radiationless transitions during the glow. This property was used by Levialdi and Luzzati (29) to detect traps in $CaSiO_3$-Mn, which were not revealed by the glow curve because of temperature quenching. These authors measured the buildup curve of the phosphor after it had been fully excited and then kept at a higher temperature for a certain length of time. The area above the buildup curve is then proportional to the number of traps emptied during the decay time. The derivative of this area as a function of the decay temperature is again a kind of glow curve and gives the approximate distribution in depth of the "invisible" traps.

The latter method has been used only in a qualitative way in order to show the presence of deep traps produced by the killer elements Co and Ni in ZnS. As has been shown, Co produces traps in

[5] The infrared stimulation spectrum of ZnS-Cu-Pb or ZnS-Cu-Mn is also hardly affected by the addition of CdS (26, 27).

ZnS-Cu which are revealed by the glow peak at 110°C. This temperature is so high that this same glow peak cannot be expected with ZnS-Ag-Co even if Co would produce traps of the same kind in this phosphor. That these traps do exist in ZnS-Ag-Co is shown by the buildup curves in Fig. 16, measured at 90° K after the phosphor had been heated to 150°C in the dark. The area above curve B_1 of ZnS-Ag is 16.7 in arbitrary units, and the area under glow curve G_1, measured afterwards, is 13.3. Hence, only 20 per cent of the light sum acquired during the buildup was lost during the glow. With ZnS-Ag-Co we find an area of 33.8 above its much slower buildup curve B_2, and only 0.8 for its glow curve G_2. This means that about twice the number of electrons that were trapped by ZnS-Ag could be stored in ZnS-Ag-Co. This can only be explained if the latter

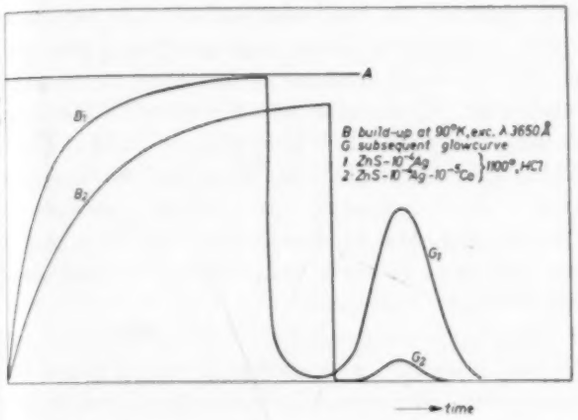

FIG. 16. Buildup curve B (with asymptote A) measured at 90°K with excitation by λ 3650 Å and subsequent glow curve G of 1: ZnS − 10^{-4} Ag and 2: ZnS − 10^{-4}Ag− 10^{-5} Co, both fired at 1100°C in HCl.

phosphor contains deep traps in addition to the shallow Cl traps.

Another example of hidden traps is furnished by ZnS-Cu-Ni. Nickel is only known as a killer, and the effect produced by it on the glow curves of ZnS phosphors is the disappearance of the high temperature glow. This is commonly ascribed to a destruction of the deep traps by nickel (2, 3). A more probable explanation, however, is found in the shift of the temperature quenching to lower temperatures. Moreover, it can be shown that Ni, instead of destroying traps, forms new ones in ZnS phosphors. These traps are again of such depth that they cannot be found in the glow curves even if copper with its favorable temperature dependence is the activator. Fig. 17 shows the buildup curves at room temperature of ZnS-Cu with increasing amounts of Ni. Before these curves were taken, the phosphors were irradiated with infrared in order to empty the deep traps. That this irradiation has a strong effect upon the speed of buildup is shown by the two curves for ZnS- 10^{-4}Cu -10^{-5}Ni. Further, a slower buildup is noticed at higher concentrations of Ni. Thus the formation of deep traps by Ni is clearly demonstrated.

The existence of deep traps in ZnS-Ag-ZnO was demonstrated by a different method. The following set of experiments was carried out with this phosphor: (*a*) warming to 120°C followed by cooling in the dark to −180°C; (*b*) excitation at 20°C followed by cooling in the dark to −180°C; (*c*) and (*d*) as (*a*) and (*b*), with subsequent excitation for one minute with UV radiation of low intensity.

The intensity of excitation at the low temperature in runs (*c*) and (*d*) was so chosen that the traps were only partially filled. After the runs (*a*) and (*b*) no thermal glow was observed. The glow curves after runs (*c*) and (*d*) showed the same shape (two peaks),

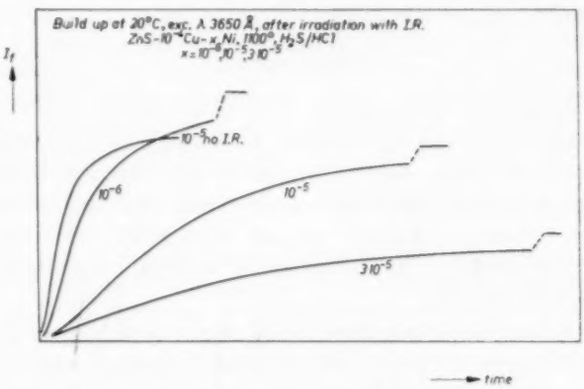

FIG. 17. Buildup curves measured at 20°C with excitation by λ 3650 Å after previous irradiation with infrared of ZnS − 10^{-4} Cu - x Ni − 1100°C, H_2S/HCl with $x = 10^{-6}$, 10^{-5}, and $3 \cdot 10^{-5}$.

but the height of the curve after (*c*) was only 70 per cent of the height of the curve after (*d*). This indicates a difference in physical condition of the phosphor after (*a*) and (*b*), and it is easily explained with the existence of deep traps which are empty after (*a*) and filled after (*b*). When the deep traps are empty, part of the excited electrons which would otherwise fill shallow traps are caught by the deep ones. Moreover, a part of the electrons released from the shallow traps during the glow will be retrapped by the deep traps. The combination of both effects will cause a lower light sum after run (*c*) than after (*d*).

There is one final point to be emphasized. Although one can deduce the presence of deep traps from the slowness of the buildup curve, one must be careful with the interpretation of experiments devised to produce a "glow curve" by indirect means. In the case of ZnS phosphors such a "glow peak" need not be due to electron traps, but is more probably associated with the activators such as Cu or Ag. The

reason is that the temperature quenching of the fluorescence is caused by a thermally activated transfer of holes from the fluorescence centers to other disturbances which may very well be the deeper traps. The occurrence of quenching instead of thermal glow at high temperatures means that the traps are deeper than the corresponding distance between the activator levels and the filled band. The decay of the light sum at elevated temperatures is then governed by the probability of escape of holes from centers, which depends on the release constant s and the activation energy ϵ for this process. For example, the indirect glow peak at 375° K found by Bull and Mason (28) for ZnS-Cu-Mn is, according to our view, not caused by the release of electrons from (Mn ?) traps, but by the release of holes from the Cu levels. With a short calculation, it can be shown that the peak at 375° K is in accordance with the ϵ-value of about 1.0 ev and the s-value of about 10^{11} sec^{-1} found for this process (12).

Discussion

From the glow curves and other more indirect evidence it has been found that traps can be produced in zinc sulfide phosphors by the following agents: (*a*) monovalent negative ions at sulfur sites; (*b*) trivalent positive ions at zinc sites; (*c*) iron-group elements (probably as 2^+ ions at zinc sites); and (*d*) oxygen.

All traps except those of (*d*) become shallower in mixed crystals with CdS or ZnSe, to a degree which is in accordance with the shift to longer wave lengths of the emission spectra. Further, in the cases (*a*) and (*b*), extra traps are formed when cadmium is substituted for zinc, but not when selenium is substituted for sulfur.

Most of these facts can be explained simply with a theory of the formation of discrete levels in ZnS phosphors, which was originally proposed by Klasens (14, 30) and which is strongly supported by Kroeger's work (15, 23). In this theory it is assumed that a group of activator levels are not levels of the activators themselves, but levels of divalent negative sulfur ions; they are lifted from the filled band by the electrostatic field of disturbances which carries a negative charge relative to the charge at the same place in the undisturbed lattice. Such disturbances can be monovalent positive ions like Ag^+, Cu^+, Au^+, and Li^+ at zinc sites, as well as trivalent negative ions like P^{3-} and As^{3-} at sulfur sites. Similarly, one may expect empty levels to be created from the conduction band by a positive charge relative to the charge at the same place in the undisturbed lattice, which can be produced by monovalent negative ions at sulfur sites or by trivalent positive ions at zinc sites. The traps formed in this manner are thus, in principle, all deformed Zn^+ levels, and the nature of the trap forming impurity has only a secondary effect on the trap depth. Since in mixed crystals of (Zn,Cd)S the conduction band is composed of Zn^+ and Cd^+ levels, one may expect that the introduction of an extra positive charge will result in the occurrence of two kinds of trap orbitals, viz., disturbed Zn^+ and Cd^+ levels.[6] A similar explanation was given by Klasens (14) for the double emission bands found by Leverenz (31) in Zn(S,Se)-Ag and Zn(S,Se)-Zn^+. The new emission peak at the long wave-length side is due to Se^{2-} levels disturbed by the neighboring activator ions with excess negative charge. Further, Kroeger (23) reports new emission bands in ZnS-ZnO activated with Ag, Cu, Au, and Zn^+, and he attributes these bands to disturbed O^{2-} levels.

The formation of new traps with mixed crystals is also reported by Bull and Garlick (32) for the As traps in willemite. These traps produce a glow peak at 285° K which remains at the same temperature when part of the zinc is replaced with beryllium. Besides this peak a new glow peak is found at 320° K which gains in height with increasing Be concentration. The formation of mixed crystals of $(Zn,Cd)_2SiO_4$-Mn-As, however, results in a shift of the glow peak to lower temperatures without giving rise to a new glow peak.

The trap levels produced by the elements Co and Ni are probably a property of the divalent ions themselves. The second ionization potentials of these atoms do not differ so much from that of zinc to make this impossible. Further, there are no indications of new Co traps coming into existence with the formation of (Zn,Cd)S, which might be expected if cobalt were present in a different state of valency than zinc.

Finally, the oxygen traps are understood least of all. The author found three glow peaks with phosphors which contained only oxygen as an impurity in addition to Cu activator. Hence there are at least three species of traps for which an explanation must be found. The shallowest traps, which give rise to the glow peak at about −125°C, are probably produced by sulfur vacancies. Due to the presence of oxygen in firing, sulfur may be removed from the lattice in form of SO_2. The sulfur vacancy thus formed has already two electrons trapped in it, but it is possible that a third one may still be attracted by it with a small binding energy. The same traps are probably present in ZnS-Cu-X^{3+} phosphors, in which the amount of Cu exceeds that of X^{3+}.

[6] Perhaps there are more than two kinds of empty levels since, for example, halogen ions surrounded by 4 Zn ions, by 3 Zn and 1 Cd ion, by 2 Zn and 2 Cd ions, etc. may all give rise to traps of different depth.

The two species of deeper traps are perhaps best explained with an idea proposed by Kroeger (23). He suggests that due to its relatively small volume an O^{2-} ion will attract relatively large cations. Now, an electron in the conduction band is equivalent to a Zn^{+} ion, so that an O^{2-} ion may act as an electron trap. According to Kroeger the monovalent activator ions are also preferably situated near oxygen ions. Such an O^{2-} ion with activator coordination will provide a shallower trap than an O^{2-} ion which is surrounded only by Zn^{2+}. As a tentative assumption we propose to consider the $X^{+}O^{2-}$complex as representing the trap of medium depth and the O^{2-} ion as forming the deepest trap.

Any discussion of this paper will appear in a Discussion Section, to be published in the June 1954 issue of the JOURNAL.

REFERENCES

1. A. F. WELLS AND M. WILKINS, Min. of Home Sec. Report RC (C) 40, 56 and 111 (1941).
2. G. F. J. GARLICK, A. F. WELLS, AND M. H. F. WILKINS, *J. Chem. Phys.*, **17,** 399 (1949).
3. G. F. J. GARLICK, Solid Luminescent Materials, Symposium at Cornell University, p. 87 (1948).
4. R. H. BUBE, *Phys. Rev.*, **80,** 655 (1950).
5. E. S. KRYLOVA, *Dokl. Akad. Nauk S.S.S.R.*, **64,** 495 (1949).
6. G. F. J. GARLICK AND A. F. GIBSON, *Proc. Phys. Soc. London*, **60,** 574 (1948).
7. A. F. GIBSON, Thesis, Birmingham University, Birmingham, England (1948).
8. F. E. WILLIAMS AND H. EYRING, *J. Chem. Phys.*, **15,** 289 (1947).
9. M. E. WISE, *Physica*, **17,** 1011 (1951).
10. M. SCHOEN, *Naturwiss.*, **38,** 235 (1951).
11. J. T. RANDALL AND M. H. F. WILKINS, *Proc. Roy. Soc. London*, **A184,** 366 (1945).
12. W. HOOGENSTRAATEN AND H. A. KLASENS, *J. Electrochem. Soc.*, **100,** 366 (1953).
13. F. A. KROEGER, J. E. HELLINGMAN, AND N. W. SMIT, *Physica*, **15,** 990 (1949).
14. H. A. KLASENS, *J. Electrochem. Soc.*, **100,** 72 (1953).
15. F. A. KROEGER AND J. DIKHOFF, *Physica*, **16,** 297 (1950).
16. F. A. KROEGER AND N. W. SMIT, *Physica*, **16,** 317 (1950).
17. R. E. SHRADER, H. W. LEVERENZ, AND E. J. WOOD, *J. Opt. Soc. Amer.*, **36,** 353 (1946).
18. G. F. J. GARLICK AND M. H. F. WILKINS, *Proc. Roy. Soc. London*, **A184,** 408 (1945).
19. G. F. J. GARLICK AND D. E. MASON, *J. (and Trans.) Electrochem. Soc.*, **96,** 90 (1949).
20. A. W. SMITH AND J. TURKEVICH, *Phys. Rev.*, **87,** 306 (1952).
21. M. L. KATS AND N. W. ZHUKOVA, *Dokl. Akad. Nauk S.S.S.R.*, **63,** 247 (1948).
22. H. W. LEVERENZ, *RCA Review*, **7,** 199 (1946).
23. F. A. KROEGER AND J. DIKHOFF, *J. Electrochem. Soc.*, **99,** 144 (1952).
24. G. F. J. GARLICK, Solid Luminescent Materials Symposium, Cornell University, p. 111 (1948).
25. G. R. FONDA, *Trans. Electrochem. Soc.*, **87,** 339 (1945).
26. G. R. FONDA, *J. Opt. Soc. Amer.*, **36,** 382 (1946).
27. N. T. MELAMED, *J. Electrochem Soc.*, **97,** 33 (1950).
28. C. BULL AND D. E. MASON, *J. Opt. Soc. Amer.*, **41,** 718 (1951).
29. A. LEVIALDI AND V. LUZZATI, *J. phys. radium*, **8,** 306, 341 (1948).
30. F. A. KROEGER, "Some Aspects of the Luminescence of Solids," p. 29, Elsevier Press, Amsterdam (1948).
31. H. W. LEVERENZ, "Luminescence of Solids," p. 200, John Wiley and Sons, Inc., New York; Chapman & Hall, London (1950).
32. C. BULL AND G. F. J. GARLICK, *J. Electrochem. Soc.*, **98,** 371 (1951).

Some Properties of Zinc Sulfide Activated with Copper and Cobalt[1]

W. Hoogenstraaten and H. A. Klasens

Philips Research Laboratories, N. V. Philips' Gloeilampenfabrieken, Eindhoven, Netherlands

ABSTRACT

Some properties of ZnS-Cu-Co phosphors under 3650 Å excitation are described, viz., the thermal glow, decay, and buildup of fluorescence, temperature dependence, and light sum. Most of the experimental results can be explained by a model in which cobalt levels act both as electron traps with a trap depth of 0.5 electron volt (ev), and as acceptors for holes, ejected thermally from copper centers with an activation energy of 1.1 ev. The possibility of excitation by 3650 Å radiation of electrons from traps to the conduction band is introduced to explain the observed intensity dependence of the light sum.

Introduction

Among the substances which have an influence on the luminescence properties of zinc sulfide there is a group generally known as killers. According to current thought, killers are additional impurities which are responsible for a drop of the fluorescence efficiency, for a decrease of the phosphorescence, and often for a strong quenching effect by infrared. These effects are shown, for instance, by zinc sulfide activated with copper or silver and containing nickel as killer. On the other hand, there is a great difference between the properties of zinc sulfides with cobalt killer depending upon whether silver or copper is the activator. With silver, both the fluorescence under steady excitation and the duration of the phosphorescence are strongly reduced by cobalt; with copper, the fluorescence is also diminished, but the phosphorescence becomes much stronger. Hence, the functions of a killer impurity cannot be generalized for all phosphors. Instead, the interaction of both killer and activator has to be considered. This is possible on the basis of the well-known band model for ZnS phosphors as discussed in general by Klasens (1). In the present paper the special case of ZnS-Cu-Co, which shows most of the properties exhibited by a large class of doubly activated phosphors, will be considered.

Experimental Part

Preparation of the Phosphors

The usual method of preparing zinc sulfide phosphors consists in firing the precipitated ZnS, mixed with the impurities and some fluxing material, in air. The phosphors then contain an amount of oxygen in the lattice which gives rise to a number of traps of different depth (2). This gives an undesirable complication of the phosphor characteristics shown by the decay and the glow curve (3). It may be avoided by firing the products without flux in a mixed atmosphere of H_2S and HCl, which removes the oxygen present in the base material and introduces the chlorine ions which are needed to stabilize the copper in the lattice (2, 4). All preparations discussed in this paper contain $3 \cdot 10^{-5}$ gram atoms Cu per mole ZnS and were fired for 30 min at 1150°C in a 50 per cent H_2S + 50 per cent HCl stream. They show the green copper fluorescence under 3650 Å excitation and, without cobalt, contain only shallow traps indicated by a single peak at −100°C in the glow curve (warming rate 2° per sec). Cobalt was introduced in concentrations ranging from $3 \cdot 10^{-4}$ to 10^{-4} gram atoms Co per mole ZnS.

Glow Curves

These were measured in the usual manner by cooling the sample with liquid air, exciting it with 3650 Å to saturation, and heating it at a uniform rate of 2° per sec (Fig. 1). Cobalt gives rise to a new glow peak at 110°C which increases in height with cobalt contents up to 10^{-5} Co and decreases for concentrations of the order of that of copper. The glow maximum is thereby shifted to higher temperatures. This glow peak due to cobalt was also found by Krylova (3), but, owing to the slower warming rate, with the maximum at 70°C.

A second effect of Co on the glow curve is the decrease in height of the original −100°C-peak, which has almost disappeared with $3 \cdot 10^{-5}$ Co. This decrease seems to be accompanied by a slight shift to lower temperatures.

It is possible to estimate the trap depth e_2 and the release constant s_2 for the cobalt traps from an

[1] Manuscript received May 21, 1952. This paper was prepared for delivery before the Philadelphia Meeting, May 4 to 8, 1952.

analysis of their glow peaks. As the recorded glow curves of Fig. 1 are not accurate enough for this purpose, the glow was measured starting at −40°C with a slower warming rate. The phosphor was previously excited at room temperature and allowed to decay for a certain time at that temperature before being cooled. In Table I the results of the calculations are shown, details of which are given in the theoretical part. The values of ϵ_2 and s_2 are about 0.51 ev and $5 \cdot 10^4$ sec^{-1}, but the figures show a marked effect of the decay time on these values. This probably indicates a distribution of the traps in depth, for during the decay the shallower traps will

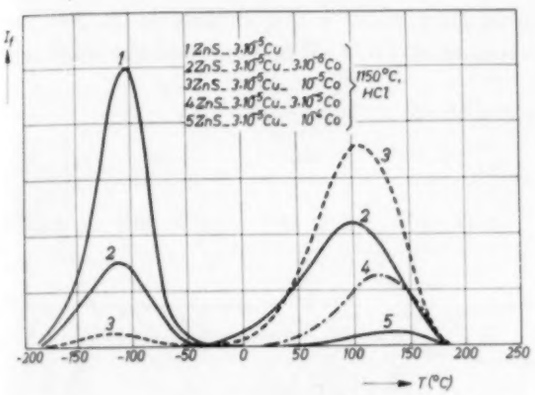

FIG. 1. Glow curves of ZnS−(3·10^{-5} Cu)-(x Co)

TABLE I. *Constants for the* Co-*trap*

Co-conc gram atoms per mole ZnS	Decay time	T_g (°K)	$\left(\frac{dT}{dt}\right)_g$ °C/sec	ϵ_1 (ev)	ϵ_2' (ev)	s_2 (sec^{-1})
	min					
$3 \cdot 10^{-6}$	1	332	$7.2\ 10^{-2}$	0.51	0.51	$2.5\ 10^4$
10^{-5}	0	332	$7.2\ 10^{-2}$	0.48	0.49	$2.3\ 10^4$
10^{-5}	1	332	$7.2\ 10^{-2}$	0.52	0.51	$9.7\ 10^4$
10^{-5}	3	334	$7.2\ 10^{-2}$	0.52	0.51	$8.4\ 10^4$
10^{-5}	15	340	$5.9\ 10^{-2}$	0.55	0.53	$1.8\ 10^5$
$3 \cdot 10^{-5}$	1	350	$4.6\ 10^{-2}$	0.46	0.51	$7.4\ 10^3$
$3 \cdot 10^{-5}$	1	370	0.179	0.49	0.48	$3.1\ 10^4$
$3 \cdot 10^{-5}$	5	374	0.179	0.54	0.54	$1.7\ 10^5$

preferentially lose their electrons, causing a higher mean ϵ_2-value for the subsequent glow curve.[2]

Decay Measurements

The decay of phosphorescence of ZnS-($3 \cdot 10^{-5}$ Cu)-(10^{-5} Co) was measured after excitation by 3650 Å at different temperatures, from $5 \cdot 10^{-3}$ sec to 10^4 sec, covering an intensity range of 10^5. For the measurements in the first 10 sec, the signal from the photomultiplier was amplified by a Philips d-c amplifier GM 4530 and fed to a high speed Hughes MK 2 A recorder. From 10 sec on, the intensity was read directly from a galvanometer. At 20°C the decay was measured after excitation with various intensities (J = 1, 6.3 10^{-2} and 5.9 10^{-3}; Fig. 2). Here the curves behave in some respects in accordance with the theory of Klasens and Wise (5) on the decay of a zinc sulfide type of phosphor containing one species of centers and one species of traps. The transition from rapid decay caused by the recombination of the free electrons to the slow decay from the traps is clearly shown by the log I

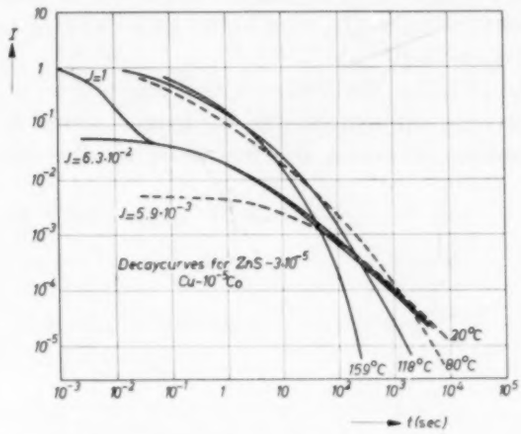

FIG. 2. Decay of fluorescence of ZnS-Cu-Co at various temperatures and initial intensities on log I vs. log t scale.

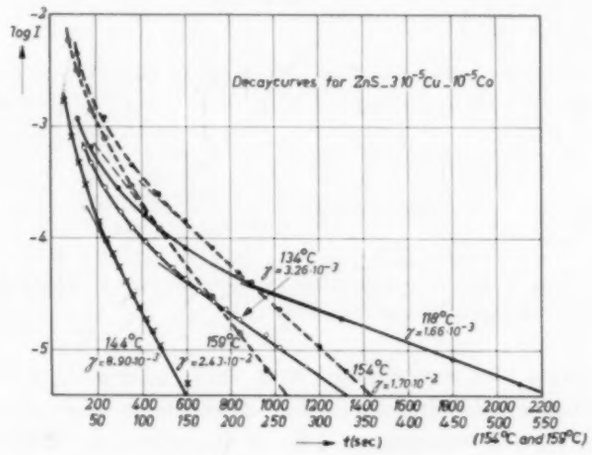

FIG. 3. Decay of fluorescence of ZnS-Cu-Co at high temperatures on log I vs. t scale.

vs. log t curve for J = 1. This transition is not shown by the decay starting from a lower initial intensity. The curves for higher temperature lie above the lower temperature curves during the first part of the decay, but later on they fall off steeply and cross the curves for lower temperatures.

In disagreement with this theory, however, is the behavior of the curves at longer times. Here all curves should tend to become straight lines with slope 2, and the curves at the same temperature should not cross. Instead, the final slope of the curves for room temperature seems to be less than

[2] The effect can also be explained by an increase of the trap depth with a decrease of the number of filled traps (6).

1, while, for high temperatures, slopes appreciably larger than 2 are observed. In fact, the decay at temperatures above 100°C is better represented by a monomolecular law, $I = A \exp -\gamma t$ for longer times (Fig. 3). The decay constants γ are given for various temperatures in Table II and are logarithmically plotted against $1/T$ in Fig. 4. From the straight line going through the points, it is found $\gamma = \gamma_0 \exp -\epsilon_1/kT$ with $\epsilon_1 = 1.1$ ev and $\gamma_0 = 1.3 \cdot 10^{11}$ sec^{-1}. The same behavior of the decay of a ZnS-Cu phosphor at high temperatures was observed by Bube (7), who found an ϵ-value of 1.0 ev and $\gamma_0 = 3 \cdot 10^{10}$ sec^{-1}.

Admittedly, the evidence that the curves of Fig. 3 become monomolecular at longer times is not complete. However, the points on semilog plot fit

there is a higher proportion of traps filled at the start of the decay. Further indications of this effect will be given later.

Temperature Dependence of Fluorescence

The curves showing the fluorescence intensity under steady excitation by 3650 Å as a function of temperature are given in Fig. 5. While the maxima have been normalized in the figure, the relative intensities actually show a strong decrease for increasing cobalt concentrations (Table III). This indicates a strong ineffective absorption by the cobalt impurity. The temperature dependence curves for high Co concentrations are especially interesting as they show a low minimum at 20°C and a maximum at 170°C. The height of the minimum de-

TABLE II. *Monomolecular part of the decay of* ZnS$-(3 \cdot 10^{-5}$ Cu$)-(10^{-4}$ Co)

Temp, °C	118	126	134	139	144	154	159
$\gamma = -\frac{d \ln I}{dt}$ (sec^{-1})	$1.66\ 10^{-3}$	$2.23\ 10^{-3}$	$3.26\ 10^{-3}$	$5.43\ 10^{-3}$	$8.90\ 10^{-3}$	$1.70\ 10^{-2}$	$2.43\ 10^{-2}$

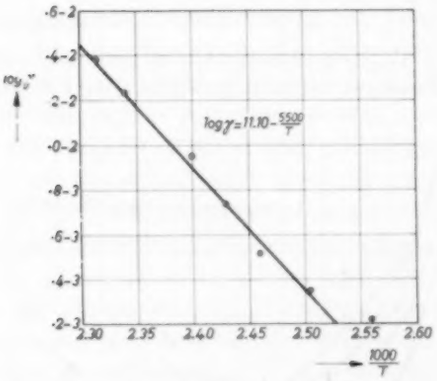

FIG. 4. Decay constants of exponential part of the decay plotted logarithmically against $1/T$.

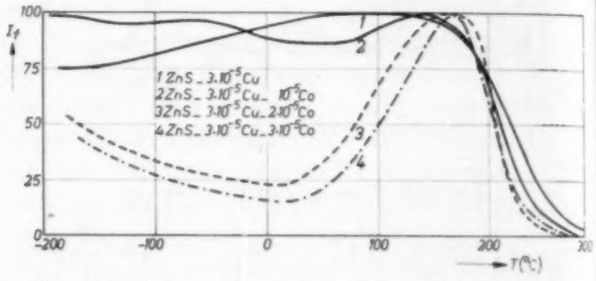

FIG. 5. Relative temperature dependence curves of ZnS$-(3 \cdot 10^{-5}$ Cu$)$-(x Co) at the same intensity of excitation by 3650 Å.

better to a straight line than those on log-log plot. Further, the slopes p on Fig. 2 tend to become quite large, for example, -4.6 for the curve at 159°C, which means that the exponent $\alpha = p/[p-1]$ in a differential equation for the decay of the type $I = -dn/dt = \gamma n^{\alpha}/L^{\alpha-1}$ will be nearly equal to unity. Finally, a strong point of evidence for the monomolecular decay is the fact that the decay constants γ derived from the semilog plots show the expected behavior as a function of temperature, from which an activation energy may be derived which is in agreement with other observations.

Another unexpected effect is the crossing of the decay curves for different exciting intensities. For $t > 200$ sec, the relative position of the three curves is reversed—the phosphorescence is stronger after low excitation than after high excitation. This can only be explained if at lower exciting intensities

creases for increasing cobalt content, so that at equal concentrations of Co and Cu the temperature dependence curve resembles the glow curve. For the descending branch at high temperatures, the often used theoretical formula $1/\eta' - 1 = A \exp -E/kT$ was tried. η' was taken to equal $I_f/I_{f\max}$. This, of course, is a somewhat doubtful procedure; as for the curves with a pronounced maximum it is not known from what level the curve would start if the process causing the minimum were absent. Indeed, the points of log $(1/\eta' - 1)$ vs. $1/T$ on Fig. 6 show a marked departure from the straight line; at high temperature, however, where the choice for $I_{f\max}$ has a lesser influence, the fit is better. So, from the high temperature part of the curves, the values of E and A given in Table IV were found. E has roughly the same value as was found for ϵ_1 from the decay curves.[3]

[3] An activation energy of 1.0 ev for the temperature quenching of ZnS-Cu phosphors was also reported by Yastrebov (8) and Garlick (9).

A decrease of the exciting intensity has two effects on the temperature dependence curve: (*a*) a shift of the maximum and minimum to lower temperatures, and (*b*) a decrease of the minimum relative to the maximum (Fig. 7).

Buildup of the Fluorescence

The buildup of the fluorescence intensity with 3650 Å excitation of ZnS-Cu-Co phosphors is a very slow process, especially if the phosphor is previously "emptied" by heating or infrared. At temperatures between −130° and 20°C the curve

TABLE III. *Relative intensities of* ZnS-$3\cdot10^{-5}$ Cu-Co

Co-conc	3650 Å		2537 Å
	I_{max}	$I_{20°C}$	$I_{20°C}$
0	100	100	100
$3\cdot10^{-6}$	67	67	56
10^{-5}	22	19	17.5
$2\cdot10^{-5}$	5.5	1.5	—
$3\cdot10^{-5}$	2.2	0.5	—

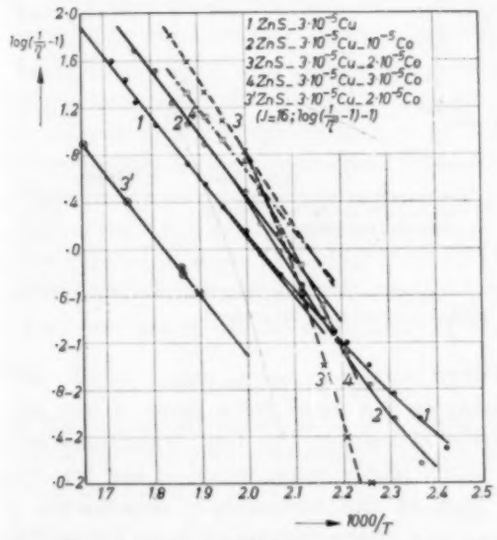

FIG. 6. $(I_{f_{max}}/I_f - 1)$ plotted logarithmically against $1/T$ for the curves of Fig. 5.

starts with a parabolic part, as shown by the curves for −122° and 18°C in Fig. 8. This behavior, which is absent in ZnS-Cu, was also found by Krylova (3). At −196°C, however, the buildup is much faster and starts linearly. After the buildup is completed, a sudden decrease of the exciting intensity causes the effect shown in Fig. 9: the fluorescence drops quickly, reaches a minimum, and then increases slowly to a new equilibrium value. This happens only at temperatures below −20°C and if the ratio of the two exciting intensities is not too small. The simplest explanation of this effect is again the assumption that at high intensities the traps are filled to a lesser degree than at lower intensities. If the intensity is decreased, the traps will accordingly capture some of the free electrons, with a resultant temporary drop of fluorescence intensity below the saturation value.

Buildup of the Light Sum

The light sum in a layer of ZnS-($3\cdot10^{-5}$ Cu)-(10^{-5} Co) was measured at −80°C after different times of excitation by 3650 Å of various intensities.[4]

TABLE IV. *Temperature dependence of* ZnS-$3\cdot10^{-5}$ Cu-Co

Co-conc gram atoms per mole ZnS	$-\frac{d\ln\left(\frac{1}{\eta'}-1\right)}{d(1/T)}$ (ev)	$\left(\frac{1}{\eta'}-1\right)_{T=\infty}$
0	1.01	$1.8\ 10^{10}$
10^{-5}	1.06	$1.4\ 10^{11}$
$2\cdot10^{-5}$	1.39	$7.8\ 10^{14}$
$3\cdot10^{-5}$	1.24	$1.3\ 10^{13}$
$2\cdot10^{-5}$ $(J = 16)$	1.37	$5.2\ 10^{13}$

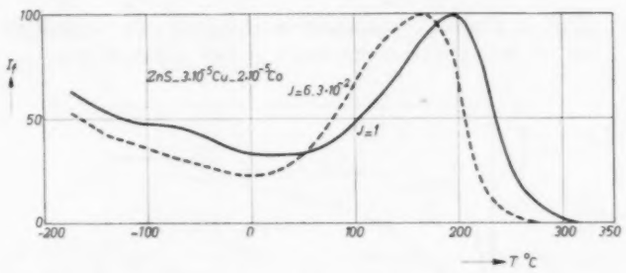

FIG. 7. Relative temperature dependence curves of ZnS−($3\cdot10^{-5}$ Cu)−($2\cdot10^{-5}$ Co) at two intensities of excitation by 3650 Å.

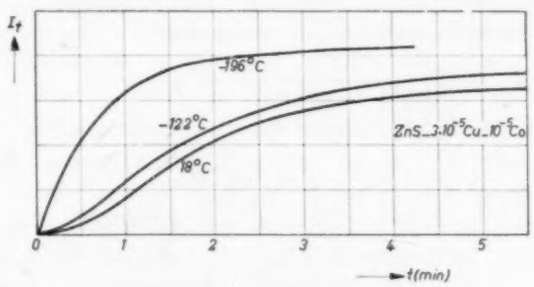

FIG. 8. Buildup of fluorescence of ZnS−($3\cdot10^{-5}$ Cu)-(10^{-5} Co) at various temperatures (excitation 3650 Å).

After excitation the sample was placed in front of a photomultiplier and warmed up at the same rate in all experiments, until the glow had disappeared. The photocurrent charged a condenser, the potential of which was measured by a triode voltmeter. By keeping the temperature during the excitation at −80°C care was taken to measure only the light

[4] The ultraviolet source was a 125-watt high pressure mercury lamp with a Woods glass filter. Infrared radiation was eliminated by a $CuSO_4$ solution. The absolute ultraviolet intensity on the sample was approximately $2\cdot10^{-2}$ watt/cm² for $J = 1$.

sum stored in the cobalt traps. The curves of Fig. 10 show the following results: (*a*) the start of the curves is superlinear as with the previous curves; (*b*) the initial buildup, as measured by the maximum slope, is roughly proportional to the exciting intensity; and (*c*) the steady state value of the light sum increases with decreasing intensity of excitation. The latter effect is the most important one as it

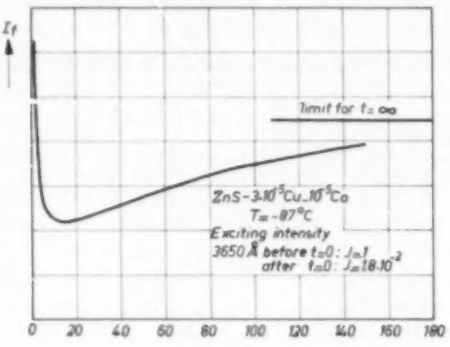

FIG. 9. Course of fluorescence intensity after a sudden drop of the excitation intensity at low temperatures.

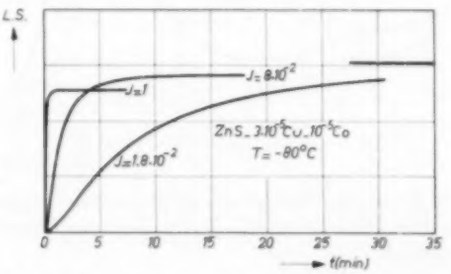

FIG. 10. Buildup of the light sum in ZnS-Cu-Co with excitation by 3650 Å at low temperature.

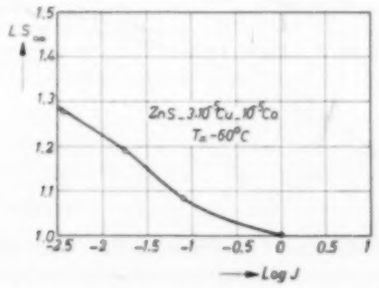

FIG. 11. Saturation value of the light sum in ZnS-Cu-Co at low temperatures as a function of the intensity of excitation by 3650 Å.

gives direct evidence of a property already derived indirectly from other experiments.

The dependence of the light sum on the excitation intensity was also clearly demonstrated by the following experiment. The phosphor was excited for 40 min; first with an intensity $J = 1$ for all 40 min, and then with $J_1 = 1$ for 10 min, and with $J_2 = 2.10^{-2}$ for 30 min. The light sum measured after the latter experiment was 17 per cent higher than that after the former. The relative value of the steady state light sum as a function of log J is shown in Fig. 11. A similar and still larger intensity dependence of the light sum in infrared phosphors was found by Urbach and coworkers (10).

DISCUSSION

For an explanation of the various results reported a very simple model is desirable. A model which is analogous to the one proposed by Schoen (11) for phosphors with killers is used here. Besides a filled and an empty band it contains filled activator levels due to copper and empty trap levels due to cobalt. Fig. 12 shows this band picture with the various transitions needed for interpretation. First consider processes [1], [3], [5], and [7]. Historically the oldest, these transitions represent fluorescence, phosphorescence, and thermal glow in the zone scheme for ZnS phosphors. The release of electrons stored in the traps is governed by the temperature

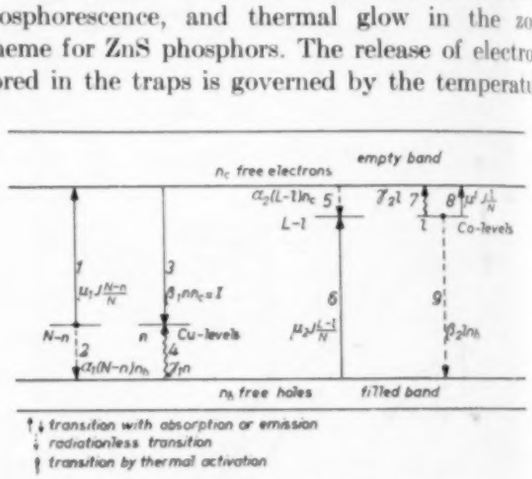

FIG. 12. Energy level diagram of ZnS-Cu-Co with various transitions referred to in text.

dependent factor $\gamma_2 = s_2 \exp -\epsilon_2/kT$, which is probably only a mean for a more or less wide distribution of values. The four transitions indicated give also a partial explanation of the low temperature part of the temperature dependence of the fluorescence. If the number of traps L is of the same order as the number of activator levels N, the capture of electrons by the traps at low temperatures will cause a considerable decrease of the number of unexcited centers. The absorption of the activators is proportional to the latter. This causes a considerable drop of the fluorescence efficiency, provided there is another competing though ineffective absorption process present.[5]

A transition of this kind is, for example, an absorption which raises electrons from the filled band to the trap levels [6], combined with a radiationless return transition [9]. The absorption by cobalt is demonstrated by the reflection spectra of zinc sulfides activated with cobalt alone (1).

Apart from lowering the efficiency of the phos-

[5] A similar explanation of a maximum in the temperature dependence of ZnS-Cu is given by Bube (12).

phor by their ineffective absorption, the cobalt impurities act as killers by contributing to the removal of holes which are created in the filled band by process [4]. This process, like [7], is a thermal transition with a rate constant $\gamma_1 = s_1 \exp -\epsilon_1/kT$. If this factor becomes large at high temperatures, the holes in the excited Cu levels leak away to the filled band, from which they may recombine with unexcited centers via [2], as well as with other disturbance levels, e.g., the filled Co traps. The latter are obviously not the only ones active in this way, for copper-activated zinc sulfides without cobalt are quenched at nearly the same temperature. At high temperatures, transition [4] may be the main factor in decreasing the number of excited Cu levels during the decay, thus causing a monomolecular part of the decay with a decay constant proportional to γ_1.

A final feature in the proposed picture is process [8], the excitation by 3650 Å of electrons from the filled traps to the conduction band. It can be shown that this transition provides an explanation for the intensity dependence of the light sum and its consequences, viz., the crossing of the decay curves, the "undershoot" effect at a sudden decrease of the excitation, and the lower level of the minimum of the temperature dependence curve at reduced intensity. It also explains why the -100°C peak in the glow curve diminishes with increasing amounts of cobalt. For the cobalt traps are only partially filled by excitation even at -180°C, with the result that during thermal glow, electrons escaping from shallower traps will be retrapped by them.

Quantitative Relationships

The mathematical consequences of the model deserve some detailed discussion. The complete equations derived from it are:

$$dn/dt = \mu_1 J(N - n)/N_+ \alpha_1 (N - n) n_h - \beta_1 n n_c - \gamma_1 n \quad \text{(I)}$$

$$dl/dt = \mu_2 J(L - l)/N_+ \alpha_2 (L - l) n_c - \beta_2 l n_h - (\gamma_2 + \mu' J/N) l \quad \text{(II)}$$

$$dn_c/dt = (\gamma_2 + \mu' J/N) l + \mu_1 J(N - n)/N - \alpha_2 (L - l) n_c - \beta_1 n n_c \quad \text{(III)}$$

$$dn_h/dt = \gamma_1 n + \mu_2 J(L - l)/N - \alpha_1 (N - n) n_h - \beta_2 l n_h \quad \text{(IV)}$$

$$n + n_h = l + n_c \quad \text{(V)}$$

$$I = \beta_1 n n_c \quad \text{(VI)}$$

Decay and the thermal glow.—Here there can be introduced an approximation which is valid either after the first few seconds of the decay or with the glow curves for a moderate heating rate. Then $n_c \ll l$, $n_h \ll n$ and it may be assumed that $dn_c/dt = dn_h/dt = 0$. With $J = 0$, this leads to the following simplified equations:

$$n = l \quad \text{(VII)}$$

$$dn/dt = -\frac{\gamma_2 \beta_1 n^2}{\alpha_2 (L - n) + \beta_1 n} - \frac{\gamma_1 \beta_2 n^2}{\alpha_1 (N - n) + \beta_2 n} \quad \text{(VIII)}$$

$$I = \frac{\gamma_2 \beta_1 n^2}{\alpha_2 (L - n) + \beta_1 n} \quad \text{(IX)}$$

It was shown in the experimental part that the decay law becomes exponential at high temperatures. Also, it will be seen that $\gamma_1 \gg \gamma_2$ at high temperatures. Hence the last term of (VIII), which is then predominant, must include a wide range of values where it is proportional to n. This will happen if $\beta_2 n \gg \alpha_1 N$, which is only possible if $\beta_2 \gg \alpha_1$.[6] In order to simplify the equations still further, it is assumed that $\alpha_2 = \beta_1$. Then,

$$\frac{dn}{dt} = -\gamma_2 n^2/L - \gamma_1 n \quad \text{(X)}$$

$$I = \gamma_2 n^2/L. \quad \text{(XI)}$$

With these two equations the decay and the glow curves of the ZnS-Cu-Co phosphors can be understood at least qualitatively. At low temperatures $\gamma_2 \gg \gamma_1$ and the only important term in (X) is $\gamma_2 n^2/L$. This gives a bimolecular law for the decay of the form $I = I_0[1 + (\gamma_2 n_0/L)t]^{-2}$. Actually, owing to a distribution of γ_2 values or to a variation of the trap depth ϵ_2 with the number of trapped electrons (6), a more complicated law must be expected. At high temperatures, however, $\gamma_1 \gg \gamma_2$—although $\epsilon_1 > \epsilon_2$—because $s_1 \gg s_2$; if $\gamma_2 n \ll \gamma_1 L$ the latter term in (X) is predominant. This leads to the decay law $I = I_0 \exp -2\gamma_1 t$, which will hold until n becomes of the order of $\alpha_1 N/\beta_2$. Accordingly, the values of γ from Table II can be identified with $2\gamma_1$, which lead to $\epsilon_1 = 1.1$ ev and $s_1 = 7 \cdot 10^{10}$ sec^{-1}.[7]

The values of ϵ_2 and s_2 may be derived from the glow curves in the following manner. In the rising part of the glow curve the value of n is approximately constant, so the intensity will be proportional to γ_2. The points of log I against $1/T$ for low values of T lie on a straight line giving the ϵ_2 values of

[6] It will happen also if the holes leak away from the Cu levels to other occupied levels further above the occupied band, whose number is large compared with n.

[7] According to Bube (7) the exponential decay with 1.0 ev activation energy would be caused by the emptying of deep traps of that depth. The present view of taking it as a property of the Cu centers agrees with that of Schön (13).

Table I. In order to find s_2 the glow maximum is calculated from (X) and (XI):

$$\frac{dI}{dt} = 2\gamma_2 \frac{n}{L}\frac{dn}{dt} + \frac{n^2}{L}\frac{d\gamma_2}{dt} = 0$$

$$2\frac{dn}{dt} + n\left(\frac{dT}{dt}\right)_g \frac{\epsilon_2}{kT_g^2} = 0$$

$$2\gamma_2 \frac{n}{L} + 2\gamma_1 = \left(\frac{dT}{dt}\right)_g \frac{\epsilon_2}{kT_g^2}$$

With $\epsilon_2 = 0.5$ ev, $T_g = 332°$ K, $(dT/dt)_g = 7.2 \cdot 10^{-2}$ degree/sec and the values of s_1 and ϵ_1 as determined above, it is found:

$$\left(\frac{dT}{dt}\right)_g \frac{\epsilon_2}{kT_g^2} = 3.8 \cdot 10^{-3}; \qquad 2\gamma_1 = 3 \cdot 10^{-6}.$$

The term $2\gamma_1$ may thus be neglected, and if finally $n \sim \frac{1}{2}L$ is taken at the maximum, we have:

$$s_2 \sim \frac{1}{T_g'}\left(\frac{dT}{dt}\right)_g x\, e^x \qquad \text{with} \qquad x = \frac{\epsilon_2}{kT_g}.$$

A check on the calculation is derived from I_g, the measured maximum of I. Thus, $I_g = \gamma_2 n_g^2/L$

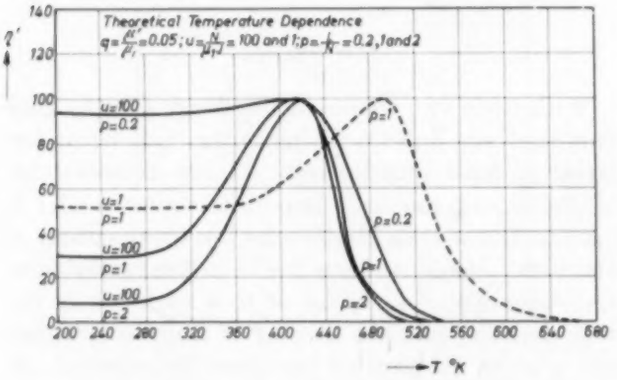

FIG. 13. Theoretical relative temperature dependence curves for ZnS-Cu-Co calculated from formulas (XIIa) and (XIIIa).

and from the intercepts of the log I vs. $1/T$ lines the quantity $I_\infty = s_2 n_0^2/L$ is known. Hence $I_g/I_\infty = (n_g/n_0)^2 e^{-\epsilon_2'/kT_g}$, and taking $n_g \sim \frac{1}{2}n_0$, this gives the values of ϵ_2' of Table I.

It is now easy to understand why at equal concentrations of Co and Cu the height of the glow peak is reduced. Since the number of filled traps can never exceed the total number of centers, the relative number of filled traps is reduced if the ratio Co/Cu increases above 1. There is a general trend of glow peaks to shift to higher temperatures as traps are less completely filled. This is partly due to kinetics, because, with decreasing n^2/L in (XI), γ_2 has to be increased by raising the temperature in order to obtain the same value of I, and partly it is due to a trap depth distribution. A shift of the glow peak to higher temperatures will cause increased temperature quenching of the later stages, and the total light sum will thus be reduced.

Temperature dependence.—For the discussion of the temperature dependence of the fluorescence it is not really permissible to make the assumption that $n_c \ll l$ and $n_h \ll n$. Without this simplification, however, the calculations would become much more complicated. Moreover, the exciting intensities with which the present temperature dependence measurements were carried out were relatively low. Finally, it is desired only to show a qualitative fit of the theoretical curves with the experimental ones. So, in the general equations (I) to (VI) one can put $dn/dt = dl/dt = dn_c/dt = dn_h/dt = 0$, eliminate n_c and n_h, and put $n = l$. As in the previous calculation, we take $\beta_2 l \gg \alpha_1 N$ and for simplicity $\alpha_2 = \beta_1$. This leads to the following equations:

$$\mu_1 J \frac{N-n}{N}\frac{L-n}{L} - \mu' J \frac{n^2}{LN} - \gamma_2 \frac{n^2}{L} - \gamma_1 n = 0 \qquad \text{(XII)}$$

$$I = \mu_1 J \frac{N-n}{N} - \gamma_1 n. \qquad \text{(XIII)}$$

Substituting $n/N = x$, $L/N = p$, $\mu'/\mu_1 = q$, $N/\mu_1 J = u$, and $I/\mu_1 J = \eta$, there results

$$(1 - q - u\gamma_2)x^2 - \{1 + p(1 + u\gamma_1)\}x + p = 0 \qquad \text{(XIIa)}$$

$$\eta = 1 - (1 + u\gamma_1)x. \qquad \text{(XIIIa)}$$

From these equations and the known temperature dependence of γ_2 and γ_1, η can be calculated as a function of T for various values of p (the number of traps), q (the absorption coefficient of the filled trap), and $1/u$ (the exciting intensity). The theoretical curves of $\eta' = \eta/\eta_{max}$ in Fig. 13 show the same qualitative behavior as the experimental ones of Fig. 5 and 7, viz.: (*a*) with increasing Co concentration the low temperature minimum decreases with respect to the maximum, and the descending branch at high temperatures shows a shift to lower temperatures; (*b*) at lower exciting intensity the maximum shifts to lower temperatures and rises with respect to the minimum.

At high temperatures, the first term of equation (XIIa) can be neglected and equations (XIIa) and (XIIIa) reduce to:

$$\frac{1}{\eta} - 1 = p(1 + u\gamma_1) \approx \frac{L}{\mu_1 J} s_1 \exp - \frac{\epsilon_1}{kT}.$$

This is the behavior shown in Fig. 6 from which were found the values of ϵ_1 and $Ls_1/\mu_1 J$ of Table IV. For the temperature dependence of ZnS-($3 \cdot 10^{-3}$

(Cu)-($2 \cdot 10^{-5}$ Co), measured at two intensities, we find indeed that $(1/\eta' - 1)_{\tau=\infty}$ is proportional to $1/J$. Further, a large increase of this value is noticed with increasing Co concentration, which cannot be explained by the increase of L alone. It is probably caused by a decrease of the effective value of J in the deeper layers of the phosphor owing to the strong absorption by Co.

The stationary state.—Finally, the stationary state at low temperatures and high excitation intensities must be considered in order to explain the intensity dependence of the light sum. This might be done by solving the original equations (I) to (VI) with $dn/dt = dl/dt$, etc. $= 0$ and $\gamma_1 = \gamma_2 = 0$. This relatively complicated calculation was performed for the limiting cases of $J \to 0$ and $J \to \infty$. However, it was found that the same result could be obtained more easily by neglecting the processes [2], [6], and [9] of Fig. 12, provided it is assumed that $\beta_2 \gg \alpha_1 \gg \beta_1, \alpha_2$ (with factors of, say, 100). In that case the hole transitions do not disturb the equilibrium brought about by the electron transitions. The equation system then reduces to:

$$\mu_1 J(N - n)/N = \beta_1 n n_c \qquad \text{(XIV)}$$

$$\mu' J\, l/N = \alpha_2(L - l)n_c \qquad \text{(XV)}$$

$$n = l + n_c\,. \qquad \text{(XVI)}$$

Eliminating n and n_c and using the abbreviations

$$z = l/L, \qquad y = \frac{\mu_1 J}{\beta_1 N^2}, \qquad L/N = p,$$

$$\mu'/\mu_1 = q, \qquad \alpha_2/\beta_1 = r, \qquad \text{and} \qquad r/q = \lambda$$

$$y = \lambda \frac{1 - z}{z}\left(\frac{p(\lambda - 1)z^2}{\lambda - (\lambda - 1)z} - \frac{(p + 1)\lambda z + \lambda}{\lambda - (\lambda - 1)z}\right) \qquad \text{(XVII)}$$

$$\frac{n_c}{L} = \frac{y}{p\lambda}\frac{z}{1 - z} = \frac{p(\lambda - 1)z^2 - (p + 1)\lambda z + \lambda}{p\lambda - p(\lambda - 1)z}\,. \qquad \text{(XVIII)}$$

The term $p(\lambda - 1)z^2 - (p + 1)\lambda z + \lambda$ in (XVII) has always one root between 0 and 1, which may be called z_0. This is the only physically interesting z value for which $y = 0$. For $z = 0$, $y = \infty$, thus with increasing J the fraction of filled traps decreases from a value of generally less than 1, to zero. This, however, is not the same as the light sum which is present in the phosphor after the excitation is stopped. During the excitation, there are free electrons in the conduction band whose number n_c can be calculated from equation (XVIII). When the excitation ceases, these free electrons will be distributed among the empty trap and activator levels. This process is governed by the two equations:

$$dn/dt = -\beta_1 n n_c \qquad \text{(XIX)}$$

$$dl/dt = \alpha_2(L - l)n_c\,. \qquad \text{(XX)}$$

Dividing (XIX) by (XX):

$$\frac{dn}{dt} = -\frac{\beta_1}{\alpha_2}\frac{n}{L - l} = -\frac{1}{r}\frac{n}{L - l},$$

and

$$\frac{n^r}{L - l} = \text{const.} \qquad \text{(XXI)}$$

When the number of free electrons is exhausted after a short time, the new values of n, l, etc., which

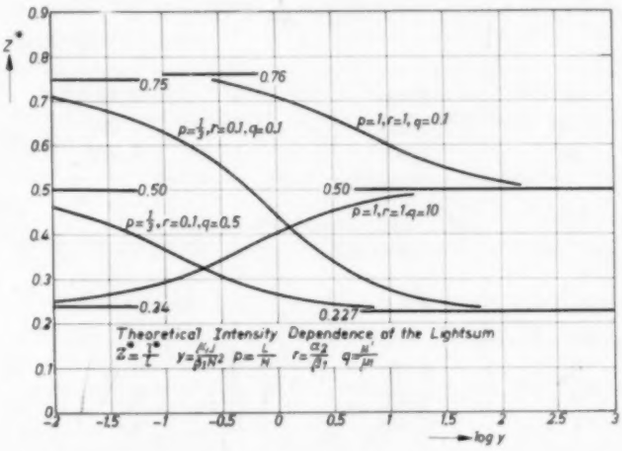

FIG. 14. Theoretical intensity dependence of the relative light sum z^* calculated from formulas (XVII), (XVIII), and (XXII).

will be designated by n^*, l^*, etc., can be calculated from (XXI) in terms of the values during excitation. With $n_c^* = 0$, $n^* = l^*$, and $z^* = l^*/L$ it is found

$$\frac{(z^*)^r}{1 - z^*} = \frac{\left(z + \frac{n_c}{L}\right)^r}{1 - z}\,. \qquad \text{(XXII)}$$

As a special case for $J = \infty$, $z = 0$, and $n_c = N$. Thus:

$$(pz_\infty^*)^r + z_\infty^* - 1 = 0. \qquad \text{(XXIII)}$$

While for $J = 0$, n_c becomes zero which leads to $z_0^* = z_0$.

If J increases from zero to infinity, the measurable light sum in the cobalt traps varies thus from z_0 to z_∞^*. In order to calculate intermediate values, we have to take a certain z, calculate y and n_c from (XVII) and (XVIII), and find the corrected z^* from (XXII). The results of some of these calculations for different values of the parameters p, r, and q are shown in Fig. 14. In Table V, values

of z_0 and z_∞^* and their ratios are given. For large q there is an increase instead of a decrease of the light sum with increasing J, especially with high r. Low r gives very small light sums, whereas with high r the traps are always nearly completely filled. The exciting intensity at which the variation of z^* becomes noticeable is roughly proportional to $\lambda = r/q$. From the present experiments with $p = \frac{1}{3}$ it is found $z_0/z_\infty^* > 1.3$; since the exciting intensities were relatively low, we can estimate the most probable values of the parameters, viz., $0.1 < q < 1$ and $r \sim 0.1$.

TABLE V. *Theoretical trap occupancy at low temperatures for $J = 0$ and ∞*

$p = 0.5$	$z_0; \frac{z_0}{z_\infty^*}$						z_∞^*
r \ q	0.1		1		10		
10^{-2}	0.128	21.9	$4.32\ 10^{-2}$	7.40	$1.40\ 10^{-2}$	2.40	$5.84\ 10^{-3}$
1	0.921	1.38	0.667	1.00	0.333	0.500	0.667
10^3	$1-10^{-4}$	$\lesssim 1$	0.999	0.999	0.990	0.990	1.000
$p = 0.33$	$z_0; \frac{z_0}{z_\infty^*}$						z_∞^*
r \ q	0.1		0.5		1		
0.1	0.75	3.30	0.50	2.20	0.396	1.75	0.227
0.5	0.918	1.62	0.75	1.33	0.65	1.15	0.565
1	0.955	1.27	0.84	1.12	0.75	1.00	0.750

Summary and Conclusion

The phosphor ZnS-Cu-Co provides a system for which the simple band picture with activators and independent traps is valid. Moreover, all transition processes that are theoretically possible in such a model are found in this case. In summary, there are the absorption [1] and emission [3] for the activator levels, which are obvious for a luminescent substance; for the Co levels there are transitions [6] and [9] of the same kind, causing the killing properties;[8] we find the capture [5] and thermal release [7] of the electrons by these same levels, which are then functioning as traps, leading to the phosphorescence and glow phenomena; further, there are the equivalent transitions [2] and [4] at the activator levels, which give rise to the thermal quenching and to the exponential decay at high temperatures. Finally, the picture is completed with absorption transitions of trapped electrons to the empty band [8], and of holes from activator levels to the filled band. This latter process has not yet been mentioned as it did not play a part in the phenomena studied; its existence, however, is very well known, for it causes the infrared quenching and stimulation of copper-activated zinc sulfides. Melamed (14) found the same quenching spectrum for ZnS-Cu-Co, Ni, or Fe with maxima at 0.78 and 1.3 μ. Irradiation in the same region causes stimulation of ZnS-Cu-Pb or Mn (15, 16). Finally, Antonov-Romanovskii (17) reports an increase of the absorption of ZnS-Cu-Co on excitation by 3650 Å in three spectral regions, viz., at 0.45, 0.8, and 1.3 μ. The latter two cause quenching, while the 0.45 μ band must obviously be identified with the absorption [8] reported here. The fact that a filled trap with a thermal activation energy of only 0.5 ev shows an absorption for 3650 Å radiation is certainly surprising. In a private communication to the authors, Kroeger pointed out that this discrepancy is removed if it is assumed that the liberation of an electron from the Co trap occurs indirectly in the following way. In ZnS-Cu-Co the cobalt is most probably incorporated in form of Co^{2+} ions at Zn sites, which by trapping electrons are transformed into Co^+ ions. The trapping of a free electron by the cobalt trap may accordingly be formulated by the reaction:

$$Zn^+ + Co^{2+} \rightarrow Zn^{2+} + Co^+ + \epsilon_2. \qquad (a)$$

It has been shown (1, 2) that a monovalent positive ion X^+ in zinc sulfide gives rise to a filled level somewhat above the filled band. This level is a disturbed S^{2-} level from the filled band and may be indicated as $S^{2-}(X^+)$. In zinc sulfide phosphors activated by silver or copper the activator levels are thus due to Ag^+ or Cu^+ ions. In the same way the filled Co trap will produce a filled $S^{2-}(Co^+)$

[8] If the empty levels are due to other impurities instead of cobalt, these transitions may also give rise to an emission (1).

level, from which, as with the normal activator levels, an electron may be excited to the conduction band by ultraviolet or blue light. This excitation is formulated by the reaction:

$$S^{2-}(Co^{+}) + Zn^{2+} + h\nu \rightarrow S^{-}(Co^{+}) + Zn^{+}. \quad (b)$$

The state symbolized by $S^{-}(Co^{+})$, which represents an empty level below the filled trap level, is not stable, but will spontaneously be transformed into $S^{2-}(Co^{2+})$ with the liberation of a certain amount of energy:

$$S^{-}(Co^{+}) \rightarrow S^{2-}(Co^{2+}) + W. \quad (c)$$

With $S^{2-}(Co^{2+})$ the original state of the Co^{2+} ion in which the trap is empty is restored, while at the same time the disturbed S^{2-} level has disappeared. Thus the net effect of the processes (*b*) and (*c*) is identical with that of a direct transition of an electron from Co^{+} to the conduction band, the result being an empty trap and a free electron in both cases.

The energy W liberated in transition (*c*) may either be radiated as fluorescence, or it may be used to bring the Co^{2+} ion, which is re-formed in the process, into one of its characteristic excited states. Considering what happens in a ZnS-Mn phosphor (18), the latter possibility is the most probable one. The energy of the excited Co^{2+} ion may then finally be radiated as fluorescence deep in the infrared, or it may be annihilated radiationless as happens in all phosphors above a certain critical temperature.

Several authors (11, 19–21) have previously advocated the concept of empty levels for the killers in order to explain the strong intensity dependence of killed phosphors, which was not correctly accounted for by the theory of filled killer levels of Wise and Klasens (22).

Arpiarian (21) mentions the fact that Co produces traps, but he rejects their identification with the killer levels, using the argument that ZnS-Cu-Co phosphors show no infrared stimulation. The absence of this, however, is clearly understood by the much stronger infrared quenching caused by the transition of holes from copper levels to the filled band. Moreover, at low temperatures where the quenching with infrared radiation is strongly reduced, infrared stimulation of ZnS-Cu-Co phosphors was indeed found.

Some of the experimental phenomena with ZnS-Cu-Co, e.g., the monomolecular part of the decay together with the high temperature glow peak, are partially due to the behavior of the two thermal release factors γ with temperature. Owing to the fact that in one of the γ factors a high value of s is combined with a high value of ϵ, and in the other a low value of s with a low value of ϵ, the values of γ_1 and γ_2 cross at a temperature of 220°C. Below this temperature we find mainly phosphorescence; above it, quenching occurs. Another factor determining the properties of the phosphor is the relative magnitude of the various recombination constants. From the correlation between s and α derived from the consideration of the equilibrium of electrons (or holes) between donor (or acceptor) levels and the nearest band, giving $s/\alpha = 2(2\pi m^{*}kT)^{3/2}/h^{3} \approx 10^{19}$, the values $\alpha_1 \sim 5\cdot10^{-9}$; $\alpha_2 \sim 5\cdot10^{-15}$ can be obtained. It is also estimated from the intensity dependence of the light sum that $\beta_1 \sim 10\alpha_2$ and that $\beta_2 \gg \alpha_1$. This leads to the following order of magnitude for the values of β: $\beta_1 \sim 5\cdot10^{-14}$, $\beta_2 \gtrsim 10^{-7}$. Apparently the cross section for the capture of holes by a center is much larger than that for electron capture.

Any discussion of this paper will appear in a Discussion Section, to be published in the June 1954 issue of the JOURNAL.

REFERENCES

1. H. A. KLASENS, *J. Electrochem. Soc.*, **100,** 72 (1953).
2. W. HOOGENSTRAATEN, *J. Electrochem. Soc.*, **100,** 356 (1953).
3. E. S. KRYLOVA, *Dokl. Ak. Nauk S.S.S.R.*, **64,** 495 (1949).
4. F. A. KROEGER, J. E. HELLINGMAN, AND N. W. SMIT, *Physica*, **15,** 990 (1949).
5. H. A. KLASENS AND M. E. WISE, *Nature*, **158,** 483 (1946).
6. M. E. WISE, *Physica*, **17,** 1011 (1951).
7. R. H. BUBE, *Phys. Rev.*, **80,** 655 (1950).
8. V. A. YASTREBOV, *J. Exp. Theoret. Phys. U.S.S.R.*, **17,** 140 (1947).
9. G. F. J. GARLICK AND A. F. GIBSON, *J. Opt. Soc. Amer.*, **39,** 935 (1949).
10. F. URBACH, H. HEMMENDINGER, AND D. PEARLMAN, Solid Luminescent Materials, Symposium at Cornell University, p. 279 (1948).
11. M. SCHOEN, *Z. Naturforsch.*, **6a,** 251 (1951)
12. R. H. BUBE, *Phys. Rev.*, **81,** 633 (1951).
13. M. SCHOEN, *Naturwissenschaften*, **31,** 203 (1943); **38,** 235 (1951).
14. N. F. MELAMED, *J. Electrochem. Soc.*, **97,** 33 (1950).
15. G. R. FONDA, *J. Opt. Soc. Amer.*, **36,** 382 (1946).
16. D. PEARLMAN, N. R. NAIL, AND F. URBACH, Solid Luminescent Materials, Symposium at Cornell University, p. 358 (1948).
17. V. V. ANTONOV-ROMANOVSKII AND I. P. SHCHUKIN, *Dokl. Ak. Nauk S.S.S.R.*, **71,** 445 (1950).
18. F. A. KROEGER, "Some Aspects of the Luminescence of Solids," p. 234, Elsevier Press, Inc., Houston (1948).
19. N. R. NAIL, F. URBACH, AND D. PEARLMAN, *J. Opt. Soc. Amer.*, **39,** 690 (1949).
20. S. ROBERTS AND F. E. WILLIAMS, *J. Opt. Soc. Amer.*, **40,** 516 (1950).
21. N. ARPIARIAN AND D. CURIE, *Compt. rend.*, **234,** 75 (1952).
22. M. E. WISE AND H. A. KLASENS, *J. Opt. Soc. Amer.*, **38,** 226 (1948).

Anodic Formation of Coatings on Magnesium, Zinc, and Cadmium[1]

KURT HUBER

Institute for Inorganic, Analytical and Physical Chemistry, University of Berne, Berne, Switzerland

ABSTRACT

A report is given of recent investigations of anodically formed coatings on magnesium, zinc, and cadmium in NaOH and Na_2CO_3 solutions. The growth of the coatings was followed by means of x-ray and electron diffraction and electron microscopy. It was found that the metal oxide was favored as initial product. Depending upon the relative magnitude of the solubility products, the coatings remained in the form of oxides or were converted into the respective hydroxides or carbonates. The semiconductance of the initial coatings was significant in determining the electrochemical behavior of the electrodes.

INTRODUCTION

For more than 100 years, it has been a matter of active controversy as to whether the passivity of metals is brought about by the formation of a coating (or film), or by a change in the nature of the metal or of its surface caused by action of the passivating agent. Recently, the general tendency has been to favor the theory which considers the formation of coatings as responsible; however, the opposing point of view still has its representatives.

Metals can be rendered passive by purely chemical action; on the other hand, the passivation of metals by anodic treatment in the appropriate solutions is particularly effective. Such anodic passivation can be more readily investigated.

The investigation of anodic passivation has usually proceeded along the lines of successive refinement of the electrical measurements. An equally suitable method, although less often encountered, has been employed by Evans and his school, and consists of examining the coatings so formed with all available means and then comparing the results of these investigations with the electrochemical behavior of the electrode. In this report, the behavior of magnesium and zinc is briefly described, followed by a somewhat more comprehensive discussion of the behavior of cadmium. These metals are particularly suitable for such studies since the anodically formed coatings can be readily isolated by means of a procedure based upon the solubility of these metals in mercury. A suitable carrier substance, paraffin, for example, is coated over the passive, film-coated metal. The metal is then placed on mercury in which it dissolves, leaving the coating attached to the carrier substance. After transfer to a suitable support, the carrier substance is removed by solvent action.

[1] Manuscript received July 30, 1952. This paper was prepared for delivery before the Philadelphia Meeting, May 4 to 8, 1952.

The disadvantage of this method lies in the fact that it can only be used for those metals which are readily soluble in mercury. These metals which may be classified as "normal" in contrast to the "inert" metals (1) differ from the latter in other characteristics, such as melting point, heat of sublimation, hardness, metal overvoltage, hydrogen overvoltage, catalytic effectiveness, etc. Therefore, any regularities observed in the behavior of these mercury-soluble metals may not necessarily be applicable to all other metals.

The electrolysis is performed in a simple apparatus. The anode consists of a rod or sheet of the metal to be investigated; the electrolyte is a solution of alkali hydroxide or carbonate, and the cathode is usually of platinum sheet (except in the case of zinc/alkali hydroxide where a zinc cathode is more advantageous because of the anodic solubility of the metal). Increasing voltages are applied to this cell by means of a potentiometric set-up, and curves showing the dependence of the anodic current density upon the cell voltage are thus obtained. The course of these curves depends primarily upon the behavior of the anode. Following this procedure, electrolysis is carried out for various constant values of cell voltage for various periods of time. The coatings formed in this manner are then compared with the electrochemical behavior of the anode.

EXPERIMENTAL RESULTS

Magnesium (2)

Magnesium in 1*N* NaOH gives the curve in Fig. 1. A short active ascent is followed by a region of passivity, with a cell voltage between approximately 0.5 and 3 v, then a longer ascent between 3 and 20 v and finally an extended region of passivity until 50 v (5 ma/cm^2). The course of the curve is not reproducible above 50 v.

Between 0.5 and 3 v, a very thin, light gray coat-

ing is formed on the magnesium anode, between 3 and 20 v a thicker, dark gray coating appears with simultaneous evolution of oxygen. Between 20 and 50 v either a smooth, light gray, firmly adherent coating is formed, if the region is reached by gradually increasing the voltage, or an invisible thin coating, if the high cell voltage is applied immediately.

Only hydroxide can be detected if the applied voltage lies in the range which quickly produced thick coatings. Such coatings were investigated by x-rays. It proved possible to produce thin coatings on the passive electrode which, after isolation, were penetrable by electrons. The electron diffraction photographs of such thin layers with a formation period of 1 to 2 minutes show primarily oxide lines. After periods of formation longer than 2 minutes, hydroxide lines appear and the coatings no longer penetrable by electrons revealed only hydroxide lines. These facts indicate that the oxide is formed as initial product on the passive electrode, but that the

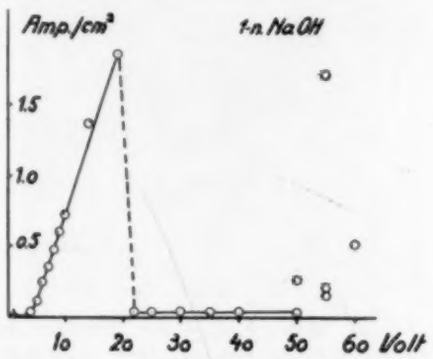

FIG. 1. Current-voltage curve for Mg in 1*N* NaOH

oxide is then quickly converted into hydroxide. Obviously the oxide is also present directly in contact with the metal in the thicker coatings but can no longer be detected in the diffraction photographs because of the relatively small amount on hand.

Zinc (3)

Fig. 2 shows current-voltage curves of zinc in solutions of alkali hydroxide and alkali carbonate. In solutions of sodium hydroxide, at lower voltages zinc at first passes actively into solution. A loose white coating precipitates on the electrode after continued electrolysis under these conditions. When a definite anodic current density is attained, the voltage suddenly jumps to the branch of the curve representing oxygen evolution. Simultaneously, a dark coating is formed on the electrode which can grow to a thickness of several microns if the electrolysis is carried out for an extended period of time.

The necessary voltage for anodic polishing lies between the voltage given by the active branch of the curve and that at which oxygen evolution takes place. These conditions can be attained by use of a bath concentration considerably higher than 1*N* and a small external circuit resistance. Under these circumstances, the metal surface is also covered with a passivating coating, but the voltage is insufficient for the discharge of gaseous oxygen (4).

The course of the curve for zinc in sodium carbonate solution is completely different. An active branch of the curve is scarcely to be observed and the current density remains small with increasing voltage. The electrode becomes a "barrier-electrode." A thin, colorless coating forms on the surface of the electrode during the electrolysis. Higher current densities temporarily appear only when voltages are reached corresponding to the current increase associated with the evolution of oxygen in the case of zinc in sodium hydroxide solution. Simultaneously,

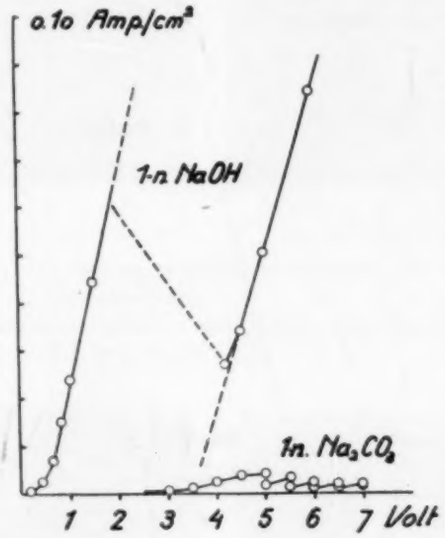

FIG. 2. Current-voltage curve for Zn in 1*N* NaOH and 1*N* Na_2CO_3.

a darkening of the color of the coating can be observed.

The precipitate formed on the active zinc anode in sodium hydroxide solution consists of γ-zinc hydroxide and a small quantity of colorless oxide. On the other hand, the coating formed on the passive electrode proves to be zinc oxide, independent of the stage of development and independent of the electrolyte. This is revealed by electron diffraction examination of the thinner coatings and x-ray analysis of the thicker ones. The different anodic behavior of zinc in solutions of sodium hydroxide and sodium carbonate does not, therefore, depend upon the fact that coatings of various compounds are formed, but rather that, depending upon the electrolyte, zinc oxide with different characteristics is produced.

In sodium hydroxide solution, a zinc oxide is formed which is colored dark due to the presence of an excess of zinc.[2] This is in accordance with the

[2] See Ref. (3), especially *Helv. Chim. Acta*, **27**, 1443 (1944).

noticeable electron conductance evidenced by this coating. On the other hand, the light colored zinc oxide formed in sodium carbonate solution scarcely conducts a current at all.

An attempt was made to measure the coating resistance in the cell zinc/oxide coating/mercury;[3] such measurements are rather difficult because even slight traces of moisture increase the conductance by several powers of ten. The following experimental facts are valid in respect to the dark colored coatings.

(*a*) The conductance increases with increasing voltage (2 to 48 v).

(*b*) The cell possesses definite rectifying characteristics. The resistance is about 10 times higher when the zinc is positive, that is, anodic.

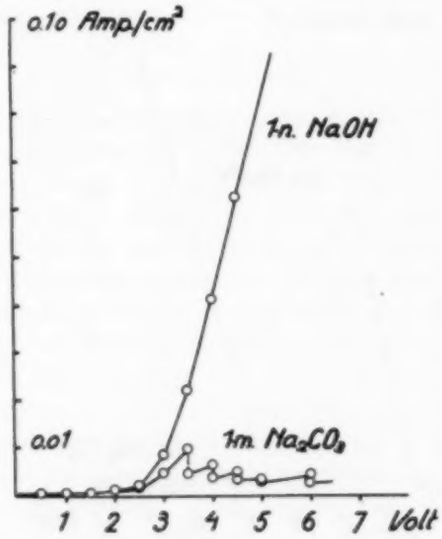

FIG. 3. Current-voltage curve for Cd in 1*N* NaOH and 1*N* Na_2CO_3.

(*c*) The resistance of the coatings is a function of time. If the zinc is the positive electrode, the resistance first passes through a maximum value, then through a flat minimum, and after ¼ hr slowly increases in value again. If the zinc is negative, the current changes only in the first few minutes and then remains approximately constant.

In spite of the uncertainty of these measurements, the resistance of the dark and light colored coatings definitely differs. The resistance of 1 cm² of the dry dark coating is on the average 10,000 to 100,000 ohms, while that of the lighter coating, although 10 to 100 times thinner, is several powers of ten greater. Therefore, the behavior of the zinc anode in the various baths used appears to be a question of semiconductance of the zinc oxide.

The structure of such coatings is equally important. It follows from the steep branch of the curve representing evolution of oxygen that after passivation of zinc in sodium hydroxide the coating resistance can have a value of only a few ohms. (This branch of the curve runs approximately parallel to the portion representing active zinc passing into solution.) Measurements gave a value of 6 to 8 ohms per cm².

A comparison of these measurements with those performed on the dry coating shows that only a small portion of the electrolyte-permeated coating is effective in offering resistance. Other observations indicate that the resistance-offering portion of the coating consists of a primary layer in contact with the metal. In the outer porous part of the coating, the current is conducted by the infiltrating electrolyte. (Based on the volume of the pores and the conductance of the electrolyte, the resistance of the porous portion of the coating is estimated to be less than 1 ohm.)

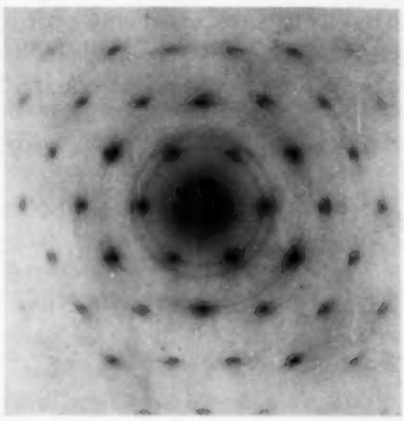

FIG. 4. Cd/2*N* KOH, 4 v, 30 sec. Electron diffraction diagram of an isolated coating. Only hydroxide interferences.

The light oxide coating formed in the carbonate baths is indeed much thinner (10 to 100 times), but it is not porous. This fact, in conjunction with the much smaller specific conductance of the coating, prevents any active oxygen evolution from taking place.

Cadmium (5)

The course of the current-voltage curves for a cadmium anode (Fig. 3) in solutions of sodium hydroxide and sodium carbonate is similar to that of the zinc anode in the corresponding solutions.

The main difference between these curves is to be found in the fact that no branch of the curve appears, representative of active cadmium passing into solution in sodium hydroxide. This is understandable because cadmium does not form the stable hydroxide complexes that zinc does. Therefore, cadmium oxide or cadmium hydroxide is much less soluble in sodium hydroxide than the corresponding

[3] See Ref. (3), especially B. Bieri, Diss. Berne (1949).

inc compounds. Cadmium hydroxide cannot be electrolytically polished in solutions of sodium hydroxide for this reason.

In solutions of sodium carbonate, a temporary increase in current density takes place as in the case of zinc (but even more pronounced) when the discharge voltage of oxygen is reached.

X-ray and electron diffraction investigations (Fig.) reveal principally only cadmium hydroxide in coatings formed on cadmium in sodium hydroxide, regardless of widely varied experimental conditions. Coatings were prepared ranging in thickness from a few hundred Å to 30 μ, in baths of 0.3 to 13N sodium or potassium hydroxide between temperatures of 5° to 100°C with cell voltages of 1 to 6 v and with periods of electrolysis ranging from a few seconds to hr.)

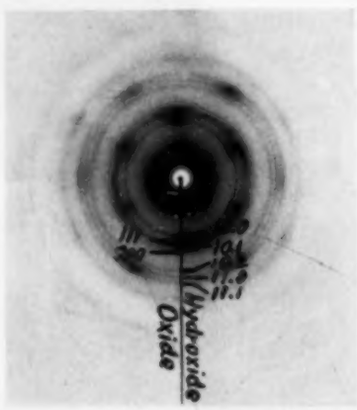

Fig. 5. Cd/2N NaOH, 4 v, 5 sec. Rinsed immediately after formation with absolute alcohol. Electron diffraction diagram of an isolated coating. Oxide interferences beside the hydroxide lines.

Extremely thin coatings with a formation period of 5 sec occasionally yield electron diffraction photographs containing oxide interference spots (Fig. 5). These are obtainable only if the electrode is immediately removed after current interruption and rinsed with absolute alcohol.

Electron microscope photographs of the coating in various stages of growth furnish a deeper insight into the nature of its structure. Fig. 6a shows the surface of an etched crystallite of cadmium (base approximately parallel to the surface) and Fig 6b the same crystallite after treatment for 30 sec at 4 v in 2N sodium hydroxide. The surface is covered with an apparently coherent film which is strewn with a great number of tiny hexagonal crystals of cadmium hydroxide. Fig. 7 represents the same situation for a differently oriented metal crystallite. The coherent coating appears in this case to have broken loose at various protruding places of the less level metal surface.

The hydroxide crystals frequently have a favored position of orientation depending upon the orientation of the underlying metal crystallites. This is particularly evident in Fig. 8 and 9 for anodic treatment carried out under identical conditions for 5 min. The former shows a place where the hydroxide plates lie principally parallel to the surface of the parent metal, and the latter where they stand perpendicular to the surface of the metal.

Fig. 6a.

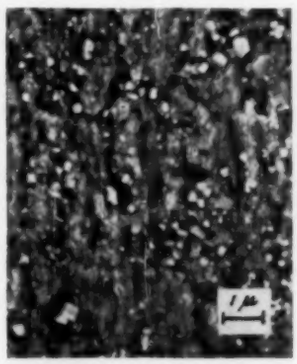

Fig. 6b.

Fig. 6a. Cd, surface of etched crystallite (electron micrograph by replica technique).

Fig. 6b. Same crystallite as in Fig. 6a after anodic treatment. 2N NaOH, 4 v, 30 sec.

Fig. 7a.

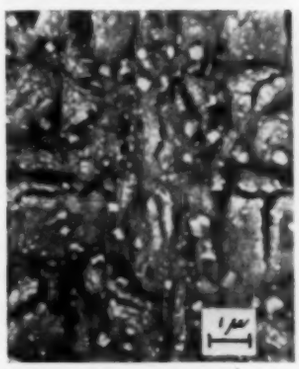

Fig. 7b.

Fig. 7a. Same as 6a for a differently oriented crystallite.

Fig. 7b. Same as Fig. 6b for a differently oriented crystallite.

Such idiomorphic crystals cannot be formed directly during the growth of the coating and it must be assumed that they are created indirectly through the solution. However, the anode is blocked for the active electrode process, i.e., dissolution of cadmium. The metal cannot be bare between the hydroxide crystals as oxygen evolution takes place simultaneously on the electrode. In this connection it is suggested that oxygen evolution can take place only on a film-coated electrode, since in general the free energy of oxidation of the metal is negative. Thus

oxidation must take place more readily than oxygen evolution itself.

It follows from the steep ascent of that branch of the current-voltage curve in which oxygen evolution takes place that the coating must be a good electron conductor with a maximum resistance of a few ohms per cm². It is obvious that, if the hydroxide crystals were to join together in a compact coating, the resistance would be much higher than that observed. Therefore, it is reasonable to suppose that the metal is covered with a thin, unstable coating. The electronic conductance of this coating is sufficiently great to permit the discharge of oxygen; the instability brings about the recrystallization through the medium of the solution, thus causing the formation of the tiny hydroxide crystals.

FIG. 8.

FIG. 9.

FIG. 8. Cd/2*N* NaOH, 4 v. Hydroxide crystals principally parallel to the metal surface.

FIG. 9. Cd/2*N* NaOH, 4 v. Hydroxide crystals perpendicular to the metal surface.

Fig. 10 is of particular interest from this standpoint. This picture represents an isolated coating through which an electron stream has been transmitted in contrast to the surface as in the other photographs. The coating is impenetrable for the greater part because of the high atomic number of cadmium, but in the middle of the picture between thicker portions of the hydroxide coating there is an electron-penetrable film on which a few tiny crystals of hydroxide are lying. This film can well be the effective primary coating.

The author's investigations have revealed that the initial coating formed on various metals in various electrolytes consists of the oxide. The evidence offered by the electron diffraction photographs of very thin coatings formed on cadmium appears to indicate that the initial product is oxide in this case also. Additional evidence is furnished by the coloration of the coating: cadmium oxide is brown to black, cadmium hydroxide is colorless. Thin coatings vary in color from brown to black depending upon the conditions of formation; thicker coatings are only somewhat yellow on the outer surface, but the inner surface which has been in contact with the metal is always still dark colored.

In thicker coatings such as are formed after anodic treatment for ¼ hour and more, the orientation of the hydroxide disappears. Fig. 11 shows the x-ray photograph of the coating of a single crystallite. No Laue spots can be observed, or even a fiber diagram, but rather completely regular Debye-Scherrer rings. The electron microscope photographs

FIG. 10. Cd/2*N* KOH, 4 v, 30 sec. Isolated coating in the transmitted electron beam. In the middle of the picture, thin primary film.

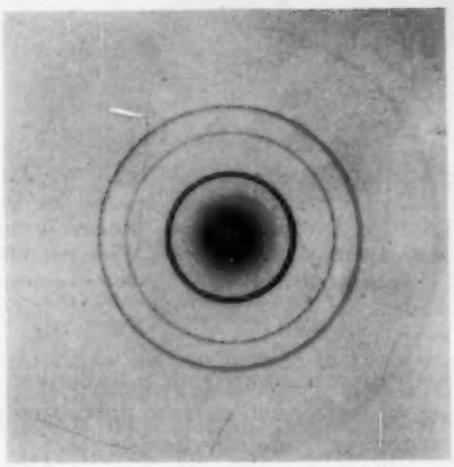

FIG. 11. Cd/2*N* KOH, 4 v, 25 min. X-ray diffraction diagram of an isolated coating of a single crystallite.

of the coating surface also reveal that there is no no longer any favored orientation of the tiny crystals.

The formation of anodic coatings on cadmium in sodium carbonate solution presents a similar picture. A fine, coherent, flexible skin is obtained by isolating a thin coating (formed at 3 v in 2*N* sodium carbonate solution for 30 minutes) with the mercury process. The thickness of such a coating can only be a fraction of a micron, as several square centimeters of surface yield only approximately ¼ mm³ of substance. X-ray diagrams indicate cadmium oxide without any doubt. Two diffuse reflections appear in the diagrams of somewhat thicker coatings in addition to the oxide

FIG. 12.

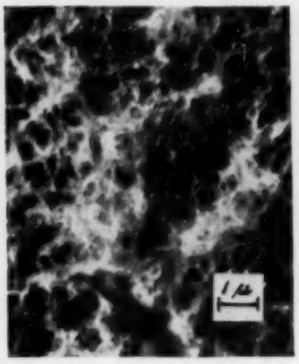

FIG. 13.

FIG. 12. Cd/2*N* Na_2CO_3, 3 v, 10 min. Coating consisting principally of oxide.

FIG. 13. Cd/2*N* Na_2CO_3, 3 v, 55 min. Formation of fibrous basic carbonate.

FIG. 14. Cd/2*N* Na_2CO_3, 5 v, 100 ft. Aggregates of normal carbonate between fibrous basic carbonate.

The morphological appearance of the basic carbonate and especially the normal carbonate indicates the secondary formation of these substances through the medium of the solution. The initial passivating film cannot consist of carbonate.

Therefore, the formation of the coating follows the following course. The oxide is first formed as the passivating film. This coating is converted, first to basic, and then to neutral carbonate by purely chemical means through contact with the electrolyte.

The coatings conduct appreciably when the evolution voltage for oxygen is reached. This conductance is only temporary and diminishes within a few minutes. The comparison of electrical and morphological observations indicates that the conductance of the coating diminishes sharply before appreciable quantities of basic or even of neutral carbonate can be detected. It follows from this that the oxide film only possesses a considerable conductance when in the form of the thinnest coating and becomes an insulator in the thicker coatings, while the products of the carbonation have scarcely any effect on the electrochemical behavior of the electrode.

SUMMARY AND DISCUSSION

In summary, see Table I [for details, see Ref. (6) and (7)].

In the passivation of magnesium in sodium hydroxide solution, oxide is first formed on the surface of the electrode although this product is quite unstable in comparison to hydroxide. The initially formed oxide is then later converted through the influence of the electrolyte into hydroxide. The solubility products can be selected as a measure of stability, the values being 10^{-6} and 10^{-11} for the oxide and hydroxide, respectively. The values given are only correct to an order of magnitude because values in the literature show little consistency, and, in addition, active states may appear which are considerably higher in energy than the stable forms. At any rate, the values which interest us differ so greatly from one another that a consideration of the order of magnitude alone is quite sufficient.

γ-zinc hydroxide precipitates on the active zinc anode during treatment in sodium hydroxide solu-

TABLE I. *Composition of coatings and solubility products*

Anode metal		Mg	Zn	Cd
Coating formed in	NaOH-solution	$MgO \rightarrow Mg(OH)_2$	ZnO	$CdO \rightarrow Cd(OH)_2$
	Na_2CO_3-solution		ZnO	$CdO \rightarrow$ Hydroxycarb. $\rightarrow$ Carbonate
Solubility product	MeO	10^{-6*}	10^{-17}	10^{-13}
	$Me(OH)_2$	10^{-11}	10^{-17}	10^{-14}
	$MeCO_3$		10^{-12}	10^{-14}

* Calculated from: $MgO + H_2O = Mg(OH)_2$, $\Delta F = 7.5$ kcal.

lines. These lines soon predominate and may be attributed to a basic carbonate. Hydroxide lines are also observed. These lines disappear when the coating has become considerably thicker (formed at 5 v in 2*N* sodium carbonate for 100 min), and the lines of the normal cadmium carbonate appear in their place.

Electron microscope photographs obtained with the replica technique reveal the following surface changes. Fig. 12 represents the condition of the surface when practically only oxide is present. Fig. 13 shows the surface after considerable quantities of basic carbonate have appeared. This fibrous substance has been observed in similar form on corroded sheets. The brush-formed aggregate of normal carbonate which is well known from corrosion experiments can be recognized in Fig. 14.

tion. The initial product on the passive zinc anode consists of oxide coating in sodium hydroxide as well as in sodium carbonate solution. A subsequent conversion into hydroxide or carbonate does not take place in accordance with the fact that the oxide and hydroxide are approximately equally insoluble while carbonate is much more soluble, as can be seen from Table I.

The situation is completely different with cadmium. The initial product formed in sodium hydroxide solution is oxide, as with zinc. This oxide, however, appears to be of a very unstable nature and is converted through subsequent change into the hydroxide. This conversion is in accordance with the fact that the solubility product of the hydroxide is about ten times smaller than that of the oxide. Cadmium oxide is formed as the initial product in sodium carbonate solution just as in the case of zinc. A further conversion into carbonate, however, as opposed to the behavior of zinc, must take place here because of the relative values of the solubility products.

The table reveals a tendency for the stable product to be formed as the final step in the reactions at the anode, while the oxide is the initial product which is formed directly from the metal.

A thick coating of the equilibrium product is certainly not completely without influence on the behavior of the electrode. Such a coating may bring about a "mechanical passivity" in that the flow of current is hindered to some extent by an insulating material. The behavior of the electrode is primarily determined, however, by the initial product which obviously consists of a thin but rather coherent film.

The following explanations are presented for discussion in connection with the anodic behavior in the region of passivity.

The current-voltage curve climbs as long as the voltage is sufficient for the reaction $4OH \rightarrow O_2 + 2H_2O + 4e$ to take place, provided that the initial coating is a good electron conductor.

A high electrical field intensity appears to be a prerequisite for electron conductance. If the coating thickness increases, the coating is converted to an insulator.

The effective coating remains permanently thin in the case of Zn/NaOH as the pores in this coating are enlarged by the solvent action of the electrolyte. This enables the electrolyte to infiltrate and take over the conductance of the current.

The coating remains thin in the case of Cd/NaOH and Mg/NaOH below approximately 20 v as the conversion of the initial coating into the stable hydroxide takes place sufficiently rapidly. Further, the hydroxide so formed does not constitute a coherent coating.

The fall in current density above 20 v in the case of Mg/NaOH probably takes place because the initial oxide coating grows faster than its subsequent conversion to hydroxide. As a result, the critical field intensity necessary for electron conductance is not attained.

In the case of Zn/Na_2CO_3 and Cd/Na_2CO_3, the the effective coating is sufficiently thin to conduct electrons for only a short time. To be sure, some current flows initially with accompanying darkening of the metal surface when the evolution voltage of oxygen is attained. However, the current soon diminishes and the coloration diminishes as well.

In the case of Cd/Na_2CO_3, a conversion of oxide to carbonate takes place to some extent, but apparently too slowly to keep the initial coating sufficiently thin to conduct. However, the effect is to bring about a much greater thickness of the coating than in the system Zn/Na_2CO_3.

Any discussion of this paper will appear in a Discussion Section, to be published in the June 1954 issue of the JOURNAL.

REFERENCES

1. R. PIONTELLI, *J. chim. phys.*, **45**, 115 (1948).
2. H. FLÜCKIGER, Dissertation given before the Faculty of Natural Sciences, University of Berne (1951). Unpublished. Microfilm of the manuscript available at "Stadt- und Hochschulbibliothek," Berne, Switzerland.
3. K. HUBER, *Z. Elektrochem.*, **48**, 26 (1942); *Helv. Chim. Acta*, **26**, 1037 (1943); **26**, 1253 (1943); **27**, 1443 (1944); *Bull. soc. chim. France*, **1949**, D154; *Chimia Switz.*, **4**, 54 (1950).
   K. HUBER AND B. BIERI, *Helv. Phys. Acta*, **21**, 375 (1948).
   B. BIERI, Dissertation given before the Faculty of Natural Sciences, University of Berne (1949). Unpublished. Microfilm of the manuscript available at "Stadt- und Hochschulbibliothek," Berne, Switzerland.
4. K. HUBER, *Z. Elektrochem.*, **55**, 165 (1951).
5. K. HUBER, Compt. rend. de la III Réunion du Comité internat. de thermodynamique et de cinétique électrochimiques. Tamburini, Milan (1952). In press.
6. F. D. ROSSINI, D. D. WAGMAN, W. H. EVANS, S. LEVINE, AND I. JAFFE, *Nat. Bur. Standards (U. S.)*, Circ. No. 500 (1952).
7. W. FEITKNECHT, Report for the subcommission for solubility data of the International Union of Pure and Applied Chemistry, analytical section. Unpublished.